



RESEARCH & DEVELOPMENT

Performance Evaluation of Strong Post Double-faced W-beam Guardrail and Strong Post Double-faced Thrie-Beam Guardrail at MASH Test Level 4 (TL-4) and Test Level 5 (TL-5) Conditions

**Howie Fang, Ph.D.
Matthew Gutowski
Emre Palta**

**Department of Mechanical Engineering & Engineering Science
The University of North Carolina at Charlotte
9201 University City Boulevard
Charlotte, NC 28223-0001**

**NCDOT Project 2015-10
FHWA/NC/2015-10
August 2017**

Technical Report Documentation Page

1. Report No. NCDOT 2015-10	2. Government Accession No.	3. Recipient's Catalog No.	
4. Title and Subtitle Performance Evaluation of Strong Post Double-faced W-beam Guardrail and Strong Post Double-faced Thrie-Beam Guardrail at MASH Test Level 4 (TL-4) and Test Level 5 (TL-5) Conditions		5. Report Date August 15, 2017	
		6. Performing Organization Code	
7. Author(s) Howie Fang, Matthew Gutowski, Emre Palta		8. Performing Organization Report No.	
9. Performing Organization Name and Address The University of North Carolina at Charlotte 9201 University City Boulevard Charlotte, NC 28223-0001		10. Work Unit No. (TRAIS)	
		11. Contract or Grant No.	
12. Sponsoring Agency Name and Address Research and Analysis Group 1 South Wilmington Street Raleigh, North Carolina 27601		13. Type of Report and Period Covered 08/16/2014 – 05/15/2017	
		14. Sponsoring Agency Code NCDOT 2015-10	
16. Abstract <i>This report summarizes the research efforts of using finite element modeling and simulations to evaluate the performance of NCDOT double-faced W-beam and Thrie-beam guardrails at different installation heights and under Manual for Assessing Safety Hardware (MASH) Test Level 4 (TL-4) and Test Level 5 (TL-5) impact conditions. A literature review is included on performance evaluation of W-beam and Thrie-beam guardrails as well as applications of finite element modeling and simulations in roadside safety research.</i> <i>The modeling and simulation work was conducted on six double-faced W-beam and Thrie-beam guardrails (with placement heights of 29 and 31 inches) placed along a six-lane 46-foot wide flat median. Two types of Thrie-beam guardrails, one utilizing a wood blockout and the other with a steel blockout, were evaluated. Under MASH TL-4 conditions, the guardrails were impacted by a 1996 Dodge Neon and a 2006 Ford F250 at 62 mph (100 km/h) and an impact angle of 25° and by a 1996 Ford F800 single-unit truck at 56 mph (90 km/h) and an impact angle of 15°. Under MASH TL-5 conditions, the guardrails were impacted by a 1996 Dodge Neon and a 2006 Ford F250 at 62 mph (100 km/h) and an impact angle of 25° and by a 1991 GMC day-cab tractor-trailer at 50 mph (80 km/h) and an impact angle of 15°. The guardrail's performance was determined by evaluating the guardrail deflection and vehicular responses based on the MASH exit box criterion, MASH evaluation criterion F, exit angles, yaw, pitch, and roll angles, transverse displacements, and transverse velocities.</i> <i>The simulation results demonstrated the effectiveness of the double-faced 29- and 31-inch W-beam guardrails and Thrie-beam guardrails, with wood- and steel-blockouts, placed on a flat median under MASH TL-4 and TL-5 impact conditions. Under impacts from the passenger vehicles (i.e., Dodge Neon and Ford F250) the W-beam and Thrie-beam guardrails with 29- and 31-inch placement heights were shown to effectively redirect the vehicles in all cases, although in some scenarios, a large exit angle was observed. Under impacts by heavy trucks (i.e., single-unit truck and tractor-trailer), the W-beam and Thrie-beam guardrails with 29- and 31-inch placement heights were shown to be effective at containing the vehicle on the impacting side, but exhibited a high likelihood for vehicle rollover. Finite element modeling and simulations were shown to provide an effective means for studying crash scenarios that are difficult and/or extremely expensive to investigate with physical crash testing.</i>			
17. Key Words <i>W-beam; Thrie-beam; Flat median; Double-faced; Median barrier; Barrier height; Roadside safety; Highway safety; Finite element</i>		18. Distribution Statement	
19. Security Classif. (of this report) Unclassified	20. Security Classif. (of this page) Unclassified	21. No. of Pages 121	22. Price

DISCLAIMER

The contents of this report reflect the views of the authors and not necessarily the views of the university. The authors are responsible for the facts and the accuracy of the data presented herein. The contents do not necessarily reflect the official views or policies of either the North Carolina Department of Transportation or the Federal Highway Administration. This report does not constitute a standard, specification, or regulation.

ACKNOWLEDGMENTS

This study was supported by the North Carolina Department of Transportation (NCDOT) under Project No. 2015-10. The authors would like to thank NCDOT personnel from the *Roadway Design Unit, Transportation Mobility & Safety, Highway Division 5, Project Services Unit, FHWA – NC Division, and Research and Development Unit* for the support and cooperation during the grant period.

EXECUTIVE SUMMARY

This report summarizes the research efforts of using finite element modeling and simulations to evaluate the performance of NCDOT double-faced W-beam and Thrie-beam guardrails at different installation heights under Manual for Assessing Safety Hardware (MASH) Test Level 4 (TL-4) and Test Level 5 (TL-5) impact conditions. A literature review is included on performance evaluation of W-beam and Thrie-beam guardrails as well as applications of finite element modeling and simulations in roadside safety research.

The modeling and simulation work was conducted on six double-faced W-beam and Thrie-beam guardrails (with placement heights of 29 and 31 inches) placed along a six-lane 46-foot wide flat median. Two types of Thrie-beam guardrails, one utilizing a wood blockout and the other with a steel blockout, were evaluated. Under MASH TL-4 conditions, the guardrails were impacted by a 1996 Dodge Neon and a 2006 Ford F250 at 62 mph (100 km/h) and an impact angle of 25° and by a 1996 Ford F800 single-unit truck at 56 mph (90 km/h) and an impact angle of 15°. Under MASH TL-5 conditions, the guardrails were impacted by a 1996 Dodge Neon and a 2006 Ford F250 at 62 mph (100 km/h) and an impact angle of 25° and by a 1991 GMC day-cab tractor-trailer at 50 mph (80 km/h) and an impact angle of 15°. The guardrail's performance was determined by evaluating the guardrail deflection and vehicular responses based on the MASH exit box criterion, MASH evaluation criterion F, exit angles, yaw, pitch, and roll angles, transverse displacements, and transverse velocities.

The simulation results demonstrated the effectiveness of the double-faced 29- and 31-inch W-beam guardrails and Thrie-beam guardrails, with wood- and steel-blockouts, placed on a flat median under MASH TL-4 and TL-5 impact conditions. Under impacts from the passenger vehicles (i.e., Dodge Neon and Ford F250) the W-beam and Thrie-beam guardrails with 29- and 31-inch placement heights were shown to effectively redirect the vehicles in all cases, although in some scenarios, a large exit angle was observed. Under impacts by heavy trucks (i.e., single-unit truck and tractor-trailer), the W-beam and Thrie-beam guardrails with 29- and 31-inch placement heights were shown to be effective at containing the vehicle on the impacting side, but exhibited a high likelihood for vehicle rollover. Finite element modeling and simulations were shown to provide an effective means for studying crash scenarios that are difficult and/or extremely expensive to investigate with physical crash testing.

TABLE OF CONTENTS

Title Page	i
Technical Report Documentation Page	ii
Disclaimer	iii
Acknowledgments	iv
Executive Summary	v
Table of Contents	vi
List of Tables	vii
List of Figures	viii
1. Introduction	1
1.1 Background	1
1.2 Research Objectives and Tasks	3
2. Literature Review	7
2.1 Performance Evaluation of Guardrails	7
2.2 Finite Element Simulations of Vehicular Crashes	14
3. Finite Element Modeling of Vehicles and Guardrails	19
3.1 FE Models of Four Vehicles	19
3.2 FE Model of the Guardrails	22
3.3 Simulation Setup	26
4. Simulation Results and Analysis	31
4.1 Case 1: Double-faced 29-inch W-beam guardrail.....	32
4.2 Case 2: Double-faced 31-inch W-beam guardrail.....	43
4.3 Case 3: Double-faced 29-inch Thrie-beam Guardrails.....	53
4.4 Case 4: Double-faced 31-inch Thrie-beam Guardrails.....	72
4.5 Comparison of Guardrails at 29- and 31-inch Placement Heights.....	89
5. Findings and Conclusions	95
6. Recommendations	98
7. Implementation and Technology Transfer Plan	99
References	100

List of Tables

Table 3.1: Specifications of the four test vehicles used in crash simulations

Table 3.2: Simulation conditions for all cases

Table 4.1: The dimension of the exit box defined in MASH

Table 4.2: Exit box dimensions for the four test vehicles of this study

Table 4.3: Simulation results of Case 1 (Double-faced 29-inch W-beam guardrail)

Table 4.4: Simulation results of Case 2 (31-inch double-faced W-beam guardrail)

Table 4.5: Simulation results of Case 3 (Double-faced 29-inch Wood- and Steel-blockout Thrie-beam Guardrails)

Table 4.6: Simulation results of Case 4 (Double-faced 31-inch Wood- and Steel-blockout Thrie-beam Guardrails)

Table 4.7: Vehicle redirection characteristics of double-faced W-beam guardrails

Table 4.8: Vehicle redirection characteristics of double-faced wood-blockout Thrie-beam guardrails

Table 4.9: Vehicle redirection characteristics of double-faced steel-blockout Thrie-beam guardrails

List of Figures

- Fig. 1.1: A strong post W-beam guardrail (top) and a Thrie-beam guardrail (bottom).
- Fig. 1.2: A double-faced W-beam guardrail (left) and a double-faced Thrie-beam guardrail (right).
- Fig. 1.3: FE models of a small passenger car, a pickup truck, a single-unit truck, and a tractor-trailer.
- Fig. 1.4: FE models of a double-faced G4(1S) W-beam guardrail, double-faced wood-blockout Thrie-beam guardrail, double-faced G4(1S) steel-blockout Thrie-beam guardrail.
- Fig. 1.5: FE model of a double-faced W-beam guardrail.
- Fig. 1.6: Evaluation of a W-beam guardrail at MASH TL-4 and TL-5 conditions.
- Fig. 1.7: Definition of vehicle responses.
- Fig. 1.8: Double-faced Thrie-beam guardrail segments with wood blockouts (left) and steel blockouts (right).
- Fig. 1.9: A steel-blockout Thrie-beam guardrail impacted by a single-unit truck (left) and a tractor-trailer (right).
-
- Fig. 3.1: FE models of the four vehicles used in crash simulations.
- Fig. 3.2: FE models of the soil foundation around a post.
- Fig. 3.3: FE models of a wood blockout (left) and steel blockout (right) on the Thrie-beam guardrails.
- Fig. 3.4: FE model of the bolt connections on the W-beam guardrails.
- Fig. 3.5: Profile views of the 29-inch double-faced guardrail FE models.
- Fig. 3.6: Full FE model of the double-faced 29-inch W-beam guardrail.
- Fig. 3.7: Full FE model of the double-faced 31-inch W-beam guardrail.
- Fig. 3.8: Full FE model of the double-faced 29-inch wood-blockout Thrie-beam guardrail.
- Fig. 3.9: Full FE model of the double-faced 31-inch wood-blockout Thrie-beam guardrail.
- Fig. 3.10: Full FE model of the double-faced 29-inch steel-blockout Thrie-beam guardrail.
- Fig. 3.11: Full FE model of the double-faced 31-inch steel-blockout Thrie-beam guardrail.
- Fig. 3.12: FE models of the double-faced 29-inch W-beam guardrail under vehicular impacts.
- Fig. 3.13: FE models of the double-faced 31-inch W-beam guardrails.
- Fig. 3.14: FE models of the double-faced 29-inch wood-blockout Thrie-beam guardrails.
- Fig. 3.15: FE models of the double-faced 29-inch steel-blockout Thrie-beam guardrails.
- Fig. 3.16: FE models of the double-faced 31-inch wood-blockout Thrie-beam guardrails.

Fig. 3.17: FE models of the double-faced 31-inch steel-blockout Thrie-beam guardrails.

Fig. 4.1: The exit-box criterion defined in MASH.

Fig. 4.2: A Dodge Neon impacting the double-faced 29-inch W-beam guardrail at 62 mph (100 km/h) and 25°.

Fig. 4.3: Yaw, pitch, and roll angles of Dodge Neon impacting the double-faced 29-inch W-beam guardrail at 62 mph (100 km/h) and 25°.

Fig. 4.4: Maximum dynamic deflection of the double-faced 29-inch W-beam guardrail at 62 mph (100 km/h) and 25° and impacted by a Dodge Neon.

Fig. 4.5: Simulations of Dodge Neon impacting the double-faced 29-inch W-beam guardrail at 62 mph (100 km/h) and 25°.

Fig. 4.6: Transverse displacement and velocity of the Dodge Neon impacting the double-faced 29-inch W-beam guardrail at 62 mph (100 km/h) and 25°.

Fig. 4.7: A Ford F250 impacting the double-faced 29-inch W-beam guardrail at 62 mph (100 km/h) and 25°.

Fig. 4.8: Yaw, pitch, and roll angles of Ford F250 impacting the double-faced 29-inch W-beam guardrail at 62 mph (100 km/h) and 25°.

Fig. 4.9: Maximum dynamic deflection of the double-faced 29-inch W-beam guardrail at 62 mph (100 km/h) and 25° and impacted by a Ford F250.

Fig. 4.10: Simulations of Ford F250 impacting the double-faced 29-inch W-beam guardrail at 62 mph (100 km/h) and 25°.

Fig. 4.11: Transverse displacement and velocity of the Ford F250 impacting the double-faced 29-inch W-beam guardrail at 62 mph (100 km/h) and 25°.

Fig. 4.12: A single-unit truck impacting the double-faced 29-inch W-beam guardrail at 56 mph (90 km/h) and 15°.

Fig. 4.13: Yaw, pitch, and roll angles of the single-unit truck impacting the double-faced 29-inch W-beam guardrail at 56 mph (90 km/h) and 15°.

Fig. 4.14: Maximum dynamic deflection of the double-faced 29-inch W-beam guardrail at 56 mph (90 km/h) and 15° and impacted by a single-unit truck.

Fig. 4.15: Simulations of the single-unit truck impacting the double-faced 29-inch W-beam guardrail at 56 mph (90 km/h) and 15°.

Fig. 4.16: Transverse displacement and velocity of the single-unit truck impacting the double-faced 29-inch W-beam guardrail at 56 mph (90 km/h) and 15°.

Fig. 4.17: A tractor-trailer impacting the double-faced 29-inch W-beam guardrail at 50 mph (80 km/h) and 15°.

- Fig. 4.18: Yaw, pitch, and roll angles of the tractor's (a) cabin and trailer's (b) tandem axle impacting the double-faced 29-inch W-beam guardrail at 50 mph (80 km/h) and 15°.
- Fig. 4.19: Maximum dynamic deflection of the double-faced 29-inch W-beam guardrail at 50 mph (80 km/h) and 15° and impacted by a tractor-trailer.
- Fig. 4.20: A tractor-trailer impacting the double-faced 29-inch W-beam guardrail at 50 mph (80 km/h) and 15°.
- Fig. 4.21: Transverse displacements and velocities of the tractor-trailer impacting the double-faced 29-inch W-beam guardrail at 50 mph (80 km/h) and 15°.
- Fig. 4.22: A Dodge Neon impacting the double-faced 31-inch W-beam guardrail at 62 mph (100 km/h) and 25°.
- Fig. 4.23: Yaw, pitch, and roll angles of Dodge Neon impacting the double-faced 31-inch W-beam guardrail at 62 mph (100 km/h) and 25°.
- Fig. 4.24: Maximum dynamic deflection of the double-faced 31-inch W-beam guardrail at 62 mph (100 km/h) and 25° and impacted by a Dodge Neon.
- Fig. 4.25: Simulations of Dodge Neon impacting the double-faced 31-inch W-beam guardrail at 62 mph (100 km/h) and 25°.
- Fig. 4.26: Transverse displacement and velocity of the Dodge Neon impacting the double-faced 31-inch W-beam guardrail at 62 mph (100 km/h) and 25°.
- Fig. 4.27: A Ford F250 impacting the double-faced 31-inch W-beam guardrail at 62 mph (100 km/h) and 25°.
- Fig. 4.28: Yaw, pitch, and roll angles of Ford F250 impacting the double-faced 31-inch W-beam guardrail at 62 mph (100 km/h) and 25°.
- Fig. 4.29: Maximum dynamic deflection of the double-faced 31-inch W-beam guardrail at 62 mph (100 km/h) and 25° and impacted by a Ford F250.
- Fig. 4.30: Simulations of Ford F250 impacting the double-faced 31-inch W-beam guardrail at 62 mph (100 km/h) and 25°.
- Fig. 4.31: Transverse displacement and velocity of the Ford F250 impacting the double-faced 31-inch W-beam guardrail at 62 mph (100 km/h) and 25°.
- Fig. 4.32: A single-unit truck impacting the double-faced 31-inch W-beam guardrail at 56 mph (90 km/h) and 15°.
- Fig. 4.33: Yaw, pitch, and roll angles of a single-unit truck impacting the double-faced 31-inch W-beam guardrail at 56 mph (90 km/h) and 15°.
- Fig. 4.34: Maximum dynamic deflection of the double-faced 31-inch W-beam guardrail at 56 mph (90 km/h) and 15° and impacted by a single-unit truck.
- Fig. 4.35: Simulations of a single-unit truck impacting the double-faced 31-inch W-beam guardrail at 56 mph (90 km/h) and 15°.

- Fig. 4.36: Transverse displacement and velocity of the single-unit truck impacting the double-faced 31-inch W-beam guardrail at 56 mph (90 km/h) and 15°.
- Fig. 4.37: A tractor-trailer impacting the double-faced 31-inch W-beam guardrail at 50 mph (80 km/h) and 15°.
- Fig. 4.38: Yaw, pitch, and roll angles of the tractor's (a) cabin and trailer's (b) tandem axle impacting the double-faced 31-inch W-beam guardrail at 50 mph (80 km/h) and 15°.
- Fig. 4.39: Maximum dynamic deflection of the double-faced 31-inch W-beam guardrail at 50 mph (80 km/h) and 15° and impacted by a tractor-trailer.
- Fig. 4.40: Simulations of a tractor-trailer impacting the double-faced 31-inch W-beam guardrail at 50 mph (80 km/h) and 15°.
- Fig. 4.41: Transverse displacement and velocities of the tractor-trailer impacting the double-faced 31-inch W-beam guardrail at 50 mph (80 km/h) and 15°.
- Fig. 4.42: A Dodge Neon impacting the double-faced 29-inch wood-blockout Thrie-beam guardrail at 62 mph (100 km/h) and 25°.
- Fig. 4.43: A Dodge Neon impacting the double-faced 29-inch steel-blockout Thrie-beam guardrail at 62 mph (100 km/h) and 25°.
- Fig. 4.44: Yaw, pitch, and roll angles of Dodge Neon impacting the double-faced 29-inch (a) wood- (b) steel-blockout Thrie-beam guardrail at 62 mph (100 km/h) and 25°.
- Fig. 4.45: Maximum dynamic deflection of the double-faced 29-inch wood-blockout Thrie-beam guardrail at 62 mph (100 km/h) and 25° and impacted by a Dodge Neon.
- Fig. 4.46: Maximum dynamic deflection of the double-faced 29-inch steel-blockout Thrie-beam guardrail at 62 mph (100 km/h) and 25° and impacted by a Dodge Neon.
- Fig. 4.47: Simulations of Dodge Neon impacting the double-faced 29-inch wood-blockout Thrie-beam guardrail at 62 mph (100 km/h) and 25°.
- Fig. 4.48: Simulations of Dodge Neon impacting the double-faced 29-inch steel-blockout Thrie-beam guardrail at 62 mph (100 km/h) and 25°.
- Fig. 4.49: Transverse displacement and velocity of the Dodge Neon impacting the double-faced 29-inch wood-blockout Thrie-beam guardrail at 62 mph (100 km/h) and 25°.
- Fig. 4.50: Transverse displacement and velocity of the Dodge Neon impacting the double-faced 29-inch steel-blockout Thrie-beam guardrail at 62 mph (100 km/h) and 25°.
- Fig. 4.51: A Ford F250 impacting the double-faced 29-inch wood-blockout Thrie-beam guardrail at 62 mph (100 km/h) and 25°.
- Fig. 4.52: A Ford F250 impacting the double-faced 29-inch steel-blockout Thrie-beam guardrail at 62 mph (100 km/h) and 25°.
- Fig. 4.53: Yaw, pitch, and roll angles of Ford F250 impacting the double-faced 29-inch (a) wood- (b) steel-blockout Thrie-beam guardrail at 62 mph (100 km/h) and 25°.

- Fig. 4.54: Maximum dynamic deflection of the double-faced 29-inch wood-blockout Thrie-beam guardrail at 62 mph (100 km/h) and 25° and impacted by a Ford F250.
- Fig. 4.55: Maximum dynamic deflection of the double-faced 29-inch steel-blockout Thrie-beam guardrail at 62 mph (100 km/h) and 25° and impacted by a Ford F250.
- Fig. 4.56: Simulations of Ford F250 impacting the double-faced 29-inch wood-blockout Thrie-beam guardrail at 62 mph (100 km/h) and 25°.
- Fig. 4.57: Simulations of Ford F250 impacting the double-faced 29-inch steel-blockout Thrie-beam guardrail at 62 mph (100 km/h) and 25°.
- Fig. 4.58: Transverse displacement and velocity of the Ford F250 impacting the double-faced 29-inch wood-blockout Thrie-beam guardrail at 62 mph (100 km/h) and 25°.
- Fig. 4.59: Transverse displacement and velocity of the Ford F250 impacting the double-faced 29-inch steel-blockout Thrie-beam guardrail at 62 mph (100 km/h) and 25°.
- Fig. 4.60: A single-unit truck impacting the double-faced 29-inch wood-blockout Thrie-beam guardrail at 56 mph (90 km/h) and 15°.
- Fig. 4.61: A single-unit truck impacting the double-faced 29-inch steel-blockout Thrie-beam guardrail at 56 mph (90 km/h) and 15°.
- Fig. 4.62: Yaw, pitch, and roll angles of single-unit trucks impacting the double-faced 29-inch (a) wood- (b) steel-blockout Thrie-beam guardrail at 62 mph (100 km/h) and 25°.
- Fig. 4.63: Maximum dynamic deflection of the double-faced 29-inch wood-blockout Thrie-beam guardrail at 56 mph (90 km/h) and 15° and impacted by a single-unit truck.
- Fig. 4.64: Maximum dynamic deflection of the double-faced 29-inch steel-blockout Thrie-beam guardrail at 56 mph (90 km/h) and 15° and impacted by a single-unit truck.
- Fig. 4.65: Simulations of single-unit truck impacting the double-faced 29-inch wood-blockout Thrie-beam guardrail at 56 mph (90 km/h) and 15°.
- Fig. 4.66: Simulations of single-unit truck impacting the double-faced 29-inch steel-blockout Thrie-beam guardrail at 56 mph (90 km/h) and 15°.
- Fig. 4.67: Transverse displacement and velocity of the single-unit truck impacting the double-faced 29-inch wood-blockout Thrie-beam guardrail at 56 mph (90 km/h) and 15°.
- Fig. 4.68: Transverse displacement and velocity of the single-unit truck impacting the double-faced 29-inch steel-blockout Thrie-beam guardrail at 56 mph (90 km/h) and 15°.
- Fig. 4.69: A tractor-trailer impacting the double-faced 29-inch wood-blockout Thrie-beam guardrail at 50 mph (80 km/h) and 15°.
- Fig. 4.70: A tractor-trailer impacting the double-faced 29-inch steel-blockout Thrie-beam guardrail at 50 mph (80 km/h) and 15°.

- Fig. 4.71: Yaw, pitch, and roll angles of the tractor's (a) cabin and trailer's (b) tandem axle impacting the double-faced 29-inch wood-blockout Thrie-beam guardrail at 50 mph (80 km/h) and 15°.
- Fig. 4.72: Yaw, pitch, and roll angles of the tractor's (a) cabin and trailer's (b) tandem axle impacting the double-faced 29-inch steel-blockout Thrie-beam guardrail at 50 mph (80 km/h) and 15°.
- Fig. 4.73: Maximum dynamic deflection of the double-faced 29-inch wood-blockout Thrie-beam guardrail at 50 mph (80 km/h) and 15° and impacted by a tractor-trailer.
- Fig. 4.74: Maximum dynamic deflection of the double-faced 29-inch steel-blockout Thrie-beam guardrail at 50 mph (80 km/h) and 15° and impacted by a tractor-trailer.
- Fig. 4.75: Simulations of tractor-trailer impacting the double-faced 29-inch wood-blockout Thrie-beam guardrail at 50 mph (80 km/h) and 15°.
- Fig. 4.76: Simulations of tractor-trailer impacting the double-faced 29-inch steel-blockout Thrie-beam guardrail at 50 mph (80 km/h) and 15°.
- Fig. 4.77: Transverse displacement and velocities of the tractor-trailer impacting the double-faced 29-inch wood-blockout Thrie-beam guardrail at 50 mph (80 km/h) and 15°.
- Fig. 4.78: Transverse displacement and velocities of the tractor-trailer impacting the double-faced 29-inch steel-blockout Thrie-beam guardrail at 50 mph (80 km/h) and 15°.
- Fig. 4.79: A Dodge Neon impacting the double-faced 31-inch wood-blockout Thrie-beam guardrail at 62 mph (100 km/h) and 25°.
- Fig. 4.80: A Dodge Neon impacting the double-faced 31-inch steel-blockout Thrie-beam guardrail at 62 mph (100 km/h) and 25°.
- Fig. 4.81: Yaw, pitch, and roll angles of Dodge Neon impacting the double-faced 31-inch (a) wood- (b) steel-blockout Thrie-beam guardrail at 62 mph (100 km/h) and 25°.
- Fig. 4.82: Maximum dynamic deflection of the double-faced 31-inch wood-blockout Thrie-beam guardrail at 62 mph (100 km/h) and 25° and impacted by a Dodge Neon.
- Fig. 4.83: Maximum dynamic deflection of the double-faced 31-inch steel-blockout Thrie-beam guardrail at 62 mph (100 km/h) and 25° and impacted by a Dodge Neon.
- Fig. 4.84: Simulations of Dodge Neon impacting the double-faced 31-inch wood-blockout Thrie-beam guardrail at 62 mph (100 km/h) and 25°.
- Fig. 4.85: Simulations of Dodge Neon impacting the double-faced 31-inch steel-blockout Thrie-beam guardrail at 62 mph (100 km/h) and 25°.
- Fig. 4.86: Transverse displacement and velocity of the Dodge Neon impacting the double-faced 31-inch wood-blockout Thrie-beam guardrail at 62 mph (100 km/h) and 25°.
- Fig. 4.87: Transverse displacement and velocity of the Dodge Neon impacting the double-faced 31-inch steel-blockout Thrie-beam guardrail at 62 mph (100 km/h) and 25°.
- Fig. 4.88: A Ford F250 impacting the double-faced 31-inch wood-blockout Thrie-beam guardrail at 62 mph (100 km/h) and 25°.

- Fig. 4.89: A Ford F250 impacting the double-faced 31-inch steel-blockout Thrie-beam guardrail at 62 mph (100 km/h) and 25°.
- Fig. 4.90: Yaw, pitch, and roll angles of Ford F250 impacting the double-faced 31-inch (a) wood- (b) steel-blockout Thrie-beam guardrail at 62 mph (100 km/h) and 25°.
- Fig. 4.91: Maximum dynamic deflection of the double-faced 31-inch wood-blockout Thrie-beam guardrail at 62 mph (100 km/h) and 25° and impacted by a Ford F250.
- Fig. 4.92: Maximum dynamic deflection of the double-faced 31-inch steel-blockout Thrie-beam guardrail at 62 mph (100 km/h) and 25° and impacted by a Ford F250.
- Fig. 4.93: Simulations of Ford F250 impacting the double-faced 31-inch wood-blockout Thrie-beam guardrail at 62 mph (100 km/h) and 25°.
- Fig. 4.94: Simulations of Ford F250 impacting the double-faced 31-inch steel-blockout Thrie-beam guardrail at 62 mph (100 km/h) and 25°.
- Fig. 4.95: Transverse displacement and velocity of the Ford F250 impacting the double-faced 31-inch wood-blockout Thrie-beam guardrail at 62 mph (100 km/h) and 25°.
- Fig. 4.96: Transverse displacement and velocity of the Ford F250 impacting the double-faced 31-inch steel-blockout Thrie-beam guardrail at 62 mph (100 km/h) and 25°.
- Fig. 4.97: A single-unit truck impacting the double-faced 31-inch wood-blockout Thrie-beam guardrail at 56 mph (90 km/h) and 15°.
- Fig. 4.98: A single-unit truck impacting the double-faced 31-inch steel-blockout Thrie-beam guardrail at 56 mph (90 km/h) and 15°.
- Fig. 4.99: Yaw, pitch, and roll angles of single-unit trucks impacting the double-faced 31-inch (a) wood- (b) steel-blockout Thrie-beam guardrail at 62 mph (100 km/h) and 25°.
- Fig. 4.100: Maximum dynamic deflection of the double-faced 31-inch wood-blockout Thrie-beam guardrail at 56 mph (90 km/h) and 15° and impacted by a single-unit truck.
- Fig. 4.101: Maximum dynamic deflection of the double-faced 31-inch steel-blockout Thrie-beam guardrail at 56 mph (90 km/h) and 15° and impacted by a single-unit truck.
- Fig. 4.102: Simulations of single-unit truck impacting the double-faced 31-inch wood-blockout Thrie-beam guardrail at 56 mph (90 km/h) and 15°.
- Fig. 4.103: Simulations of single-unit truck impacting the double-faced 31-inch steel-blockout Thrie-beam guardrail at 56 mph (90 km/h) and 15°.
- Fig. 4.104: Transverse displacement and velocity of the single-unit truck impacting the double-faced 31-inch wood-blockout Thrie-beam guardrail at 56 mph (90 km/h) and 15°.
- Fig. 4.105: Transverse displacement and velocity of the single-unit truck impacting the double-faced 31-inch steel-blockout Thrie-beam guardrail at 56 mph (90 km/h) and 15°.

- Fig. 4.106: A tractor-trailer impacting the double-faced 31-inch wood-blockout Thrie-beam guardrail at 50 mph (80 km/h) and 15°.
- Fig. 4.107: A tractor-trailer impacting the double-faced 31-inch steel-blockout Thrie-beam guardrail at 50 mph (80 km/h) and 15°.
- Fig. 4.108: Yaw, pitch, and roll angles of the tractor-trailer impacting the double-faced 31-inch wood-blockout Thrie-beam guardrail at 50 mph (80 km/h) and 15°.
- Fig. 4.109: Yaw, pitch, and roll angles of the tractor-trailer impacting the double-faced 31-inch steel-blockout Thrie-beam guardrail at 50 mph (80 km/h) and 15°.
- Fig. 4.110: Maximum dynamic deflection of the double-faced 31-inch wood-blockout Thrie-beam guardrail at 50 mph (80 km/h) and 15° and impacted by a tractor-trailer.
- Fig. 4.111: Maximum dynamic deflection of the double-faced 31-inch steel-blockout Thrie-beam guardrail at 50 mph (80 km/h) and 15° and impacted by a tractor-trailer.
- Fig. 4.112: Simulations of tractor-trailer impacting the double-faced 31-inch wood-blockout Thrie-beam guardrail at 50 mph (80 km/h) and 15°.
- Fig. 4.113: Simulations of tractor-trailer impacting the double-faced 31-inch steel-blockout Thrie-beam guardrail at 50 mph (80 km/h) and 15°.
- Fig. 4.114: Transverse displacement and velocities of the tractor-trailer impacting the double-faced 31-inch wood-blockout Thrie-beam guardrail at 50 mph (80 km/h) and 15°.
- Fig. 4.115: Transverse displacement and velocities of the tractor-trailer impacting the double-faced 31-inch steel-blockout Thrie-beam guardrail at 50 mph (80 km/h) and 15°.

1. Introduction

Roadside barrier systems are important devices to ensure transportation safety; they serve the purpose of safely redirecting errant vehicles and preventing runaway vehicles from intruding into oncoming travel lanes. Over the years, different types of barriers have been developed and are categorized into rigid (e.g., concrete barriers), semi-rigid (e.g., W-beam guardrails), and flexible (e.g., cable barriers) systems. W-beam guardrails are widely used safety devices on U.S. highways. Figure 1.1 shows a strong post W-beam and Thrie-beam guardrails that are commonly used on U.S. highways. W-beam and Thrie-beam guardrails usually require substantial replacement or repairs after major vehicle crashes, because even low-energy impacts can bend and damage the rails and displace the posts such that the barrier may not perform properly in a subsequent crash event. Evaluations of the in-service W-beam and Thrie-beam guardrails showed that these systems generally had satisfactory safety performance.

All barrier systems used on U.S. highways are designed according to the Roadside Design Guide of the American Association of State Highway and Transportation Officials (AASHTO). They must be tested to satisfy the safety criteria specified by Manual for Assessing Safety Hardware (MASH), a replacement of the old standard – Report 350 of the National Cooperative Highway Research Program (NCHRP). Some of the test conditions in MASH are more severe than those in NCHRP Report 350 and the language of emphasizing the importance of in-service evaluation is added to MASH. Although the current barrier systems that passed NCHRP Report 350 are not required to pass the corresponding MASH criteria, it is important to evaluate their performance under MASH test conditions for practical safety concerns. Currently, the W-beam and Thrie-beam guardrails are required to comply with MASH Test Level 3 (TL-3) conditions, i.e., under the impacts of a small passenger car (1100C) and a pickup truck (2270P) at 62 mph (100 km/h) and 25 degree.



Fig. 1.1: A strong post W-beam guardrail (top) and a Thrie-beam guardrail (bottom).

1.1 Background

The single-faced W-beam and Thrie-beam guardrails shown in Fig. 1.1 generally perform well under vehicular impacts at MASH TL-3 conditions. When used as highway median barriers, two separate guardrails are typically installed, with one on each side of the median. While preventing cross-median crashes, the two guardrails create logistical challenges for maintenance operations (e.g. guardrail repairs and landscaping upkeep). A practical solution adopted by state DOT engineers is to replace the two separate single-faced guardrails with a combined double-faced guardrail, as shown in Fig. 1.2. In a previous NCDOT research

project, a 27-inch double-faced W-beam guardrail was evaluated on a six-lane, 46-ft median divided freeway under the TL-3 conditions of NCHRP Report 350. The research results showed that the double-faced W-beam guardrails outperformed the single-faced guardrails and were recommended for use in locations where two separate single-faced guardrails were to be installed.



Fig. 1.2: A double-faced W-beam guardrail (left) and a double-faced Thrie-beam guardrail (right).

Research on the standard G4(1S) W-beam guardrails shows that they may not meet the TL-3 criteria of NCHRP Report 350 at 27-inch installation height. A revision to the guardrail height is required for new installations of G4(1S) guardrails under TL-3 conditions. According to the USDOT memorandum issued in May 2010 (Nicol 2010), transportation agencies should ensure a minimum height of 27¾ inches (measured from grade to top of the rail) for newly installed G4(1S) guardrails. The generic or proprietary designs of 31-inch high guardrails are also recommended to transportation agencies for consideration of adoption as the standard for all new installations instead of the G4(1S) system. The installation height of 31 inches is the nominal height measured from grade to the top of the rail and includes a construction tolerance of plus or minus one inch. These new 31-inch guardrails are shown to have improved crash-test performance under TL-3 conditions of NCHRP Report 350 and increased capacity to safely contain and redirect higher center-of-gravity vehicles such as pickup trucks and SUVs.

In recent years, NCDOT changed the standard rail height of single-faced W-beam guardrails from 27 inches to 29 and 31 inches for new guardrail installations. Accordingly, the double-faced W-beam and Thrie-beam guardrails, if chosen, will need to be installed at the new rail heights. The double-faced guardrails used in highway medians are adopted based on their compliance with MASH TL-3 conditions and the lower cost of initial installations. Questions often arise about the DOT's design decisions and how the guardrail systems function under different conditions. The performance of the 29- and 31-inch double-faced W-beam and Thrie-beam guardrails has not been fully evaluated under MASH TL-4 and TL-5 impact conditions. To understand the performance of these guardrail systems at higher test level impact conditions (i.e., higher than the required TL-3 test conditions), the functionality of guardrail components, i.e., the rails, offset blocks, and guardrail posts, need to be evaluated.

1.2 Research Objectives and Tasks

In this study, full-scale finite element (FE) simulations were employed to evaluate the performance of the strong post double-faced W-beam and Thrie-beam guardrails at MASH TL-4 and TL-5 impact conditions. The research project had six major tasks as stated below.

Task 1: Literature Review and Data Collection

A comprehensive literature review was conducted on crash testing, modeling and simulations that are related, in particular, to W-beam and Thrie-beam guardrails to assist with model validation and crash simulations. State DOTs and research institutions were contacted to collect information on their experience of related research issues.

Task 2: FE Model Development and Validation

In this task, the FE models of four different sized vehicles, as shown in Figure 1.3, were obtained: a 1996 Dodge Neon (small passenger car) with a mass of 2,400 lb (1,090 kg), a 2006 Ford F250 pickup truck with a mass of 5,504 lb (2,499 kg), a 1996 Ford F800 single-unit truck with a total mass of 22,046 lb (10,000 kg), and a 1991 GMC day-cab tractor-trailer with a total mass of 80,000 lb (36,287 kg). These FE models were validated using crash test data and were shown to be appropriate for crash simulations. The FE models of the double-faced W-beam guardrails were obtained from a previous NCDOT project and modified to meet the requirements of the proposed work. The models of double-faced Thrie-beam guardrails were created based on a single-faced Thrie-beam model available from the National Crash Analysis Center. All of the FE models were verified based on NCDOT designs and validated using available simulation results and/or test data from literature. Figure 1.4 shows the FE models of a double-faced G4(1S) W-beam guardrail, a double-faced wood-blockout Thrie-beam guardrail, and a double-faced steel-blockout Thrie-beam guardrail. These models were used in the simulation work of this study.

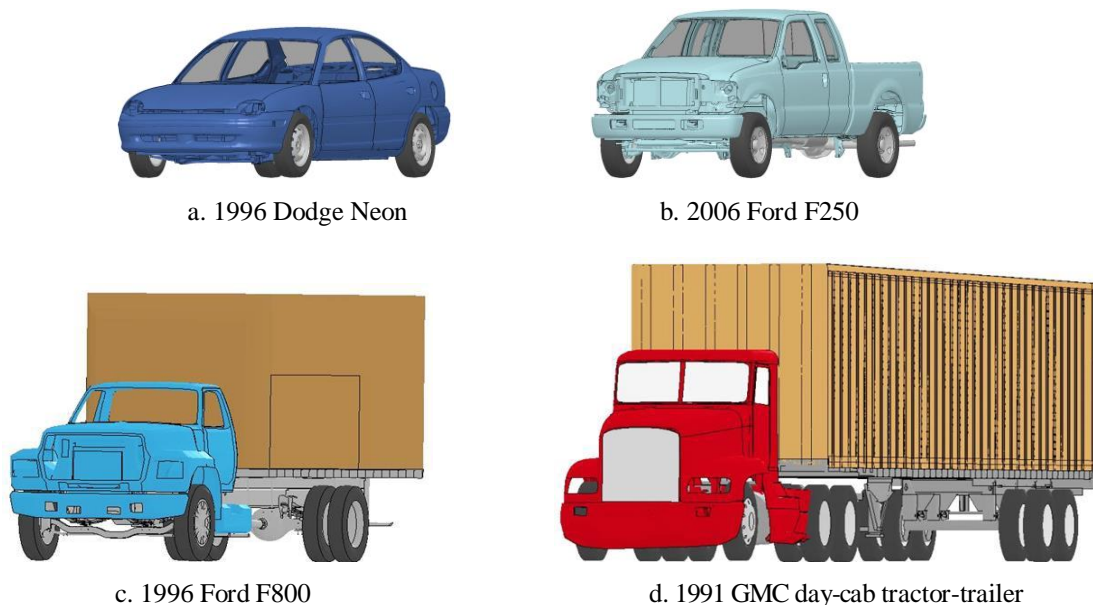


Fig. 1.3: FE models of a small passenger car, a pickup truck, a single-unit truck, and a tractor-trailer.

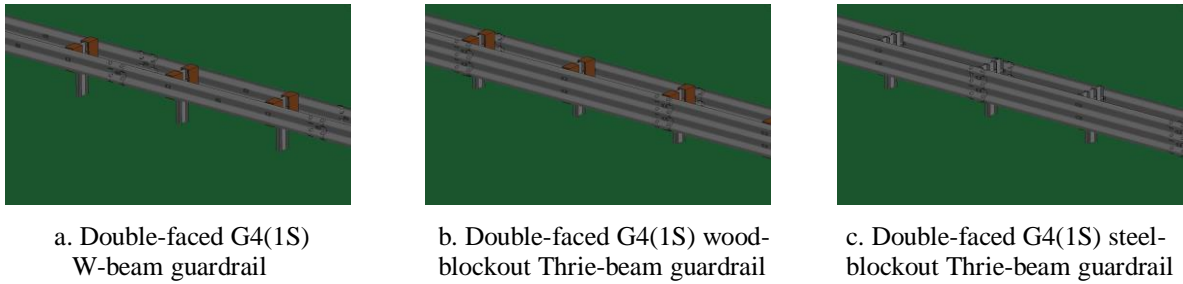


Fig. 1.4: FE models of a double-faced G4(1S) W-beam guardrail, double-faced wood-blockout Thrie-beam guardrail, double-faced G4(1S) steel-blockout Thrie-beam guardrail.

Task 3: Performance Evaluation of Double-faced 29-inch W-beam Guardrails (TL-4 & TL-5)

In this task, the 29-inch double-faced W-beam guardrail was evaluated at MASH TL-4 and TL-5 impact conditions. At MASH TL-4 impact conditions, the guardrail was impacted by the Dodge Neon and Ford F250 at 62 mph (100 km/h) and a 25° impact angle, and by the Ford F800 single-unit truck at 56 mph (90 km/h) and a 15° impact angle. At MASH TL-5 conditions, the guardrail was impacted by the Dodge Neon and Ford F250 at 62 mph (100 km/h) and a 25° impact angle, and by the tractor-trailer at 50 mph (80 km/h) and a 15° impact angle. Figure 1.5 shows the complete FE model of a double-faced W-beam guardrail and Fig. 1.6 illustrates the MASH TL-4 and TL-5 conditions.

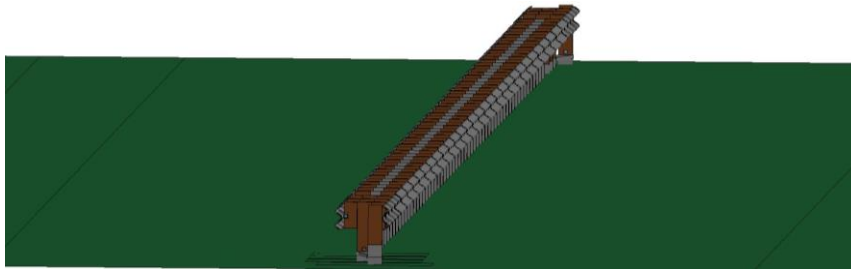


Fig. 1.5: FE model of a double-faced W-beam guardrail.

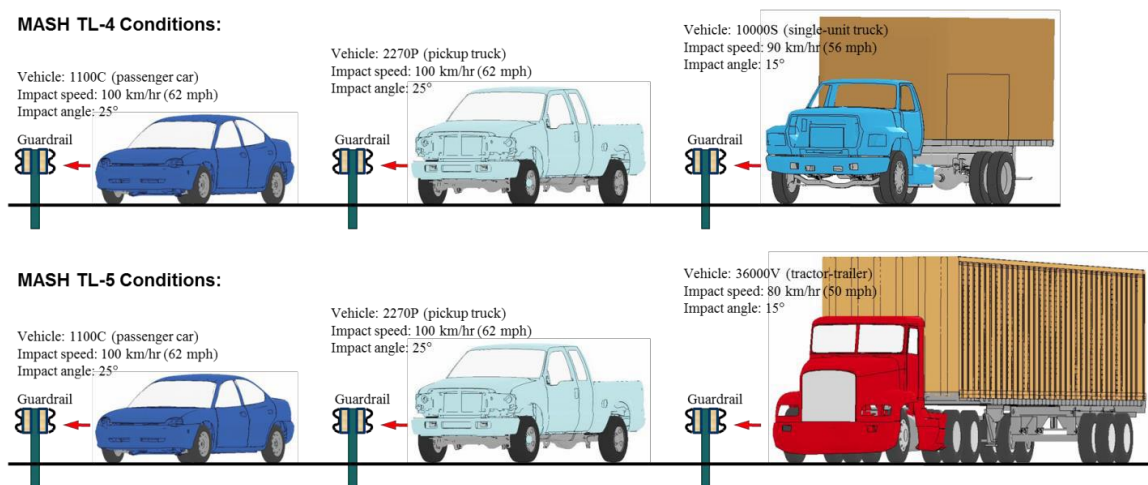


Fig. 1.6: Evaluation of a W-beam guardrail at MASH TL-4 and TL-5 conditions.

The vehicle's responses in terms of redirection, rollover, lateral displacements, and velocities were analyzed to determine the effectiveness of the 29-inch double-faced W-beam guardrails. In evaluating the vehicle's responses, the MASH evaluation criterion N was adopted, which utilizes the exit box criterion. Additionally, the MASH evaluation criterion F requires that vehicle remains upright and the maximum roll and pitch angles of the impacting vehicle do not exceed 75° . An exception to the MASH evaluation criterion F applies to heavy vehicles, in which MASH states: "although it is preferable all vehicles remain upright, this requirement is not applicable for tests involving the 10000S (i.e., single-unit truck) and 36000V (i.e., tractor-trailer) vehicles." This exception allows a 90° roll for heavy vehicle impacts and relies on the fact that the primary goal of the impact scenario is to demonstrate the guardrail's ability to contain and redirect the impacting vehicles. Figure 1.7 shows the definition of the three rotational responses (roll, pitch, and yaw) along with the corresponding translational responses (surge, sway, and heave). The time histories of the three response parameters, i.e., roll, pitch, and yaw angles, were recorded for the entire period of simulations. The maximum roll and pitch angles were extracted and compared with the MASH evaluation criterion F . In addition to the above-mentioned MASH evaluation criteria, the time histories of the vehicle's transverse displacements and velocities were also examined for performance evaluation. The effectiveness of the 29-inch W-beam guardrails was determined based on analysis of simulation results for both small and large vehicles.

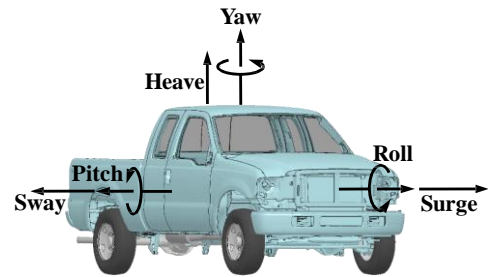


Fig. 1.7: Definition of vehicle responses.

Task 4: Performance Evaluation of Double-faced 31-inch W-beam Guardrails (TL-4 & TL-5)

In this task, the double-faced 31-inch W-beam guardrail was evaluated under MASH TL-4 and TL-5 impact conditions. The impact conditions and evaluation criteria were the same as those used for the 29-inch W-beam guardrail stated in Task 3.

Task 5: Performance Evaluation of Double-faced 29-inch Thrie-beam Guardrails (TL-4 & TL-5)

For each of the double-faced Thrie-beam guardrails, two designs were evaluated. In the first design, the guardrail was offset from the post with a wood blockout. In the second design, the guardrail was offset from the post with a steel blockout. Figure 1.8 shows the single segments of the two double-faced Thrie-beam guardrails with their respective wood and steel-blockouts. The performance of each design of the double-faced Thrie-beam guardrails was evaluated and compared to determine their effectiveness. The double-faced 29-inch Thrie-beam guardrails were evaluated in this task at MASH TL-4 and TL-5 impact conditions. The impact conditions and evaluation criteria are the same as those stated in Task 3. Figure 1.9 shows examples of the scenarios of the Ford F800 single-unit truck and the day cab tractor-trailer impacting the steel-blockout Thrie-beam guardrail that were simulated in this task.

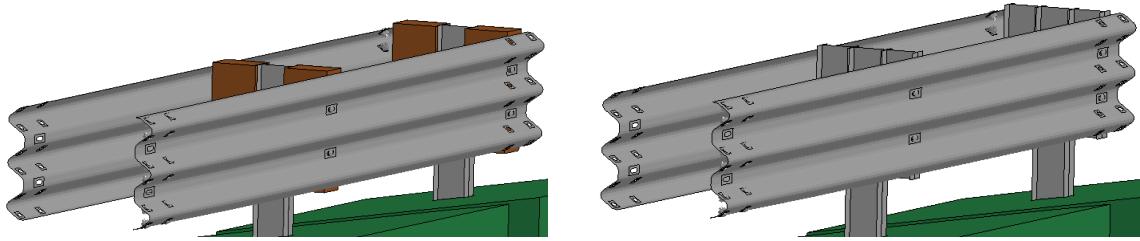


Fig. 1.8: Double-faced Thrie-beam guardrail segments with wood blockouts (left) and steel blockouts (right).

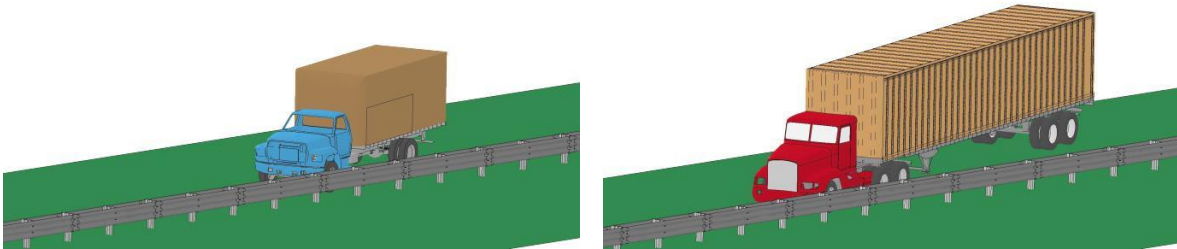


Fig. 1.9: A steel-blockout Thrie-beam guardrail impacted by a single-unit truck (left) and a tractor-trailer (right).

Task 6: Performance Evaluation of Double-faced 31-inch Thrie-beam Guardrails (TL-4 & TL-5)

The double-faced 31-inch wood- and steel-blockout Thrie-beam guardrails were evaluated in this task at MASH TL-4 and TL-5 impact conditions. The impact conditions and evaluation criteria are the same as those stated in Task 3.

Task 7: Final Report

This final report provides a comprehensive summary of research activities, findings, and outcomes for this project. It synthesizes literature review, FE modeling efforts, simulation results, and the performance evaluation of 29- and 31-inch double-faced W-beam and Thrie-beam guardrails on six-lane, 46-foot median divided freeways.

2. Literature Review

Highway median barriers have been developed and used on U.S. highways for decades to contain and redirect errant vehicles and prevent secondary impacts. These median barriers are sorted into three main categories: rigid (e.g., concrete barriers), semi-rigid (e.g., W-beam and Thrie-beam guardrails), and flexible systems (e.g., cable barriers). Presently, semi-rigid guardrails are the most commonly used barriers across the United States. This section will provide a comprehensive summary of studies related to W-beam and Thrie-beam guardrail systems. The topics cover performance evaluation (in-service and crash testing) and the application of FE modeling and simulations for highway safety research.

2.1 Performance Evaluation of Guardrails

In the 1960s, Jehu (1968) published a study where full-scale dynamic testing was conducted in the United States, Germany, Netherlands, and the United Kingdom. Within the United States, New York State pioneered the development of weak-post barrier systems through analytical models and full-scale vehicle crash tests. In 1965, the state's roadside and median barrier standards were changed to include only weak-post barriers. In the early 1970s, a study by Zweden and Bryden (1977) was conducted to evaluate the field performance of the older strong-post barriers and newly developed weak-post barriers based on New York State accident data collected between 1967 to 1970. A statistical analysis was conducted to compare the performance of the collected barrier systems based on accident data including occupant injury, vehicular responses, and post-impact maintenance. This study generated a number of significant conclusions on the performance of weak- and strong-post barriers. Although there was no significant difference in fatality rates between the two barrier systems, weak-post barriers exhibited a combined fatality/serious injury rate significantly lower than that for strong-post barriers. The resulting occupant injury appeared to be linked to barrier stiffness since both barrier systems had lower injury severity rates than other stiffer median barriers. With respect to barrier penetrations, the weak-post barriers demonstrated a lower penetration rate than the strong-post barriers, which might be due to the lack of consistency between early strong-post barrier designs. The study also indicated that barrier penetrations on weak-post systems were typically due to the low rail heights, and that barrier end terminals (i.e., the first and the last 50 feet of the barrier) had higher rates of penetration and serious injury than the midsections. The study also related barrier damage to their stiffness. It was found that stiffer barriers (e.g., strong-post barriers) had less damage or shorter damaged sections than weaker barriers (e.g., weak-post barriers). The study also determined that despite their longer damage lengths, weak-post barriers were on average less expensive to repair than strong-post barriers.

In 1981, Bryden and Hahn (1981) conducted a series of crash tests of vehicles impacting corrugated steel Thrie-beam guardrails to determine rail deflections, structural adequacy, vehicle decelerations, and vehicle damages. The results of these tests were used to determine the usability of a ten-gauge Thrie-beam guardrail for bridge rails and double-faced median barriers. Although the tests were not extensive, they were the earliest testing involving Thrie-beam guardrails on which impact limits were set from the conclusion of the crash tests.

In the early 1990s, the Traffic Engineering Branch of the North Carolina Department of Transportation (NCDOT) conducted a study of accidents on North Carolina's interstate

highways in which vehicles crossed the median and entered the opposing travel lanes (Lynch et al. 1993). The study analyzed accidents that occurred during the period from April 1, 1988 through October 31, 1991. The objectives of this study were to identify interstate locations with unusually high cross-median accidents, to determine possible safety improvements, to develop a priority listing of these locations with recommended improvements, and to develop a model for identifying potentially dangerous locations on North Carolina interstate highways. Data collected in the study showed that 105 fatalities resulted from 751 cross-median crashes took place in North Carolina. These crashes represented three percent of total crashes but 32% of total fatalities on interstate highways during the study period. One of the outcomes of this study was the recommendation to construct median barriers at 24 locations along the interstate highways in North Carolina.

Using data collected from Connecticut, Iowa, and North Carolina from 1997 to 1999, Ray and Weir (2001) conducted an in-service performance evaluation of four guardrail systems: the G1 cable guiderail, G2 weak-post W-beam guardrail, and the G4(1S) and G4(1W) strong-post W-beam guardrails. The study focused primarily on estimating the number of unreported collisions and the true distribution of occupant injuries. The collisions were measured in terms of collision characteristics, occupant injury, and barrier damage. Within the sample size limitations of the data collected in the study, no statistically significant difference was found between the performance of the guardrails in the three states, and there was no difference between the performance of G1 and G2 guardrails and between G1 and G4(1W) guardrails.

In the study conducted by Ross et al. (1993), uniform procedures were developed for evaluating the safety performance of candidate roadside hardware systems, including longitudinal barriers, crash cushions, breakaway supports, truck-mounted attenuators, and work zone traffic control devices. The report from this study, the National Cooperative Highway Research Program (NCHRP) Report 350, was adopted as the standard guideline for evaluating the safety performance of roadside safety devices until it was replaced by the new standard, Manual for Assessing Safety Hardware (MASH 2009). The evaluation of devices in NCHRP 350 was facilitated through three main criteria: structural adequacy, occupant risk, and post-impact vehicle trajectory. Structural adequacy referred to how well the device performed its intended task (i.e. a guardrail preventing a vehicle from striking a shielded object). The occupant risk criteria attempted to quantify the probability of severe occupant injury. The post-impact vehicle trajectory was adopted to ensure that the device would not cause subsequent harm (i.e. a vehicle being unsafely redirected back into traffic). The guidelines recognized the infinite number of roadside hardware installations and crash configurations. Therefore, standardized installation configurations and practical high-frequency impact scenarios were used to provide a basis for comparing the performance of similar devices. A matter of particular note was the multi-service level concept that provided six different test levels to allow for more or less stringent performance evaluation (ideally depending on the ultimate usage/placement of the hardware).

Although the NCHRP Report 350 specified six different test levels, the warrants for devices satisfying an individual test level was outside the scope of the document and was left to the judgment of the transportation agency implementing the hardware. Generally speaking, devices tested to the lower test levels, i.e., TL-1 and TL-2, were mostly used on roadways

with a smaller traffic volume and lower travel speeds, and devices tested to the higher levels, i.e., TL-3 to TL-6, were typically used on roadways with a larger volume and higher speeds.

In the NCHRP Project 22-14 (2001), “Improvement of the Procedures for the Safety Performance Evaluation of Roadside Features,” updates were incorporated to the NCHRP Report 350 based on assessments at TL-3 conditions, which was the basic level used for devices on the National Highway System. In the report published by Mak and Bligh (2002), the effects of higher impact speeds and additional impact angles were considered for TL-3 conditions. These additional parameters were considered due to the fact that a number of states had changed maximum speed limits on some of their highways to 75 mph (121 km/h) and not all crashes were occurring at an impact angle of 25° or less. These parameters often caused a concern on the stability of the test vehicle instead of containment capability. The study reported that increasing the impact speed to 68.4 mph (110 km/h) would have significant effects on many of the existing roadside safety devices. Although some barriers could accommodate higher impact speeds with minor modifications, some other barriers would require major changes and yet some barriers might never be able to accommodate higher impact speeds due to design constraints. Increasing the impact speed could result in a whole new generation of roadside safety hardware. In return, the higher impact speed would only account for an additional 2.8% of the crashes and increase the percentage of covered crashes (i.e., crashes with impact speeds equal to or less than the design test speed) from approximately 90% to 92.7%. The reduction of the impact angle from 25° to 20° created controversial arguments including the possibility for existing W-beam guardrail systems to have difficulty containing vehicles at higher impact speeds. It was emphasized that the selection of impact conditions was more of a policy decision than a technical issue to be resolved when updating the NCHRP Report 350 guidelines.

Donnell et al. (2002) reviewed the methods used to assess median safety on interstates and expressways in Pennsylvania, upon observations of cross-median collisions (CMCs) on highways where median barriers were not warranted by the Pennsylvania DOT design policy. A literature review and qualitatively assessment of median safety practices for various state DOTs were conducted and used to provide input for quantitative data collection. Negative binomial regression models were used to model CMC frequencies on earth-divided highways. The qualitative results from the study recommended that three-strand cable barriers, strong-post W-beam guardrails, or concrete barriers be used as median barriers warranted by site conditions. The quantitative results showed that CMCs were rare events and that nearly 15% involved fatalities. Additional findings concluded that CMC rates at earth-divided highways decreased as the median width was increased, that CMCs appeared more likely to occur downstream of interchange entrance ramps, and that CMCs were more likely to involve adverse pavement surface conditions (e.g., wet or icy) than other crashes.

In 2003, NCHRP Project 22-16, “Development of an Improved Roadside Barrier System,” was created to develop a cost-effective and nonproprietary roadside barrier system that would be capable of passing the NCHRP Report 350 requirements. The report summarized the research efforts and findings of five new or improved guardrail systems. Although the guardrails were not testing using full-scale crash tests due to the project not continuing to

Phase II, the models were recommended based on their performance improvements, overall cost, maintainability, and system versatility.

Ray et al. (2003) reviewed literature on in-service evaluations and identified previously found effective methods. The in-service performance of commonly used barriers and terminals was examined by collecting data in the following three areas: crash, maintenance, and inventory information. A procedure manual for planning and conducting in-service evaluations of roadside hardware was developed based on the methods used and the lessons learned in the evaluation study. The manual was subsequently used as a guide for an in-service evaluation project performed in Washington State by a different research team and modified based on their experiences and recommendations.

A median barrier guideline was developed for Texas to assist highway engineers in the evaluation of median barrier needs, with the intention of achieving the highest practical level of median safety (Miaou et al. 2005; Bligh et al. 2006). In this work, statistical crash models for various types of median-related crashes were developed based on an analysis of crash data in Texas. Using estimates from the frequency and severity models and the crash costs used by Texas Department of Transportation, an economic analysis of the median barrier need was performed. Guidelines for installing median barriers on divided, access-controlled freeways were developed as a function of average annual daily traffic and median width. A guidance to assist engineers evaluating median barriers needed on existing highway facilities was also developed based on the mean cross-median crash rate.

Under the guidelines of NCHRP Project 22-9, “Improved Methods for the Cost-Effectiveness Evaluation of Roadside Safety Features,” Mak and Sicking (2003) developed the Roadside Safety Analysis Program (RSAP). The main objective of Project 22-9 was to develop an improved cost effective analysis procedure for assessing roadside safety improvements. The RSAP incorporated two integrated programs: the Main Analysis Program containing the cost-effectiveness procedure and algorithms, and the User Interface Program providing a user-friendly environment for data input and review of results. The cost-effectiveness procedure incorporated in RSAP was based on the concept of incremental benefit/cost analysis. In 2009, NCHRP Project 22-27 (2012), “Roadside Safety Analysis Program (RSAP) Update,” was started to assist the American Association of State Highway and Transportation Officials (AASHTO) Technical Committee on Roadside Safety to develop the next edition of the AASHTO *Roadside Design Guide* (AASHTO 2011). The objectives of this project were to rewrite the software, update the manuals, improve user interface, and update the embedded default data tables of the RSAP.

In a project funded by the New Jersey DOT, Gabler et al. (2005) evaluated the post-impact performance of two median barrier systems: a three-strand cable median barrier system and a modified Thrie-beam median barrier system. In this project, FE modeling was adopted as a major means of the investigation. The project also included field investigation of crashes into the subject barriers and a survey of the median barrier experience of other state DOTs. This study concluded that the Thrie-beam median barrier was capable of containing and redirecting passenger vehicles, as well as a limited number of heavy vehicles. The Thrie-beam median

barrier also reduced the incidence of higher severity cross-median collisions but increased the number of less severe collisions.

In a subsequent study also funded by the New Jersey DOT, Gabler and Gabauer (2006) investigated the fatalities and injuries in accidents involving W-beam guardrails on New Jersey highways. It was found from the study that the guardrails generally performed well in vehicular crashes and only accounted for 1.5% of total highway fatalities. This study also showed that occupant injuries in guardrail crashes were not a major issue unless the vehicle had a rollover; three-fourths of all occupants exposed to guardrail crashes suffered no injuries. Some of the issues related to the guardrail performance were also identified. For example, the study showed that over half of all the fatal collisions with guardrails involved secondary events, i.e., either a second impact or a rollover. It was also found that 14% of all fatal crashes on guardrails resulted in a rollover and that light trucks had a significantly greater chance of vaulting and/or rollover than other vehicles when colliding with the guardrail.

Reid et al. (2007) developed a new guardrail system that could perform effectively for larger vehicles with a higher center of mass and a higher bumper height. The new rail, named Buffalo Rail, had deeper cross-section, thicker rail width, and a wider post spacing than the G4(1S) W-beam guardrail system. The tests were performed with a 1,500 lb (680 kg) pickup truck that passed the TL-3 requirements of NCHRP Report 350.

The NCHRP Project 22-21 (2011) focused on typical cross-section designs for a construction or reconstruction project rather than on the exact cross-section design at a particular point. The typical cross-section designs were determined early in the design process before adjustments were made to account for variations along the alignment (e.g., horizontal and vertical curves, interchanges and intersections, and special drainage requirements). Project 22-21 was started on January 2006 and was completed in April 2011. The final report of Project 22-21 contained guidance that practitioners can use to evaluate the safety implications of various median cross-section designs, including barrier type and placement guidelines (based on the NCHRP Project 22-22 (2010)), so that a cost-effective design could be achieved.

In 2009, the Manual for Assessing Safety Hardware (MASH) was published to supersede the previous roadside safety standard, NCHRP Report 350. MASH presented uniform guidelines for crash testing permanent and temporary highway safety features and recommends evaluation criteria to assess test results. MASH does not supersede any guidelines for the design of roadside safety hardware, which are contained within the AASHTO *Roadside Design Guide*. As of January 1, 2011, the Federal Highway Administration (FHWA) has required that all new product designs be tested using MASH test criteria for use on the National Highway System. A few of the significant changes from NCHRP Report 350 to MASH include:

- The weight of the small car test vehicle was increased from 1,800 lbs. (820C) to 2,420 lbs. (1100C)
- The impact angle of the small test vehicle was increased from 20° to 25°
- The weight of the pickup truck test vehicle was increased from 4,400 lbs. (2000P) to 5,000 lbs. (2270P)

- The mass of the single-unit truck in TL-4 was increased from 18,000 lbs. (8,000 kg) to 22,000 lbs. (10,000 kg) and the impact speed was increased from 50 mph (80 km/h) to 56 mph (90 km/h).

In a study conducted by Hu and Donnell (2010), they analyzed the severity of median barrier crashes using five years of data from rural divided highways in North Carolina. The criteria used for the analysis included median barrier type, the barrier's offset distance from the edge of the travel lane, roadway segment characteristics, roadway surface conditions, driver and vehicle characteristics, median barrier placement, and median cross-slope data. The major conclusion of this study was that less severe crash outcomes pertained to those on cable median barriers when compared to concrete barriers and W-beam guardrails. It was also observed that the barrier's offset distance from the travel lane was associated with a lower probability of severe crashes.

In 2010, Hampton et al. (2010) conducted crash tests and finite element analysis (FEA) on already damaged sections of the G4(1S) W-beam guardrails, which had not previously been conducted. The FEA work will be discussed in depth in the following section. Two crash tests were performed by the MGA Research Corporation for the NCHRP Project 22-23, "Criteria for Restoration of Longitudinal Barriers," to evaluate the performance of guardrails with prescribed rail and post deflections. The first crash test was conducted at 30 mph (48.3 km/h) with an impact angle of 25° and resulted in a 36 ft (10.97 m) damaged section of the guardrail with a maximum deflection of 1.21 ft (0.37 m). The second crash test was performed in the damaged location with undesirable results. The guardrail provided minimal resistance to the impacting vehicle as it vaulted over the guardrail. These results were due to a failed link present in the guardrail that separated the rail from the post. The study concluded that a deflection of 0.92 ft (0.279 m) or more on the post and rail would result in vehicle vaulting over the median barrier.

Gabauer et al. (2010) also conducted research on the performance of G4(1S) guardrails with minor damage already done to sections. They assessed five types of damage using the pendulum impact tests: vertical tear, horizontal tear, splice damage, twisted blockout, and missing blockout. W-beam ruptures were observed in tests with vertical tear damage due to the a stress concentration caused by the tear and thus were recommended for repair with high priority. There was no evidence of rail rupture near the location of a horizontal tear, but there was an observed splice failure in the higher speed tests. The recommendation for a horizontal tear was that tears less than 12 inches in length and 0.5 inches in width would not significantly affect the performance of the barrier and should be repaired with medium priority. The splice damage was simulated with one of the bolts having lost all bearing capacity and had a performance indistinguishable from the undamaged barrier. The recommended repair priority for missing bolt was medium for a single bolt and high for more than one bolt. A twisted blockout had little to no effect on the performance of the guardrail and was recommended to have a low repair priority. The performance of the guardrail with a missing blockout was marginal to unacceptable for the higher speed tests with a medium priority for repair. Further investigations with full-scale crashes would help evaluate the trajectory and stability of the impacting vehicle due to the limitations of the pendulum tests.

Ochoa and Ochoa (2011) completed a study to optimize guardrails for rural roadways in the United States, Europe, and some developing countries. In order to optimize a W-beam guardrail, the main methods for identifying failures had to be defined and considered. For the conventional strong-post W-beam guardrails, the relatively high release load varied by approximately 360% and was further compounded by another 40% due to variations in the yield strength of guardrail panels. A physics-based guardrail analysis was performed to determine the solution of optimizing the release load in relation to post section properties. This optimization was accomplished by introducing an improved fastening system that incorporated a separate, deformable release member to consistently provide a predefined release load of around 1,700 lb (7,565 N) with a maximum variation of 20%. The versatile W-beam guardrail incorporating these improvements was successfully crash tested and accepted by FHWA at NCHRP Report 350 and MASH TL-3 conditions.

In 2011, AASHTO published the new *Roadside Design Guide*, which presented a synthesis of current information and operating practices related to roadside safety. The guide was intended to be used as a resource document from which individual highway agencies could develop standards and policies. It was focused on safety treatments that could minimize the likelihood of serious injuries when a motorist leaves the roadway. The 2011 edition was updated to include hardware systems that had been tested to meet the evaluation criteria contained in NCHRP Report 350. It also included an outline of the most current evaluation criteria contained in MASH.

In 2012, Findley et al. (2012) conducted a statewide structural and safety investigation on the performance of weathered steel beam guardrails (WSBG) in North Carolina. This research was performed at the Institute of Transportation Research and Education at North Carolina State University. This study was prompted when New Hampshire found that the WSBG deteriorates at a much faster rate compared to the galvanized steel guardrail (GSG) in the northeast due to the harsher weather conditions. The study concluded that in all test sites across North Carolina, there were no structural concerns about using WSBG. Additionally, the research suggested a lower percentage of injury collisions associated with WSBG installations than the GSG installations at comparable sites. However, this study used a small sample size and further investigation was needed for a more robust comparison.

Alluri et al. (2012) evaluated the safety performance of the G4(1S) guardrail system installed on both limited and non-limited access facilities in Florida. The effectiveness of the guardrail was measured by the percentage of vehicles prevented from crossing the guardrail during a crash. From 2006 to 2010, there were a total of 7,290 crashes involving the G4(1S) guardrails on limited access facilities and 1,384 on non-limited access facilities. For the limited access facilities, 95.3% of the vehicles were prevented from crossing over the guardrail, which broke down into 97.5% for cars and 91.6% for light trucks (included vans and trucks with four rear tires). For guardrails installed at median and roadside locations, 95.5% of all vehicles were prevented from crossing over at median locations and 94.5% at roadside locations. Medium and heavy trucks were found to have a significantly lower crossover prevention percentage of 78%, due to the fact that the safety requirements of the guardrail system were not for these vehicle types. The severity of crossover crashes was found to be higher than that of non-crossover crashes, with over-rides being the most severe cases. Similar findings were

observed on the non-limited access facilities that had a higher percentage of preventing vehicular penetrations at median locations than at roadside locations.

Researchers at the Midwest Roadside Safety Facility (MwRSF) performed a study on the safety performance of the Midwest Guardrail System (MGS) with no blockout. This revised design could possibly be used at locations where the required 12-inch blockout would not work well and an alternative was required. They successfully crash tested the non-proprietary design of the MGS with a rail height of 31 inches using a passenger car and a pickup truck under MASH TL-3 conditions (Schrum et al. 2013). The results of this report suggested that the MGS with no blockout could be used on roadways where the width of the blockout was a limiting factor and the standard MGS with blockouts was recommended for other locations.

2.2 Finite Element Simulations of Vehicular Crashes

Mackerle (2003) provided a bibliography of 271 references published between 1998 and 2002 on crash simulations using FEA and on impact-induced injuries. This bibliography categorized the references into four different topic areas: 1) Crash and impact simulations where occupants were not included; 2) Impact-induced injuries; 3) Human surrogates; and 4) Injury protection. Topics in the first area included crashworthiness of aircrafts and helicopters, automobiles, and vehicle rail structures. The second area of research utilized two major types of models for humans, the crash dummy and real human body models. Research topics in this area were mainly on biomechanics and impact analyses for various human injuries. Topics on human surrogates focused on the development FE models of hybrid and other types of human dummies. These dummy models were used to obtain dynamic responses of the whole human body during impacts, which were difficult to measure experimentally. In the area of injury protection, FEA were utilized to simulate and analyze injury protection systems such as seat belts, air bags, and collapsible structures to reduce serious or fatal injuries. The references included in Mackerle's bibliography were generally useful to the work on FE crash simulations; however, only a few references under injury protection were related to roadside safety.

Most publicly available FE models of vehicles and roadside safety structures were initially developed at the FHWA National Crash Analysis Center (NCAC) at George Washington University. Since the 1990s, significant efforts have been put on the development of FE models for crash analysis. Most of these models are available as LS-DYNA input files from NCAC's website (NCAC web1). A list of references on these modeling efforts and the simulation work performed at NCAC is also available from NCAC's website (NCAC web2).

The modeling and simulation efforts from NCAC can be found in several representative works. Marzougui et al. (2000) developed the FE model of an F-shaped portable concrete barrier (PCB) and validated the model with full-scale crash test data. With the proven fidelity and accuracy of the modeling methodology, models for two modified PCB designs were created and used in FE simulations to evaluate their safety performance. A third design was then developed based on the simulation results. In the work by Zaouk et al. (2000a, 2000b), a detailed FE model of a 1996 Dodge Neon was developed. The three dimensional geometric data of each component was obtained by using a passive digitizing arm and then imported into a preprocessor for mesh generation, part connections, and material property assignments.

Tensile tests were conducted on specimens to obtain the material properties of the various sheet metal components. The body-in-white model was used in the simulation of a frontal impact and the results were compared with test data to evaluate the accuracy and validity of the model. Kan et al. (2001) developed an integrated FE model that included the vehicular structure, interior components, occupant (Hybrid III dummy), and airbag for crashworthiness evaluation. The integrated model was then used in a case study to demonstrate the potential benefit of the integrated simulation and analysis approach. This approach would further improve the engineering practice with cost savings, while also producing more accurate and consistent analysis results. Marzougui et al. (2004) developed a detailed suspension model and incorporated it into the previously developed FE model of a Chevrolet C2500 pickup truck (Zaouk et al. 1997). Pendulum tests were conducted at the FHWA Federal Outdoor Impact Laboratory (FOIL) and the test data were compared with simulation results of deformations, displacements, and accelerations at various locations. Crash simulations were performed using the upgraded vehicle model and the results were compared with crash data from previously conducted full-scale tests.

To facilitate the use of FE simulations to evaluate roadside safety structures at higher test levels specified by NCHRP Report 350, Mohan et al. (2007) improved and validated a previously developed model of a 1996 Ford F800 single-unit truck. This 18,000-lb (8,172-kg) truck was used as the standard TL-4 vehicle in NCHRP Report 350. Simulations were performed using the improved model and the results were compared with those from a full-scale crash test. The global kinematics and the acceleration time histories of the truck from simulations were found to correlate well with the test data. The research also suggested considering frictions between the tires and barrier and between the tires and ground to correlate with the vehicle's yaw angle.

In a study by Marzougui et al. (2007), the FE model of a W-beam guardrail was developed and validated using full-scale crash test data. The model was shown to give an accurate representation of the real system based on comparison of the vehicle's roll and yaw angles. Using the validated model, they performed four simulations of a passenger truck impacting the W-beam guardrails with different rail heights. The simulation results showed that the effectiveness of the barrier to redirect a vehicle could be compromised when the rail height was lower than the recommended value.

Researchers from the roadside safety group at Worcester Polytechnic Institute utilized FE models in a number of roadside safety studies. Ray (1996a) analyzed the data from full-scale crash tests and developed a criterion using statistical parameters to assess the repeatability of a full-scale crash test. The simulation results were also compared to crash test data. Ray (1996b) reviewed the history of using FEA in roadside safety research and presented the vehicle, occupant, and roadside hardware models that had been developed to date. Ray and Patzner (1997) developed a nonlinear FE model of a modified eccentric loader terminal (MELT) that was common for W-beam guardrails and used it in simulating a full-scale crash test involving a small passenger car. Based on a comparison of simulation results with crash test data, the FE model was recommended to be used in the evaluation of new design alternatives. In the work of Patzner et al. (1999), the effects of post and soil strengths on the overall performance of the MELT terminal system using a nonlinear FE model was examined.

A matrix of twelve simulations of particular full-scale crash test scenarios was used to establish the combinations of post and soil strengths from which favorable situation(s) could be identified. This parametric study showed that certain combinations of soil and post strengths could increase the hazardous possibilities of tire snagging, pocketing, or rail penetration, while other combinations produced results that are more favorable.

In the work of Plaxico et al. (2000), they compared the impact performance of two strong-post W-beam guardrails, the G4(2W) and G4(1W). After validating the FE model for the G4(2W) guardrail with data from a full-scale crash test, the FE model of the G4(1W) guardrail was developed. The two guardrails were compared with respect to deflection, vehicle redirection, and occupant risk factors. The two systems were found to perform similarly in collisions and satisfied the requirements of the NCHRP Report 350 at Test Level 3-11 conditions. Using LS-DYNA simulations and laboratory experiments, Plaxico et al. (2003) investigated the failure mechanism of the bolted connection of a W-beam rail to a guardrail post, which could have a significant effect on the performance of a guardrail system. A computationally efficient and accurate FE model of the rail-to-post connection was developed for use in the performance evaluation of guardrail systems using LS-DYNA. Using LS-DYNA simulations, Atahan (2002) analyzed a strong-post W-beam guardrail system that failed in a previously conducted full-scale crash test. After identifying the cause of failure and incorporating necessary improvements, a new W-beam guardrail was developed with improved performance based on simulation results. Orengo et al. (2003) presented a method to model tire deflation in LS-DYNA simulations along with examples of using this improved model. The simulation results showed that deflated tires had significantly different behaviors from those of inflated tires as observed in real world crashes and in full-scale crash tests. A vehicle's kinematics were found to be strongly coupled to the behaviors of deflated tires. Therefore, modeling such behaviors was deemed critical to roadside hardware simulations. In a separate study by Ray et al. (2004), LS-DYNA simulations were used to determine if an extruded aluminum bridge rail would pass the full-scale crash tests for TL-3 and TL-4 conditions of NCHRP Report 350. The simulation results, which were supported by a subsequent AASHTO load and resistance factor design (LRFD) analysis, indicated a high likelihood of passing the crash tests.

FE simulations have also been used by researchers at the Midwest Roadside Safety Facility (MwRSF). Reid (1996) utilized FEA to study the influence of material properties on automobile crash structures and attempted to develop crashworthiness guidelines for design engineers. In one of his later works, Reid (1998) demonstrated with two simple examples, contact definition and damping, how potential modeling issues could easily be overlooked in FE impact simulations. Reid also suggested ways to check for modeling errors and methods to make improvements. In a collaborative work to improve the FE model of a Chevrolet C2500 pickup truck (Reid and Marzougui 2002; Tiso et al. 2002), structural modeling methods were introduced for model improvement through refining meshes, using more sophisticated material models, adding details to simplified components, and improving connections between components. Suspension modeling, which was critical to the correct vehicle dynamic responses, was also investigated in this collaborative work and a new model was successfully developed with significant improvements.

To educate roadside safety engineers and promote the use of simulations, Reid (2004) summarized ten years of the simulation efforts on the development of new roadside safety accessories performed at the MwRSF. In the work of Reid and Hiser (2004), they studied the friction effects between solid elements and for component connections, as well as their interactions in crash modeling and analysis. In their work on modeling bolted connections that allowed for slippage, Reid and Hiser (2005) investigated two modeling techniques that were based on discrete-spring clamping and stressed clamping using deformable elements. The simulation results for both models compared well with test data, with the stressed clamping model using deformable elements having good accuracy accompanied with a significantly increased computational cost. Hiser and Reid (2005) also investigated improved FE modeling methods for slip base structures, which could have a considerable potential for reducing the amount of crash resistance and thus occupant injury. They developed and evaluated two bolt-preloading methods, with one using discrete spring elements and the other using pre-stressed solid elements. Similar to their findings in the work of modeling hook-bolts, they found that the method using solid elements was more accurate than that using discrete spring elements when the impact conditions became more severe. The results showed that the slip base model was acceptable in both end-on and length of need impact simulations.

FE simulations were also found in the work of other researchers in roadside safety research. Whitworth et al. (2004) evaluated the crashworthiness of a modified W-beam guardrail using detailed FE models of a guardrail and a Chevrolet C2500 pickup truck. The simulation results were compared and found to be in agreement with crash test data in terms of roll and yaw angles. Simulations were also performed to evaluate the effects of rail mounting height and routed/non-routed blockouts on the safety performance of the system. In the work of Bligh et al. (2004), FEA was utilized to develop new roadside features to address three roadside safety issues. An alternative design to the popular T6 tubular W-beam bridge rail was developed to address problems with vehicle instability observed in full-scale crash testing. A retrofit connection to Texas DOT's grid-slot portable concrete barrier was developed to limit dynamic barrier deflections to levels that were more practical for work zone deployments.

One of the important parameters in evaluating the performance of barrier systems is the vehicular impact height, which varies depending on the trajectory of the vehicle along the median and the lateral offset of the barrier. Using LS-DYNA simulations, Ferdous et al. (2011) evaluated the performances of the modified G4(1S) W-beam guardrail, modified Thrie-beam guardrail, Midwest Guardrail System, and modified weak post W-beam guardrail. Each model was validated based on the results of existing crash tests. Using vehicle models meeting the requirements of NCHRP Report 350, the override and under-ride limits for each guardrail were identified. The performance limit of each barrier was determined by parametrically varying the vehicle impact height to determine the heights at which override or rollover for the pickup truck and under-ride for the small passenger car would occur.

In 2012, Marzougui et al. (2012) investigated some barrier systems, which passed the requirements of NCHRP Report 350 but failed to pass the MASH requirements, to determine if the barrier systems could be retrofitted with various modifications to improve the performance. The modifications were conducted on six G9 Thrie-beam guardrails and three G4(1S) W-beam guardrails using FE simulations. The simulation results showed that with the

proposed modifications, the guardrails that originally failed to pass the MASH requirements were able to retain the vehicle under MASH TL-3 conditions and reduce the propensity to vault over the guardrails.

Hampton et al. (2013) performed a similar simulation in an effort of evaluating the performance of strong-post W-beam guardrails with missing posts under impact conditions specified by NCHRP Report 350. The effects of missing posts on the guardrail's performance were quantitatively evaluated using FE models of crash tests under impacts of a 4,409-lb (2,000-kg) pickup truck. Simulations where one, two, or three posts were removed from the guardrails were conducted with varying points of impact to evaluate the effects of missing posts. The FE simulation results demonstrated that guardrails with even one missing post could have a remarkably decreased performance under vehicular impacts due to tire snagging. It was also observed that both the maximum deflection and maximum rail tension were greatly increased as more posts were removed from the guardrail. The overall conclusions of the study were that the guardrail performance could be significantly reduced even with one missing post and that post replacement should be a high-priority repair for guardrail maintenance.

In the work of Mongiardini and Reid (2013), they investigated relevant phenomena in simulation models that would help create a more accurate representation of the kinematics and dynamics of an actual full-scale crash test. Modifications to the steering system, tire size, and bumper failure mechanism were analyzed. A properly working steering system was found to have an insignificant role because the vehicle was redirected by the barrier system, and the tires were forced to slide over the ground. Although the bumper usually plays a relatively minimal role in a full-scale crash test, the definition of a failure mechanism for the front bumper was found to be crucial for simulating the vehicle kinematics. Without this failure mechanism, the bumper would restrict the tire from steering properly when the tire contacted the barrier post. This caused the tire to roll over the second post during impact, thus limiting the proper redirection of the vehicle. Similarly, the correct modeling of tire size was essential for simulating the interaction between the tire and posts.

FE simulations, particularly conducted with LS-DYNA, have been used increasingly more in roadside safety research. In addition to the abovementioned references, FHWA published several manuals on using LS-DYNA material models and evaluation of these models (Hallquist 2017; Lewis 2004; LSTC 2016; Murray et al. 2005; Murray 2007; Reid et al. 2004). These references can also be useful in the crash modeling work using LS-DYNA.

3. Finite Element Modeling of Vehicles and Guardrails

The simulation work of this study involved FE models of four vehicles (i.e., a 1996 Dodge Neon, a 2006 Ford F250, a 1996 F800 single-unit truck, and a 1991 GMC day cab tractor-trailer) and three NCDOT guardrails each with 29- and 31-inch placement heights. The three guardrails were: 1) double-faced wood-blockout W-beam guardrail; 2) double-faced wood-blockout Thrie-beam guardrail; and 3) double-faced steel-blockout Thrie-beam guardrail. All crash simulations were conducted at MASH TL-4 and TL-5 conditions. At TL-4 conditions, the guardrails were impacted by a 1996 Dodge Neon and a 2006 Ford F250 at 62 mph (100 km/h) and an impact angle of 25°, and by a 1996 Ford F800 single-unit truck at 56 mph (90 km/h) and an impact angle of 15°. At TL-5 conditions, the guardrails were impacted by a 1996 Dodge Neon and a 2006 Ford F250 at 62 mph (100 km/h) and an impact angle of 25°, and by a 1991 GMC day-cab tractor-trailer at 50 mph (80 km/h) and an impact angle of 15°. In all simulation cases, the vehicle departed the travel lane at the prescribed speed and angle before impacting the guardrail. The impact speed was defined in the vehicle's travel direction, and the impact angle was defined as the angle between the vehicle's travel direction and the guardrail's longitudinal direction.

3.1 FE Models of Four Vehicles

Figure 3.1 shows the FE models of the four vehicles used in this project, a 1996 Dodge Neon passenger car (MASH 1100C), a 2006 Ford F250 pickup truck (MASH 2270P), a 1996 Ford F800 single-unit truck (MASH 10000S), and a 1991 GMC day-cab tractor-trailer (MASH 36000V). Table 3.1 gives the specifications of the four vehicles relevant to this study.

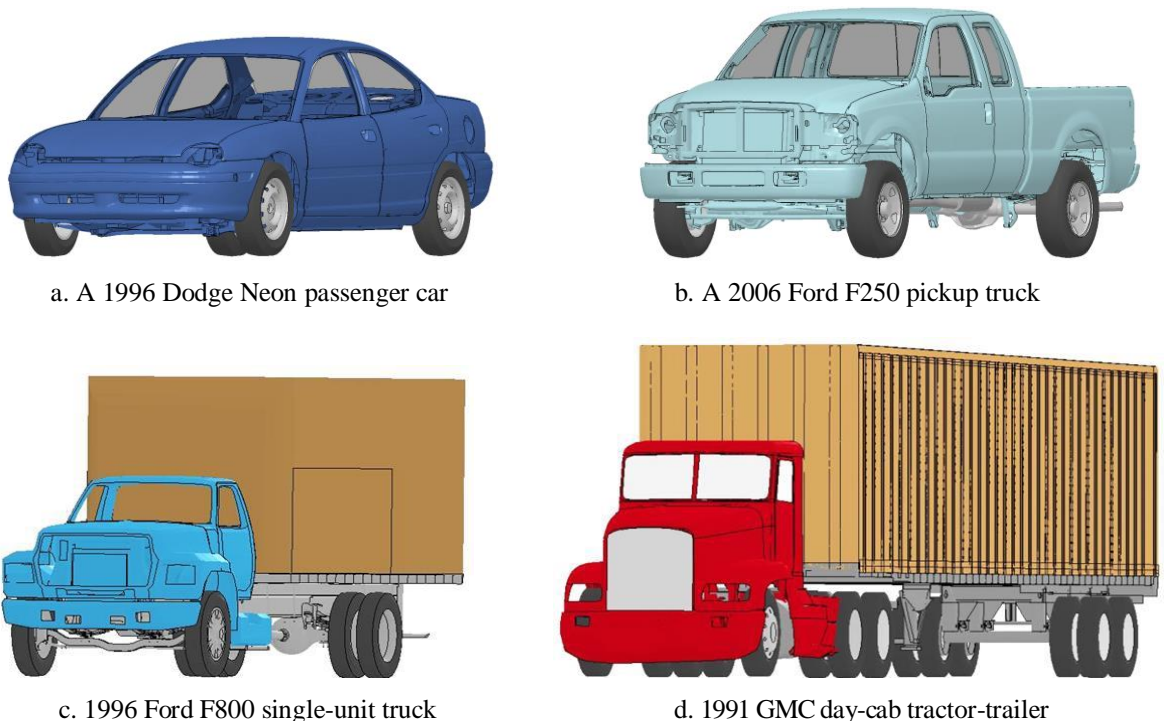


Fig. 3.1: FE models of the four vehicles used in crash simulations.

Table 3.1: Specifications of the four test vehicles used in crash simulations

Specification	Test Vehicle			
	1996 Dodge Neon	2006 Ford F250	1996 Ford F800	1991 Tractor-trailer
Curb weight*	2,414 lb (1,095 kg)	5,689 lb (2,580 kg)	16217 lb (7,456 kg)	79,718 lb (36,159 kg)
Overall length	171.8 in (4.36 m)	226.4 in (5.75 m)	337.5 in (8.57 m)	697 in (17.7 m)
Overall width	67.5 in (1.71 m)	79.9 in (2.03 m)	96.2 in (2.44 m)	245.3 in (6.23 m)
Overall height	52.8 in (1.34 m)	76.5 in (1.94 m)	131.5 in (3.34 m)	158.4 in (4.02 m)
C.G. height**	20.2 in (0.51 m)	28.5 in (0.72 m)	51.66 in (1.31 m)	64.44 in (1.64 m)
Ground clearance	5.7 in (145 mm)	8.7 in (222 mm)	10.1 in (257.4 mm)	8.8 in (223.5 mm)

* The curb weight is the weight of the vehicle with all standard equipment and amenities, but without any passengers, cargo, or any other separately loaded items.

** C.G. = Center of Gravity

The FE model of the 1996 Dodge Neon had a total of 339 parts that were discretized into 283,683 nodes and 270,727 elements (2,852 solid, 92 beam, 267,775 shell, and 8 discrete elements). Ten different constitutive models were used, including the piecewise linear plasticity model defined for most steel components, the rigid model for mounting hardware, the elastic model for the tires and other rubber components, the Blatz-Ko rubber model for nearly incompressible rubber cushions, the viscous damping model for the shock absorbers, the low-density foam model for the radiator core, the spot-weld model for sheet metal connections, the null material model defined for contact purposes, the linear elastic spring model for the spring-damper connection of the front suspension, and the crushable foam model for the bumper energy absorber. Hourglass control was used on components that could potentially experience large deformations. The FE model of the Dodge Neon was originally developed at NCAC and validated with the NHTSA’s New Car Assessment Program (NCAP) Frontal-Impact Test 2320. (NCAC, 2007a)

The FE model of the 2006 Ford F250 was composed of a total of 746 parts that were discretized into 737,986 nodes and 735,895 elements (25,905 solid, 2,305 beam, 707,656 shell, and 29 discrete elements). Eleven different constitutive models were used, including the piecewise linear plasticity model defined for most steel components, the rigid model for mounting hardware, the elastic model for the tires and other rubber components, the linear and nonlinear elastic spring model for the suspension springs, the viscous damping model for the shock absorbers, the low-density foam model for the radiator core, the spot-weld model for sheet metal connections, the viscoelastic model for radiator support mounts, the Blatz-Ko rubber model for nearly incompressible rubber cushions, and the null material model for contact purposes. Hourglass control was used on various components that could potentially experience large deformations. The FE model of the Ford F250 was originally developed at NCAC and validated with the NHTSA’s New Car Assessment Program (NCAP) Frontal-Impact Test 5820. (NCAC, 2008)

The FE model of the 2006 Ford F800 single-unit truck was composed of a total of 138 parts that were discretized into 172,793 nodes and 166,925 elements (886 solid, 548 beam, 165,386 shell, and 58 discrete elements). Seven different constitutive models were used, including the

piecewise linear plasticity model defined for most steel components, the rigid model for mounting hardware, the elastic model for the tires and other rubber components, the nonlinear elastic spring model for the suspension springs, the nonlinear viscous damping model for the shock absorbers, and the null material model for contact purposes. Hourglass control was used on various components that could potentially experience large deformations. The FE model of the Ford F800 was originally developed at NCAC and further improved at the National Transportation Research Center Inc. (NTRCI) and Oak Ridge National Laboratory (ORNL) and validated against the Texas Transportation Institute (TTI) Test 471470-17 (Mak and Menges 1998).

The FE model of the tractor-trailer consisted of a 1991 GMC WG65T day-cab tractor, 1990 Stoughton 48-ft box trailer, and a 50,000 lb (22,677 kg) ballast trailer load. The complete tractor-trailer model had a total of 495 parts that were discretized into 527,418 nodes and 466,578 elements (78,089 solid, 851 beam, 387,440 shell, and 27 discrete elements). Twelve different constitutive models were used, including the piecewise linear plasticity model defined for most steel components, the rigid model for mounting hardware, the elastic model for the tires, trailer walls, and other rubber components, the nonlinear elastic spring model and Maxwell spring model for the tractor and trailer air-ride suspension, the linear and nonlinear viscous damping model for the shock absorbers, the spot-weld model for sheet metal connections, the viscoelastic model for radiator support mounts, simplified Johnson-Cook model for trailer walls and roof, the simplified rubber with damage model for nearly incompressible rubber cushions, and the null material model for contact purposes. Hourglass control was used on various components that could potentially experience large deformations. The FE model of the tractor was originally developed as a 1992 Freightliner FLD120 sleeper-cab tractor at NCAC and validated at Federal Outdoor Impact Laboratory (FOIL) using Test No. 03008 (Marzougui 2003; Plaxico et al. 2008). The sleeper-cab tractor was adapted to a day-cab tractor modeled after a 1991 GMC WG65T day-cab tractor at NTRCI (Plaxico et al. 2009). The trailer FE model was created from scratch at NTRCI using a purchased 1990 Stoughton box trailer to model component dimensions and used in coupon tests to accurately define material properties (Plaxico et al. 2009). The ballast load in the trailer was modeled after the payload configuration in the full-scale test the complete tractor-trailer model was used for validation (Plaxico et al. 2010). The full-scale test used for validation was the Midwest Roadside Safety Facility Crash Test TL5CMB-2 (Rosenbaugh et al. 2007).

Simulations of the vehicles crashing into roadside barriers imposed significant challenges to the numerical models due to the large, nonlinear deformations and the large numbers of components contacting each other. For example, in the simulations of the tractor-trailer crashing into the W-beam guardrail, the W-beam rails and posts experienced severe deformations when redirecting the tractor-trailer. The vehicle's wheel, fender, bumper cover, front suspension, and a number of other parts on the tractor and trailer were in contact with the guardrail post, rail, and blockout. These contacts needed to be handled by selecting the appropriate contact algorithms to eliminate the unrealistic penetrations of interfering elements. Otherwise, the simulations would encounter great numerical difficulties and result in unrealistic behaviors of the vehicle and/or guardrail (e.g., the vehicle being entangled with the guardrail components). The FE model of the Dodge Neon experienced a similar issue with elements on the bumper cover penetrating the guardrail and becoming entangled due to a

contact definition that was used in the original model but inappropriate for the applications in this study. The contact definition between the vehicle's bumper and the guardrail was changed to resolve the outstanding contact issues. Before running simulations for this project, simulations were conducted using the four vehicle models to ensure appropriate contacts being defined for all parts in the vehicles, W-beam, and Thrie-beam guardrails.

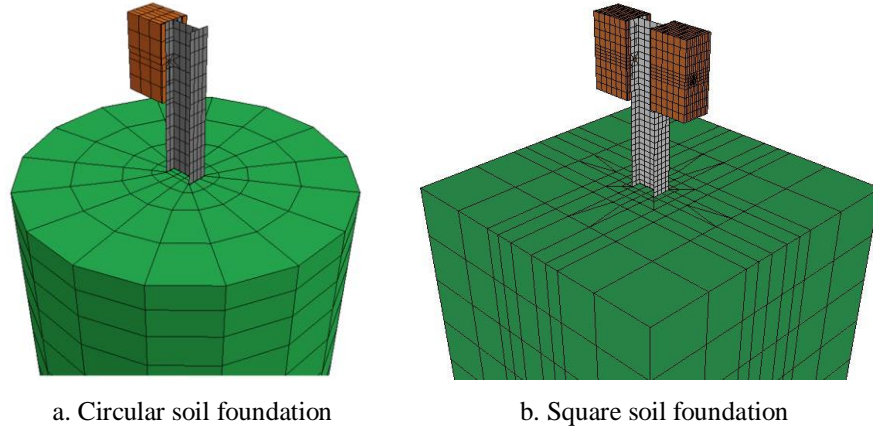
3.2 FE Models of the Guardrails

The FE models of the guardrails used in this study included strong-post double-faced wood-blockout W-beam, wood-blockout Thrie-beam, steel-blockout Thrie-beam guardrails. The FE model of the single-faced G4(1S) strong-post W-beam guardrail was originally developed at NCAC and validated using NCHRP Report 350's TL-3 conditions in full-scale crash tests at Texas A&M Transportation Institute (NCAC, 2007b). The strong-post double-faced wood-blockout W-beam guardrail was created and validated in a previous NCDOT research project (Fang et. al., 2015). The two variations of the strong-post double-faced Thrie-beam guardrails were created in accordance with the most current NCDOT Roadway Standard Drawings (NCDOT 2012) and AASHTO's Roadside Design Guide (AASHTO 2011).

The FE model of the double-faced W-beam guardrail contained six different constitutive models: the piecewise linear plasticity model for most steel components, the elastic model for the wood blockouts and terminal posts, the soil and foam model for the soils around posts, the rigid model for the bolts, nuts and road surface, the nonlinear elastic spring model for the bolt-tensioning spring in the long-bolts (used to attach the rails and wood blockouts to the posts), and the null material model used for contact purposes. The FE model of the double-faced wood-blockout Thrie-beam guardrail contained the same six constitutive models as the W-beam guardrail. The steel-blockout Thrie-beam guardrail contained five of the six constitutive models of the other guardrails, omitting the elastic model used for the wood blockouts.

In the original NCAC W-beam model, the soil around each post was a cylindrical block suitable for flat-terrain conditions. In this study, the guardrail model including the soil foundations was obtained from a previous NCDOT research project (Fang et al., 2010, 2013) in which an FE model of a square soil foundation was developed. The square soil model used the same material model and properties as the original NCAC soil model, and was compared and found identical to the circular soil model using simulations of a vehicular crash test. Figure 3.2 shows the original NCAC soil model and the square-shaped soil model used for this study.

The FE models of Thrie-beam guardrails for this study were created according to the NCDOT Roadway Standard Drawings and AASHTO's Roadside Design Guide. The Thrie-beam guardrails utilized the soil and post components from the W-beam guardrail model. The Thrie-beam rail was obtained from NCAC's model of a W-beam-to-Thrie-beam transition barrier used to transition from a semi-rigid W-beam guardrail to a rigid concrete barrier. This model was verified to be consistent with the TTI test 404211-4 and FE model from Atahan & Cansiz's study in 2005 (Buth et. al. 1998; Atahan and Cansiz 2005). Two blockouts for the Thrie-beam guardrails were selected, a steel-blockout and a wood-blockout. Figure 3.3 illustrates the wood and steel blockouts used on the Thrie-beam guardrails.



a. Circular soil foundation

b. Square soil foundation

Fig. 3.2: FE models of the soil foundation around a post.

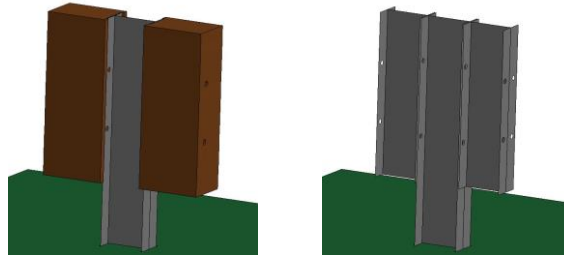


Fig. 3.3: FE models of a wood blockout (left) and steel blockout (right) on the Thrie-beam guardrails.

In this study, the bolt and nut connections on the W-bam and Thrie-beam guardrails incorporated a failure mechanism that could separate the bolt and nut upon reaching the failure point (defined by a threshold value of the force). Due to the increased impact energy from the larger vehicles used in this study, i.e., MASH TL-4 and TL-5 impact conditions, the failure mechanism was modeled in the bolt connections using the individual components to realistically emulate the bolt-nut connection behavior in an impact. Figure 3.4 illustrates the bolt connections of the W-beam guardrail. This modification along with resolutions to other contact issues (e.g., initial penetrations due to mismatched geometries) were found to significantly improve the FE model's accuracy, stability, and efficiency.

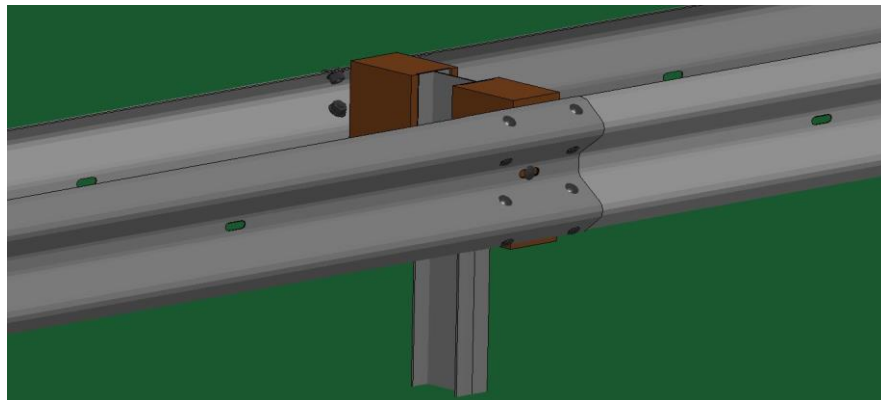


Fig. 3.4: FE model of the bolt connections on the W-beam guardrails.

Figure 3.5 shows profile views of the FE models of the double-faced W-beam, wood-blockout Thrie-beam, and steel-blockout Thrie-beam guardrails at a 29-inch installation height. Each of the three guardrail models has a corresponding 31-inch guardrail model.

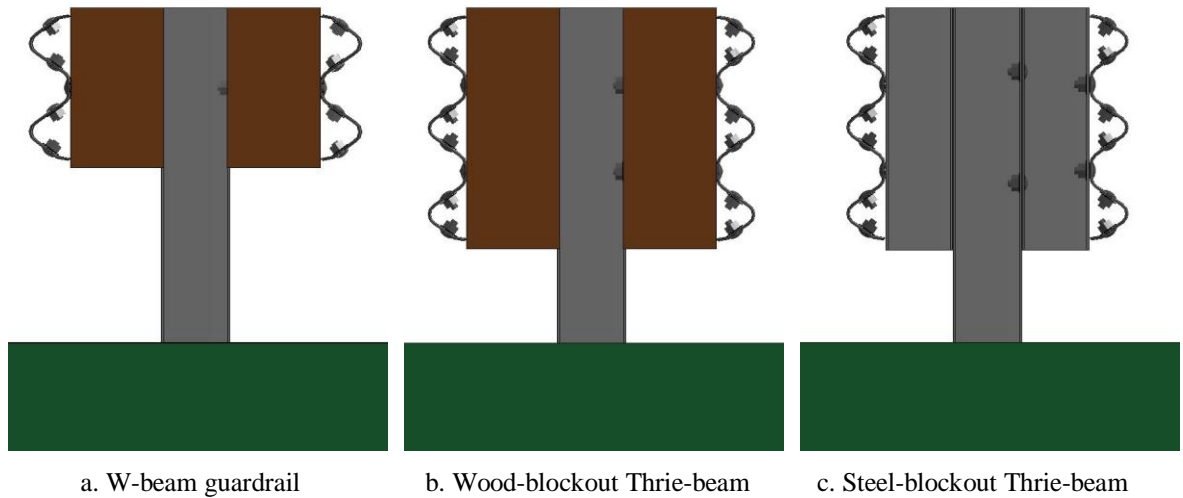


Fig. 3.5: Profile views of the 29-inch double-faced guardrail FE models.

The FE model of a single guardrail segment was duplicated to create the entire 400-ft (122-m) section of the guardrails required for this study. The duplication of the guardrail sections were completed with an in-house code developed to replicate not only the parts, nodes, elements, and material properties, but also the contact definitions defined among the parts in each segment as well as between adjacent guardrail segments. The FE models of the end terminals were then attached to the guardrail segments to create a full guardrail model. Figures 3.6 and 3.7 illustrate the full FE models of the 29- and 31-inch double-faced W-beam guardrails, respectively, placed on a flat surface. Figures 3.8 and 3.9 illustrate the full FE models of the 29- and 31-inch double-faced wood-blockout Thrie-beam guardrails, respectively. Figures 3.10 and 3.11 illustrate the full FE models of the 29- and 31-inch double-faced steel-blockout Thrie-beam guardrails, respectively.

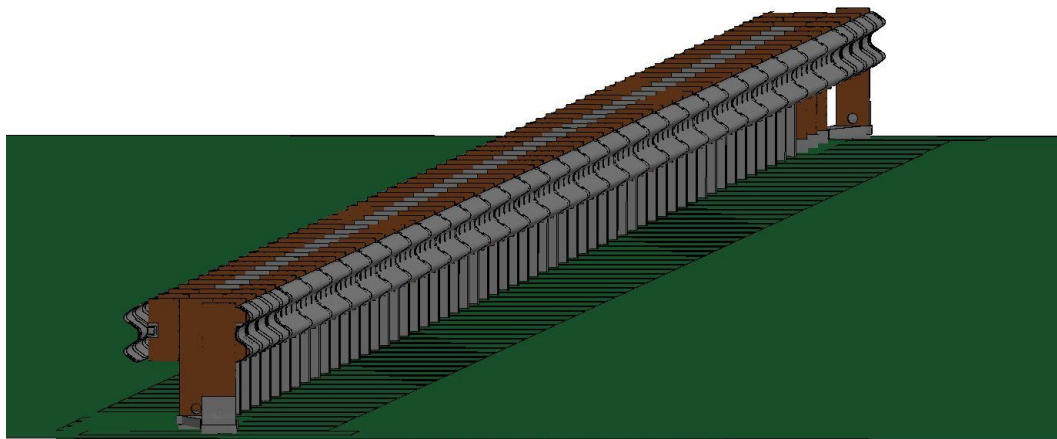


Fig. 3.6: Full FE model of the double-faced 29-inch W-beam guardrail.

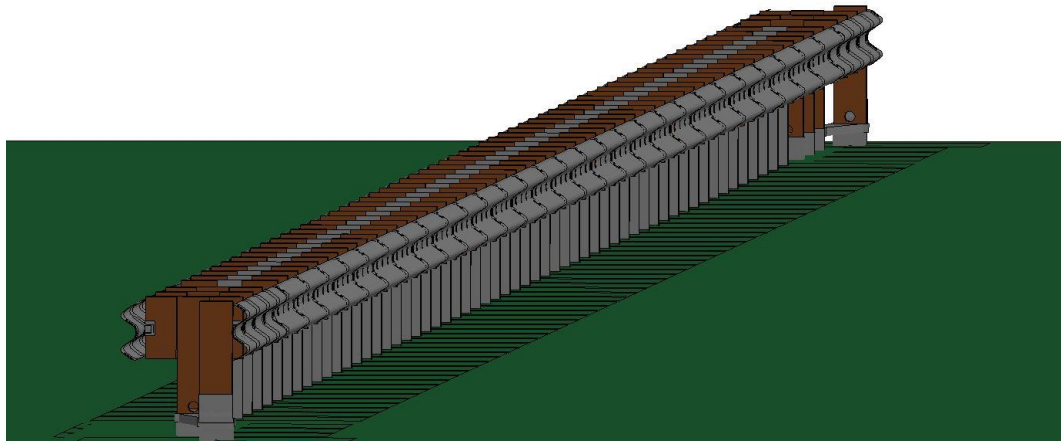


Fig. 3.7: Full FE model of the double-faced 31-inch W-beam guardrail.

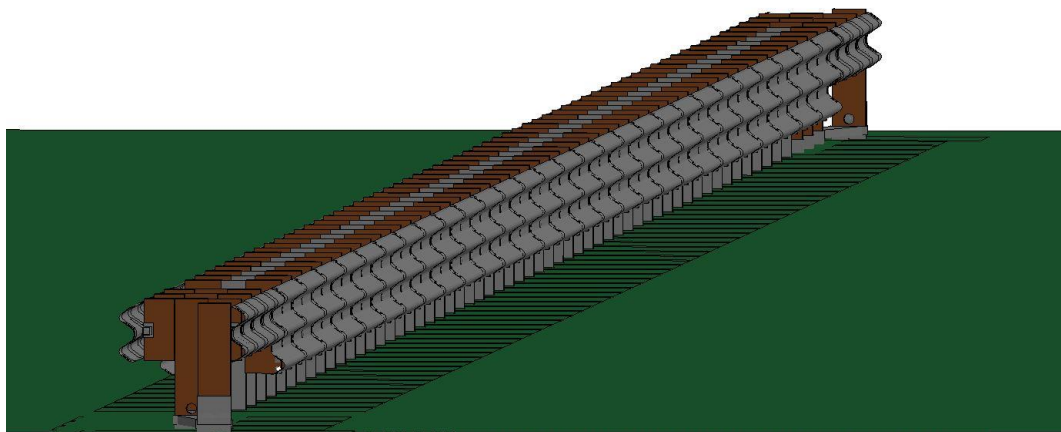


Fig. 3.8: Full FE model of the double-faced 29-inch wood-blockout Thrie-beam guardrail.

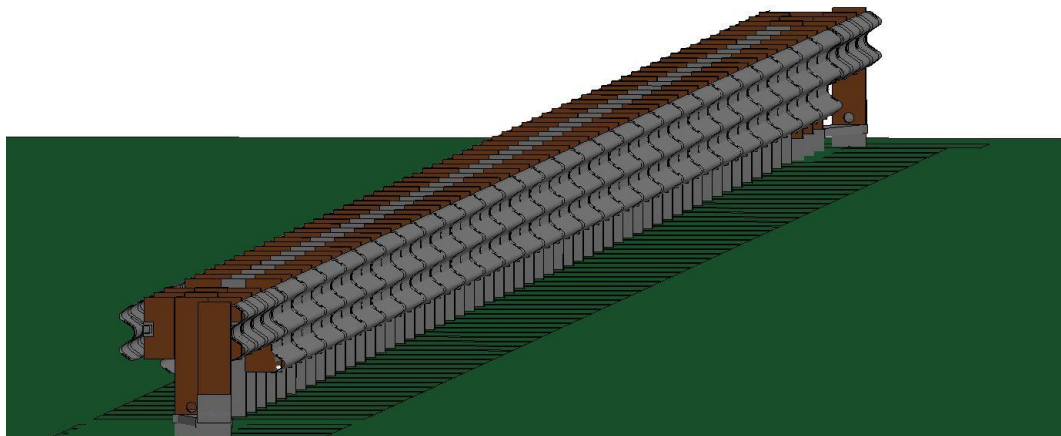


Fig. 3.9: Full FE model of the double-faced 31-inch wood-blockout Thrie-beam guardrail.

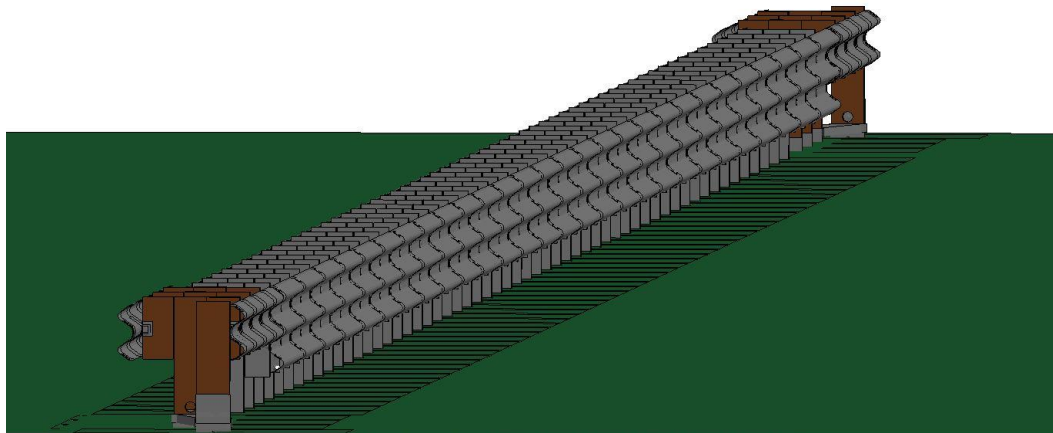


Fig. 3.10: Full FE model of the double-faced 29-inch steel-blockout Thrie-beam guardrail.

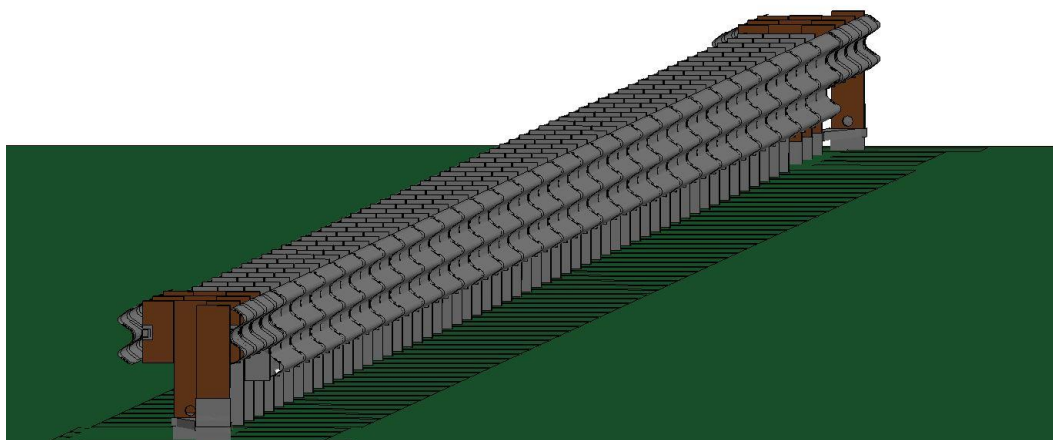


Fig. 3.11: Full FE model of the double-faced 31-inch steel-blockout Thrie-beam guardrail.

3.3 Simulation Setup

The three guardrail models, each with two barrier heights (i.e., 29 and 31 inches), were combined with the four vehicle models to conduct the simulation work of this study. These simulations were divided into four major categories based on the guardrail type and installation heights:

- Case 1: Double-faced 29-inch W-beam Guardrail evaluated at MASH TL-4 and TL-5 conditions.
- Case 2: Double-faced 31-inch W-beam Guardrail evaluated at MASH TL-4 and TL-5 conditions.
- Case 3: Double-faced 29-inch Thrie-beam Guardrails with wood and steel blockouts and evaluated at MASH TL-4 and TL-5 conditions.
- Case 4: Double-faced 31-inch Thrie-beam Guardrail with wood and steel blockouts and evaluated at MASH TL-4 and TL-5 conditions.

Figure 3.12 shows full simulation models for each of the four vehicle impacts against the double-faced 29-inch W-beam guardrail in Case 1. Figure 3.13 show the full simulation models for each of the four vehicle impacts against the double-faced 31-inch W-beam guardrail in Case 2. Figures 3.14 and 3.15 show the full simulation models of the double-faced 29-inch

wood- and steel-blockout Thrie-beam guardrails, respectively, impacted by the four test vehicles in Case 3. Lastly, Figures 3.16 and 3.17 show the simulation models of the double-faced 31-inch wood- and steel-blockout Thrie-beam guardrails, respectively, impacted by the four test vehicles in Case 4.

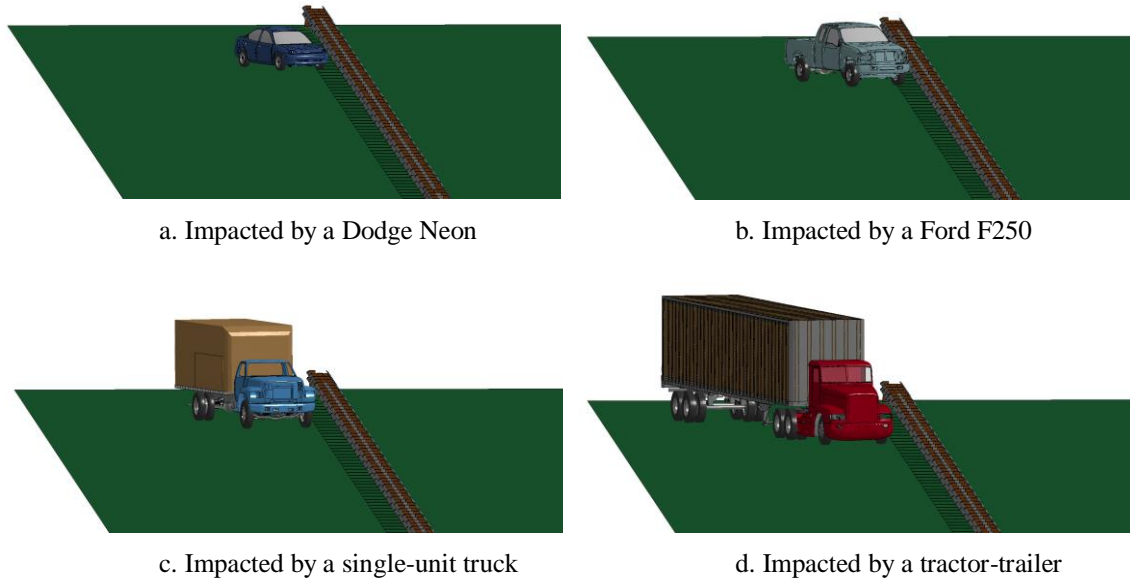


Fig. 3.12: FE models of the double-faced 29-inch W-beam guardrail under vehicular impacts.

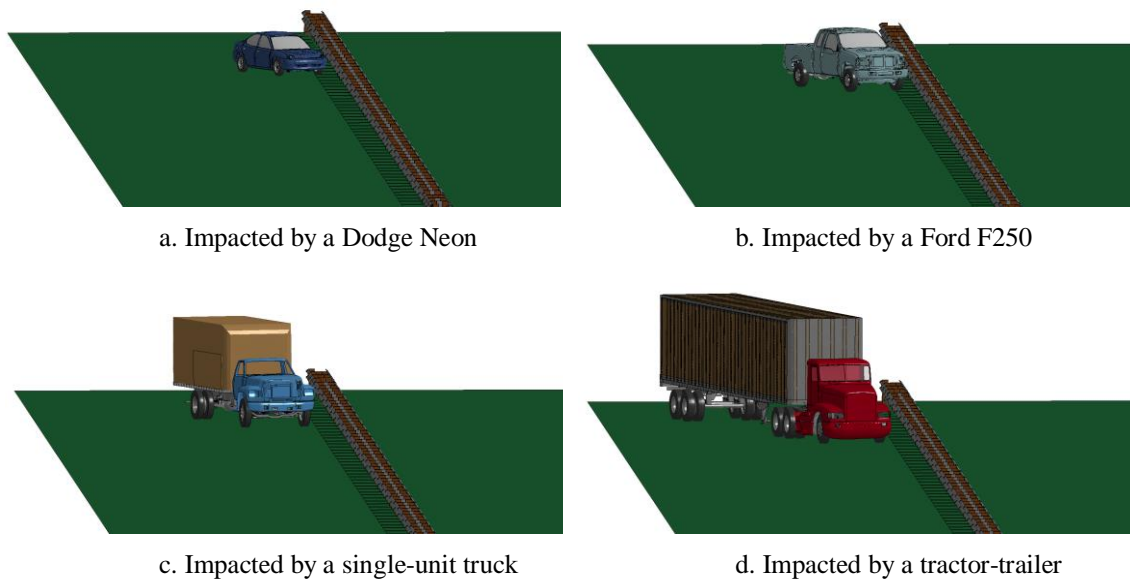
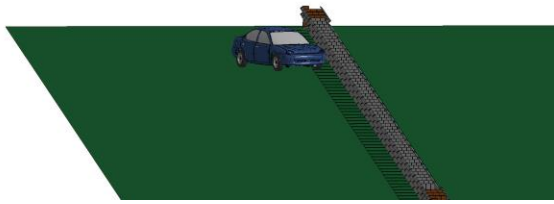
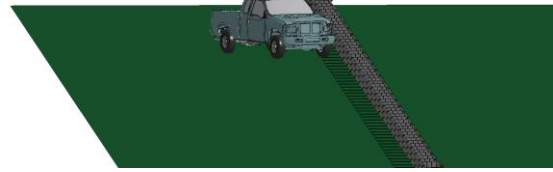


Fig. 3.13: FE models of the double-faced 31-inch W-beam guardrails.



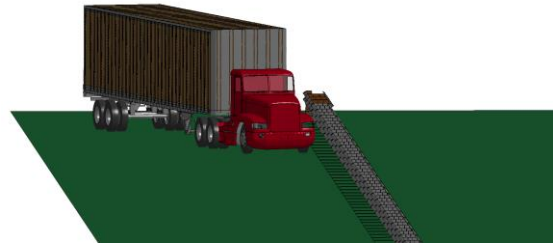
a. Impacted by a Dodge Neon



b. Impacted by a Ford F250

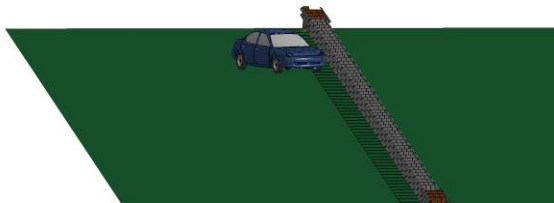


c. Impacted by a single-unit truck

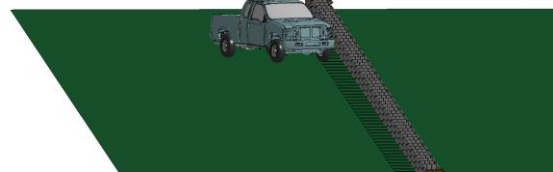


d. Impacted by a tractor-trailer

Fig. 3.14: FE models of the double-faced 29-inch wood-blockout Thrie-beam guardrails.



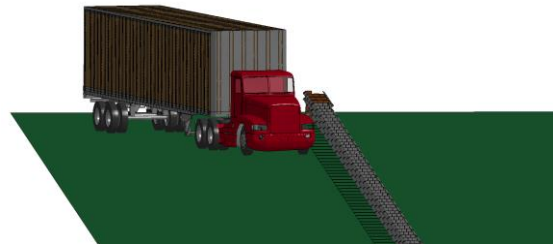
a. Impacted by a Dodge Neon



b. Impacted by a Ford F250



c. Impacted by a single-unit truck



d. Impacted by a tractor-trailer

Fig. 3.15: FE models of the double-faced 29-inch steel-blockout Thrie-beam guardrails.

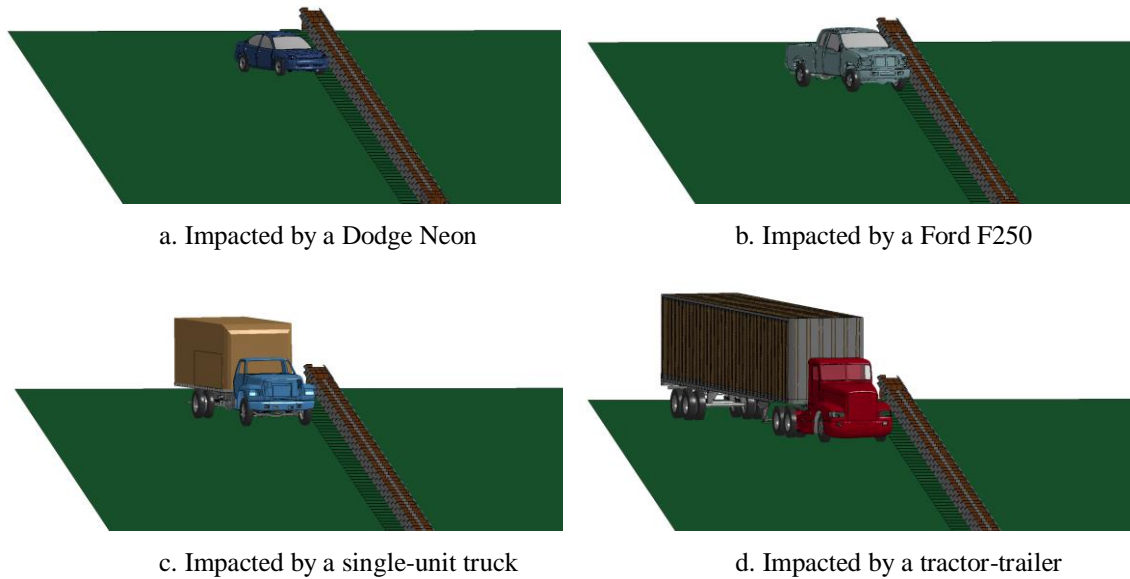


Fig. 3.16: FE models of the double-faced 31-inch wood-blockout Thrie-beam guardrails.

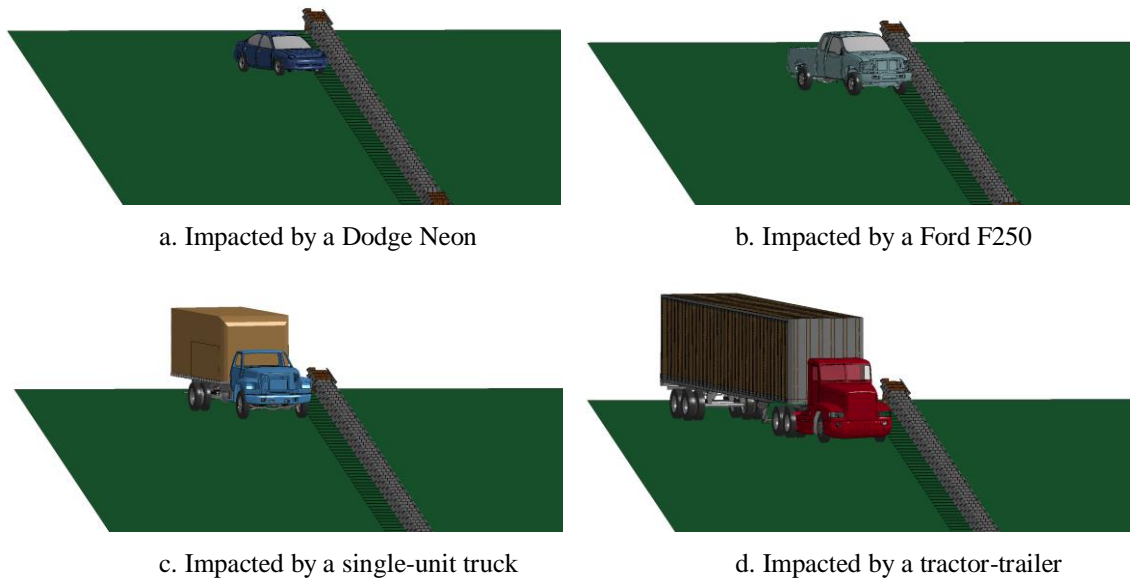


Fig. 3.17: FE models of the double-faced 31-inch steel-blockout Thrie-beam guardrails.

Table 3.2 summarizes the simulation conditions for all four cases. For each case, the guardrail is evaluated under MASH TL-4 and TL-5 impact conditions. The impact speeds were 62 mph (100 km/hr) for the Dodge Neon and Ford F250, 56 mph (90 km/hr) for the single-unit truck, and 50 mph (80 km/hr) for the tractor-trailer. The impact angles were 25° for the Dodge Neon and Ford F250 and 15° for the single-unit truck and tractor-trailer.

Table 3.2: Simulation conditions for all cases

Case No.	Guardrail Model	Impacting Vehicles	Impact Speed	Impact Angle
1	Double-faced 29-inch W-beam Guardrail	Dodge Neon	62 mph (100 km/h)	25°
		Ford F250		
		Single-Unit Truck	56 mph (90 km/h)	15°
		Tractor-Trailer	50 mph (80 km/h)	
2	Double-faced 31-inch W-beam Guardrail	Dodge Neon	62 mph (100 km/h)	25°
		Ford F250		
		Single-Unit Truck	56 mph (90 km/h)	15°
		Tractor-Trailer	50 mph (80 km/h)	
3	Double-faced 29-inch Thrie-beam Guardrails with wood- and steel-blockouts	Dodge Neon	62 mph (100 km/h)	25°
		Ford F250		
		Single-Unit Truck	56 mph (90 km/h)	15°
		Tractor-Trailer	50 mph (80 km/h)	
4	Double-faced 31-inch Thrie-beam Guardrails with wood- and steel-blockouts	Dodge Neon	62 mph (100 km/h)	25°
		Ford F250		
		Single-Unit Truck	56 mph (90 km/h)	15°
		Tractor-Trailer	50 mph (80 km/h)	

Based on Table 3.2, Cases 1 and 2 each required a total of 6 simulations (i.e., MASH TL-4 includes Dodge Neon, Ford F250, and single-unit truck impacts and TL-5 includes Dodge Neon, Ford F250, and tractor-trailer impacts). Cases 3 and 4 each had a total of 12 simulations since they both included two types of blockouts, i.e., wood- and steel-blockouts. It should be noted that the impacts by the Dodge Neon and Ford F250 at MASH TL-4 conditions were identical to those at MASH TL-5 conditions for each case. Thus, the impacts by the Dodge Neon and Ford F250 in each case will only be discussed once to eliminate redundancy. This effectively reduces to the total number of collective simulations to 24.

4. Simulation Results and Analysis

The simulation results for the four cases in Table 3.2 are presented in this section. The performance of the double-faced W-beam and Thrie-beam guardrails under vehicular impacts from four test vehicles were evaluated using vehicular responses classified by the MASH exit box criterion. The simulation results of the guardrail damage and the vehicles' yaw, pitch, and roll angles as well as transverse displacements and velocities were also examined to provide a comprehensive understanding of vehicular responses.

The exit box criterion is used to determine vehicle redirection characteristics based on the vehicle's response after impacting a longitudinal barrier. Figure 4.1 illustrates the definition of the exit box, which begins at the last contact point of the vehicle's tire track with the initial location of the barrier's face. The size of the exit box (i.e., the side lengths, A and B , of the rectangular area) is determined by the type and size of the impacting vehicle. Table 4.1 gives the definition of the dimensions A and B in the MASH exit box criterion.

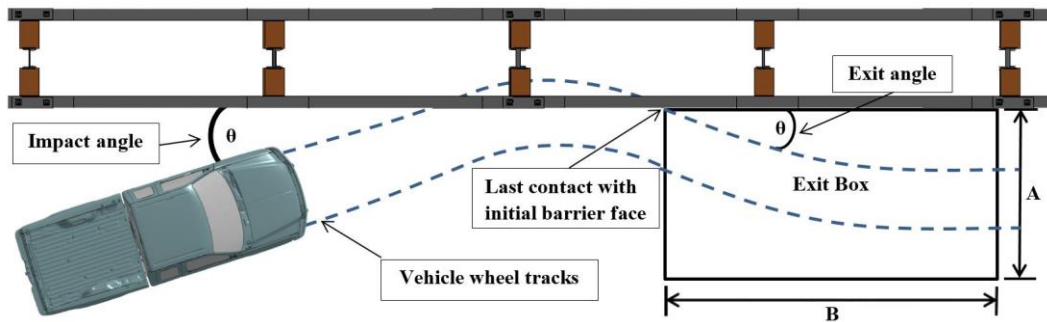


Fig. 4.1: The exit-box criterion defined in MASH.

Table 4.1: The dimension of the exit box defined in MASH

Vehicle Type	Exit Box Dimension	
	A	B
Cars or Pickup Trucks	$7.2 + V_W + 0.16V_L$ (ft)	32.8 ft (10 m)
Other Vehicles (i.e., Single-Unit Truck, Tractor-Trailer)	$14.4 + V_W + 0.16V_L$ (ft)	65.6 ft (20 m)

In Table 4.1, V_W and V_L stand for the vehicle's width and length, respectively. According to the exit box criterion, if all four tires of the vehicle remain inside the exit box for the distance B , the case is considered to be a safe redirect. The safe redirection defined here means the exit angle of the impacting vehicle is small enough to effectively eliminate the possibility of the vehicle returning to the roadway and causing a second accident. One scenario that is categorized as safe by the MASH evaluation criterion N is, if the vehicle remains upright and in contact with the guardrail while reducing its velocity to zero. When this scenario is present, no exit box is required. Another scenario in which an exit box is not required is when the vehicle fails to remain upright and rolls onto the guardrail. As stated in MASH, "although it is preferable all vehicles remain upright, this requirement is not applicable for tests involving the

10000S (i.e., single-unit truck) and 36000V (i.e., tractor-trailer) vehicles.” This exception allows a 90° roll for heavy vehicle impacts and relies on the fact that the primary goal of the impact scenario is to demonstrate the guardrail’s ability to contain and redirect the impacting vehicles. Although the exit box criterion is a useful tool for determining the post-impact vehicular trajectories, use of this criterion alone is not sufficient to determine if the vehicle has been safely redirected. In addition, a large exit angle and/or spin-out, which may be caused by pocketing and/or snagging of the vehicle on the guardrail posts, may still be present even for a case determined as a safe redirect by the exit box criterion.

Table 4.2 gives the exit box dimensions for the Dodge Neon, Ford F250, single-unit truck, and tractor-trailer, obtained using the formula in Table 4.1 and the data in Table 3.1. These four exit boxes were used to assess the post-impact vehicular responses from the simulation results.

Table 4.2: Exit box dimensions for the four test vehicles of this study

Vehicle	Exit Box Dimension	
	A	B
Dodge Neon	15.1 ft (4.60 m)	32.8 ft (10.0 m)
Ford F250	16.9 ft (5.15 m)	32.8 ft (10.0 m)
Single-Unit Truck	26.9 ft (8.21 m)	65.6 ft (20.0 m)
Tractor-trailer	32.9 ft (10.04 m)	65.6 ft (20.0 m)

4.1 Case 1: Double-faced 29-inch W-beam Guardrail

In this case, the strong-post double-faced 29-inch W-beam guardrail was evaluated under MASH TL-4 and TL-5 impact conditions using a small sedan, a pickup truck, a single-unit truck, and a tractor-trailer. An impact angle of 25° was used for the small sedan, and pickup truck and an impact angle of 15° was used for the single-unit truck and tractor-trailer. The impact speed of 62 mph (100 km/h) was used for the small sedan and pickup truck, 56 mph (90 km/h) for the single-unit truck, and 50 mph (80 km/h) for the tractor-trailer. Since the impacts by the small sedan and pickup truck are identical in MASH TL-4 and TL-5 conditions, the simulation results are only listed and discussed once. Table 4.3 gives a summary of the simulation results for Case 1 on the guardrail performance in terms of vehicular responses.

Table 4.3: Simulation results of Case 1 (Double-faced 29-inch W-beam guardrail)

Test Vehicle	MASH Level	Impact Angle	Impact Velocity	Simulation Results
Dodge Neon	TL-4 & TL-5	25°	62 mph (100 km/h)	The vehicle failed the exit box criterion due to vehicle spin-out with a large exit angle
Ford F250	TL-4 & TL-5	25°	62 mph (100 km/h)	The vehicle passed the exit box criterion and was safely redirected
Single-Unit Truck	TL-4	15°	56 mph (90 km/h)	The vehicle failed to remain upright and rolled onto the guardrail
Tractor-Trailer	TL-5	15°	50 mph (80 km/h)	The vehicle passed the exit box criterion and was safely redirected

4.1.1 Dodge Neon Impact at MASH TL-4 & TL-5 Conditions

Figure 4.2 shows a top-view vehicle trajectory of the Dodge Neon impacting the double-faced 29-inch W-beam guardrail at 62 mph (100 km/h) and 25°. The W-beam guardrail is shown in its deformed state with the vehicle's tire tracks outlined in white. The exit box, shown by the yellow dotted rectangle, is placed at the last point of contact of the vehicle's tire tracks with the initial guardrail face. It was observed that the Dodge Neon experienced tire snagging on the guardrail post, causing vehicle spin-out with a large exit angle. According to the MASH exit box criterion, since the vehicle's trajectory was primarily transverse away from the guardrail and did not travel the length of the exit box, the simulated impact was determined to fail to meet the exit box criterion.

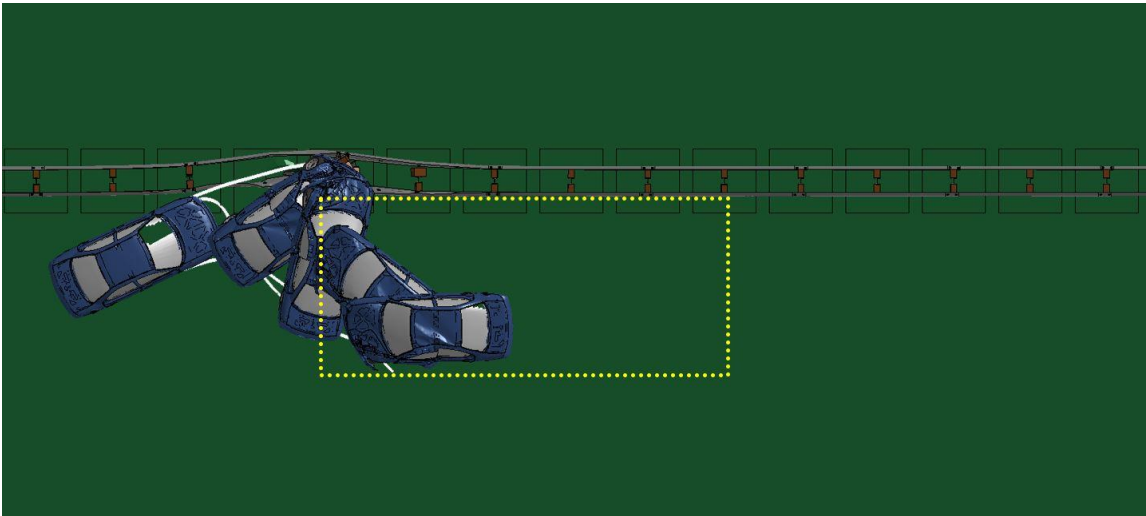


Fig. 4.2: A Dodge Neon impacting the double-faced 29-inch W-beam guardrail at 62 mph (100 km/h) and 25°.

The yaw, pitch, and roll angles of the Dodge Neon while impacting the double-faced 29-inch W-beam guardrail are shown in Fig. 4.3. The exit angle was determined by calculating the angle between the initial guardrail face and the left (i.e., driver's side) longitudinal face of the vehicle. The exit angle of the Dodge Neon impact determined to be 118°. The vehicle was not safely redirected due to tire snagging on a post and prematurely leaving the exit box with a continuous spin as indicated by the increasing yaw angle. It can be seen from the time histories of the yaw angles in Fig. 4.3 that the Dodge Neon was first redirected (during the first 0.1 seconds as indicated by the negative yaw angles) and then began to rotate in the opposite direction while losing contact with the guardrail. The positive rotation continued after the vehicle lost contact with the guardrail, resulting in a large exit angle. It was observed from the simulation results that the Dodge Neon partially under-rode the 29-inch W-beam guardrail and directly contacted the post, causing pocketing and snagging on the front left tire of the vehicle. The roll and pitch angles were less than thirteen degrees in both positive and negative directions, satisfying the MASH evaluation criterion F , which specifies a maximum 75° roll or pitch angle.

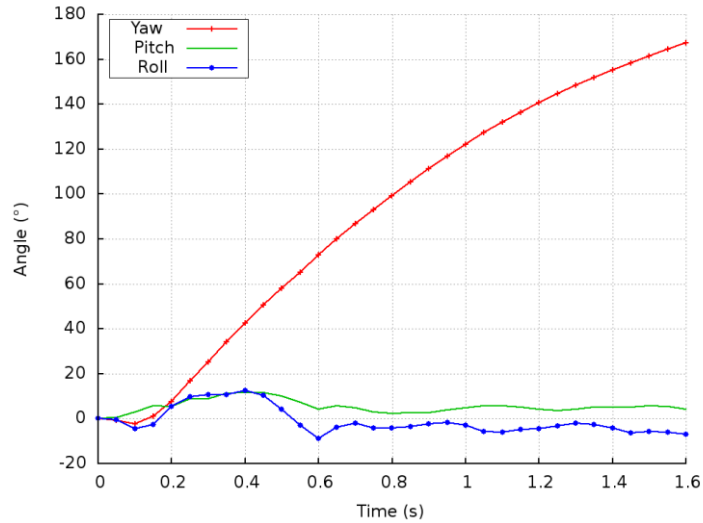


Fig. 4.3: Yaw, pitch, and roll angles of Dodge Neon impacting the double-faced 29-inch W-beam guardrail at 62 mph (100 km/h) and 25°.

The maximum dynamic deflection of the guardrail was measured on either the front-side or the backside rail during the impact. Figure 4.4 shows the maximum dynamic deflections of the 29-inch guardrail, 2.11 ft (0.64 m), under impact by the Dodge Neon at 62 mph (100 km/h). It can be seen that the damaged guardrail sections are small and localized with surrounding guardrail sections undamaged; this serves as an indication of a relatively low-severity impact from the small car. The damaged section of guardrail included three posts across two double-faced guardrail segments.

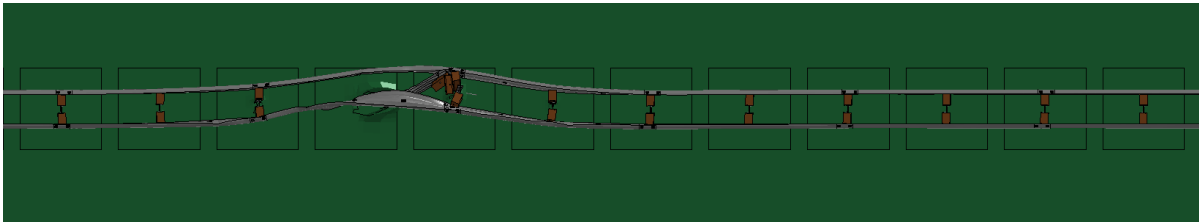


Fig. 4.4: Maximum dynamic deflection of the double-faced 29-inch W-beam guardrail at 62 mph (100 km/h) and 25° and impacted by a Dodge Neon.

Figure 4.5 shows detailed views of the vehicle-barrier interaction at 0.18 seconds when the maximum deflection of the guardrail occurs during impact on the double-faced 29-inch W-beam guardrail. Figure 4.6 shows the time histories of transverse displacement and velocity measured at the center of gravity (CG) of the vehicle. The maximum dynamic deflection at 0.18 seconds as seen in Fig. 4.5 directly correlates to the change in direction of the transverse displacement seen in Fig. 4.6a. The transverse displacement and velocity, exit box criterion, along with the exit angle, could all be used to determine if a redirection was safe or subjected to a possible secondary collision. For example, if the transverse velocity of a redirected vehicle remained large, the redirection could be followed by a secondary collision if the exit angle was also large. For the case of the Dodge Neon impacting the double-faced 29-inch W-beam guardrail, the transverse velocity was approximately 5.5 mph (9 km/h) towards the travel lane.

The small transverse velocity still has the possibility of causing a secondary impact due to the large exit angle from the vehicle spin-out.

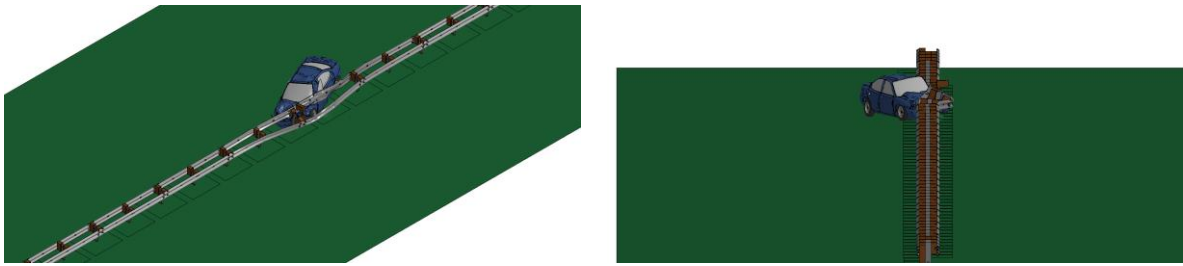


Fig. 4.5: Simulations of Dodge Neon impacting the double-faced 29-inch W-beam guardrail at 62 mph (100 km/h) and 25°.

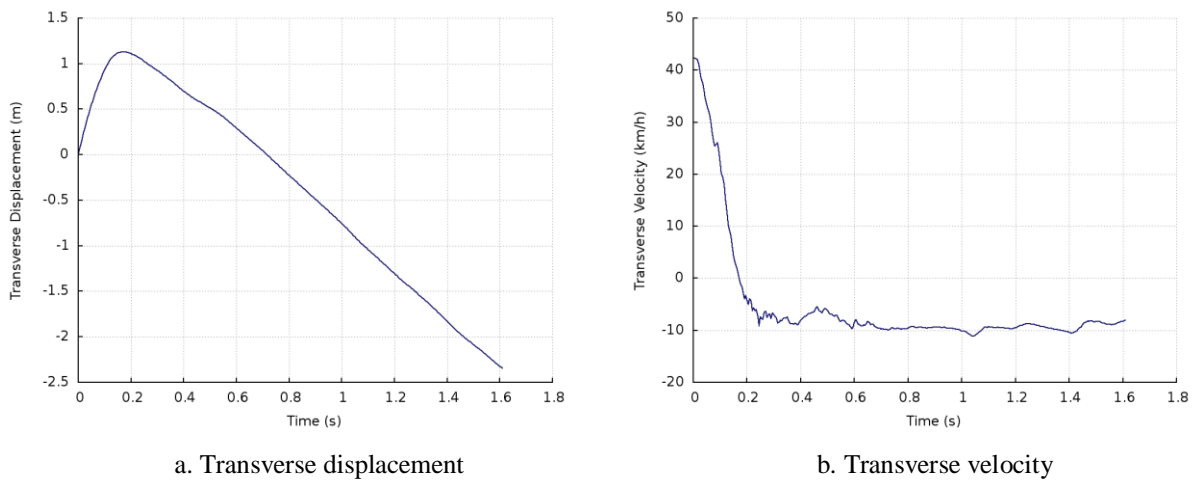


Fig. 4.6: Transverse displacement and velocity of the Dodge Neon impacting the double-faced 29-inch W-beam guardrail at 62 mph (100 km/h) and 25°.

4.1.2 Ford F250 Impact at MASH TL-4 & TL-5 Conditions

Under impact from the Ford F250 at 62 mph (100 km/h) and 25°, the double-faced 29-inch W-beam guardrail redirected the vehicle with a small exit angle. Figure 4.7 shows the top view of the vehicle trajectory from a Ford F250 impacting the double-faced 29-inch W-beam guardrail. The vehicle tire tracks are outlined in white and the exit box, shown by the yellow dotted rectangle, was placed at the last point of contact of the vehicle's tire tracks to the initial guardrail face. Due to the small exit angle, the vehicle traversed the length of the exit box with the tire tracks exiting along the right side of the exit box. This post impact trajectory is defined as a safe redirect according to the MASH exit box criterion.

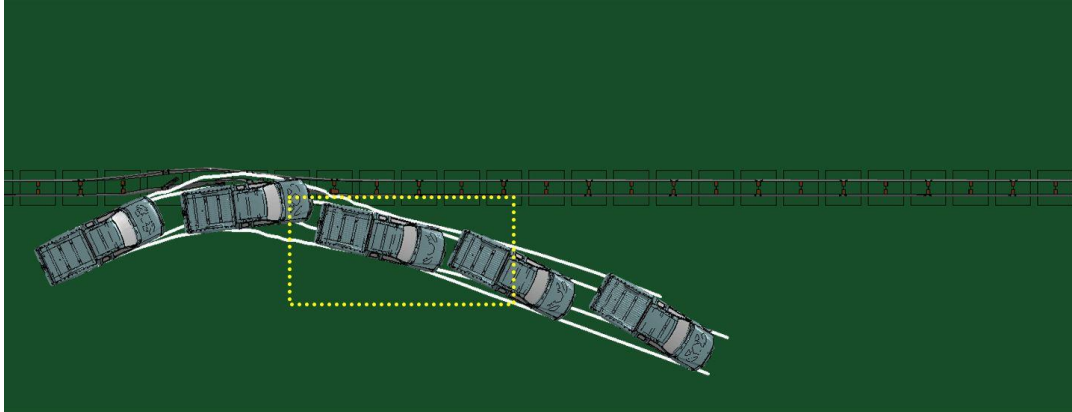


Fig. 4.7: A Ford F250 impacting the double-faced 29-inch W-beam guardrail at 62 mph (100 km/h) and 25°.

Figure 4.8 shows the yaw, pitch, and roll angles of the Ford F250 while impacting the double-faced 29-inch W-beam guardrail at 62 mph (100 km/h) and 25°. The exit angle was determined to be -8° by adding the impact angle (i.e., 25°) to the yaw angle at the point of last contact with the guardrail at 0.75 seconds (i.e., -33°). Additionally, the roll and pitch angles in the Ford F250 impact were less than ten degrees in both positive and negative directions and thus passed the MASH evaluation criterion F, which specified a maximum 75° roll or pitch angle.

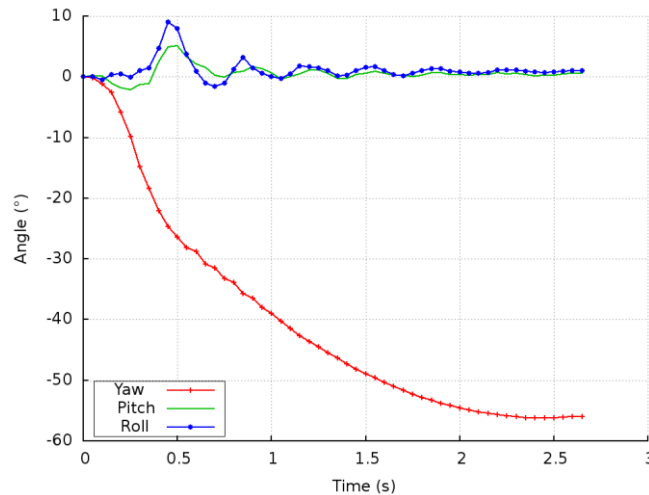


Fig. 4.8: Yaw, pitch, and roll angles of Ford F250 impacting the double-faced 29-inch W-beam guardrail at 62 mph (100 km/h) and 25°.

Figure 4.9 shows the maximum dynamic deflection of the double-faced 29-inch W-beam guardrail impacted by the Ford F250 at 62 mph (100 km/h) and 25°. This maximum dynamic deflection was determined to be 3.6 ft (1.1 m), occurred at 0.21 seconds. It can be seen that the maximum dynamic deflection of the guardrail under the impact by Ford F250 was significantly larger than that by the Dodge Neon (seen in Fig. 4.4). This increased deflection can be attributed to the additional impact energy from the larger vehicle. The damaged guardrail section spans three double-faced guardrail segments and five posts, leaving the remaining double-faced guardrail segments undeformed structurally.

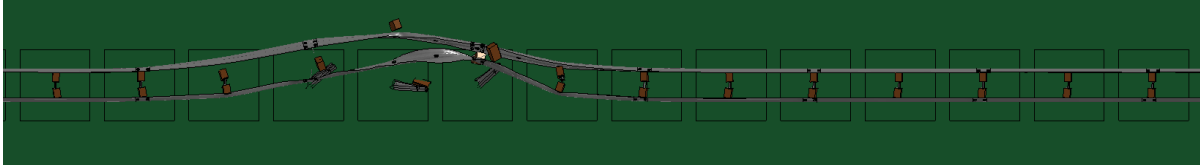


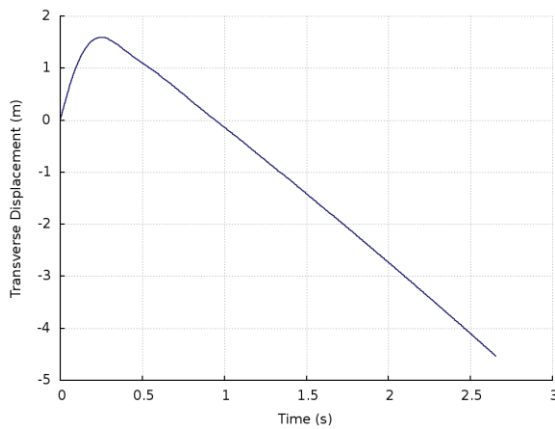
Fig. 4.9: Maximum dynamic deflection of the double-faced 29-inch W-beam guardrail at 62 mph (100 km/h) and 25° and impacted by a Ford F250.

Figure 4.10 shows the Ford F250 impacting the double-faced 29-inch W-beam guardrail at the state of maximum guardrail deflection. Due to the vehicle's higher ride profile, the Ford F250 had a better engagement with the guardrail than the Dodge Neon.

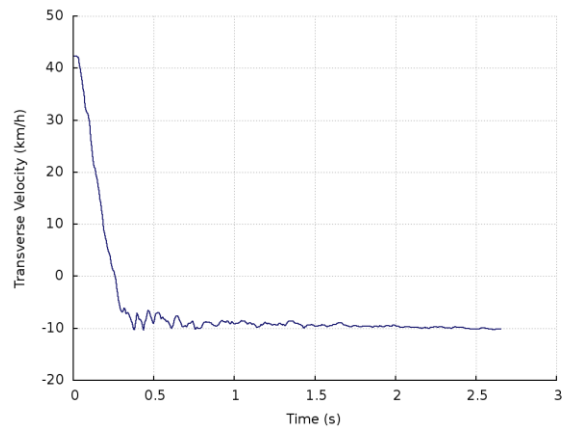


Fig. 4.10: Simulations of Ford F250 impacting the double-faced 29-inch W-beam guardrail at 62 mph (100 km/h) and 25°.

Figure 4.11 show the time histories of transverse displacement and velocity measured at the CG of the Ford F250 in the impact scenario. The maximum deflection at 0.21 seconds as seen in Fig. 4.9 directly correlates to the change in direction of the transverse displacement seen in Fig. 4.11a. The transverse velocity was approximately 6.2 mph (10 km/h) towards the travel lane, indicating a potential chance of being involved in a secondary collision depending on how close the travel lane is located. The results in Figs. 4.8 to 4.11, along with those of the Dodge Neon, indicated the performance of the double-faced 29-inch W-beam guardrail impacted by a pickup truck and a passenger car at MASH TL-4 and TL-5 impact conditions.



a. Transverse displacement



b. Transverse velocity

Fig. 4.11: Transverse displacement and velocity of the Ford F250 impacting the double-faced 29-inch W-beam guardrail at 62 mph (100 km/h) and 25°.

4.1.3 Single-unit Truck Impact at MASH TL-4 Conditions

Figure 4.12 shows the top view of vehicle trajectory of the single-unit truck impacting the double-faced 29-inch W-beam guardrail at 56 mph (90 km/h) and 15°. The W-beam guardrail is shown in its deformed state with the tire tracks outlined in white. Upon impacting the guardrail, the vehicle failed to remain upright and rolled onto the guardrail. Due to this impact behavior, an exit box was not required. The vehicle's rollover could be attributed to the high center of gravity and long rigid wheelbase that did not allow the tail end to articulate after impacting the guardrail at the front end of the truck. The tail end of the truck became airborne as the vehicle continued to interact with the guardrail. It should be noted that the single-unit truck was not required to remain upright as per MASH, "although it is preferable all vehicles remain upright, this requirement is not applicable for tests involving the 10000S (i.e., single-unit truck) and 36000V (i.e., tractor-trailer) vehicles." This exception of allowing a roll for heavy vehicle impacts was based on that the primary goal of the impact scenario was to demonstrate the guardrails ability to contain and redirect the vehicle.

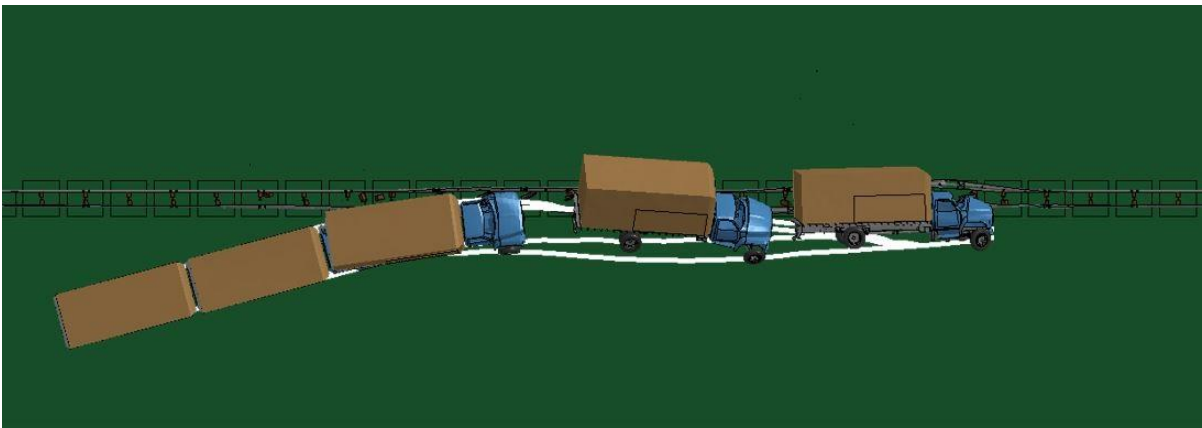


Fig. 4.12: A single-unit truck impacting the double-faced 29-inch W-beam guardrail at 56 mph (90 km/h) and 15°.

Figure 4.13 shows the yaw, pitch, and roll angles of the single-unit truck impacting the double-faced 29-inch W-beam guardrail at 56 mph (90 km/h) and 15°. Due to the vehicle's high CG point, once the vehicle's roll angle surpassed 45° at 1.05 seconds, a rollover scenario was imminent. Since the vehicle failed to remain upright, the impact did not pass the MASH evaluation criterion F for the roll angle, which specified a maximum 75° roll or pitch angle.

The maximum dynamic deflection of the double-faced 29-inch W-beam guardrail under impact by the single-unit truck at 56 mph (90 km/h) and 15° is shown in Fig. 4.14. The maximum dynamic deflection of 2.2 ft (0.7 m) occurred at 0.76 seconds, which corresponded to the instance when the yaw angle transitioned from an increasing to decreasing yaw angle. Figure 4.15 shows detailed views of the single-unit truck at the maximum dynamic deflection while impacting the double-faced 29-inch W-beam guardrail at 56 mph (90 km/h) and 15°.

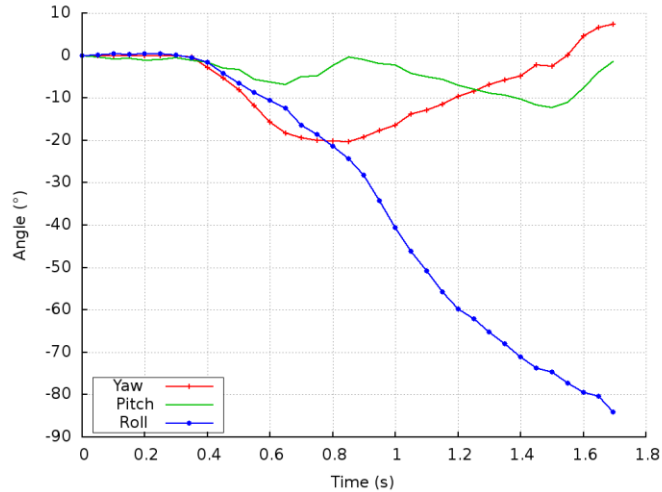


Fig. 4.13: Yaw, pitch, and roll angles of the single-unit truck impacting the double-faced 29-inch W-beam guardrail at 56 mph (90 km/h) and 15°.

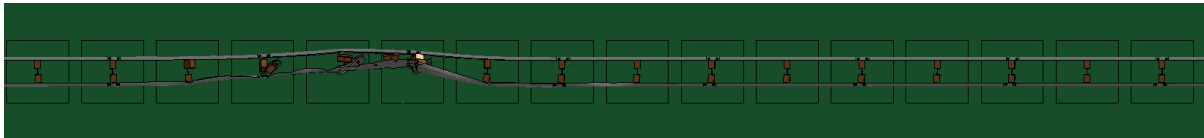


Fig. 4.14: Maximum dynamic deflection of the double-faced 29-inch W-beam guardrail at 56 mph (90 km/h) and 15° and impacted by a single-unit truck.



Fig. 4.15: Simulations of the single-unit truck impacting the double-faced 29-inch W-beam guardrail at 56 mph (90 km/h) and 15°.

Figure 4.16 shows the time histories of transverse displacement and velocity measured at the CG of the single-unit truck in the truck cabin. From Fig. 4.16a, it can be seen that the transverse displacement did not transition to decreasing values after impacting the guardrail, indicating that the vehicle was not redirected. Figure 4.16b shows that the transverse velocity is essentially reduced to zero after the vehicle begins to roll onto the guardrail.

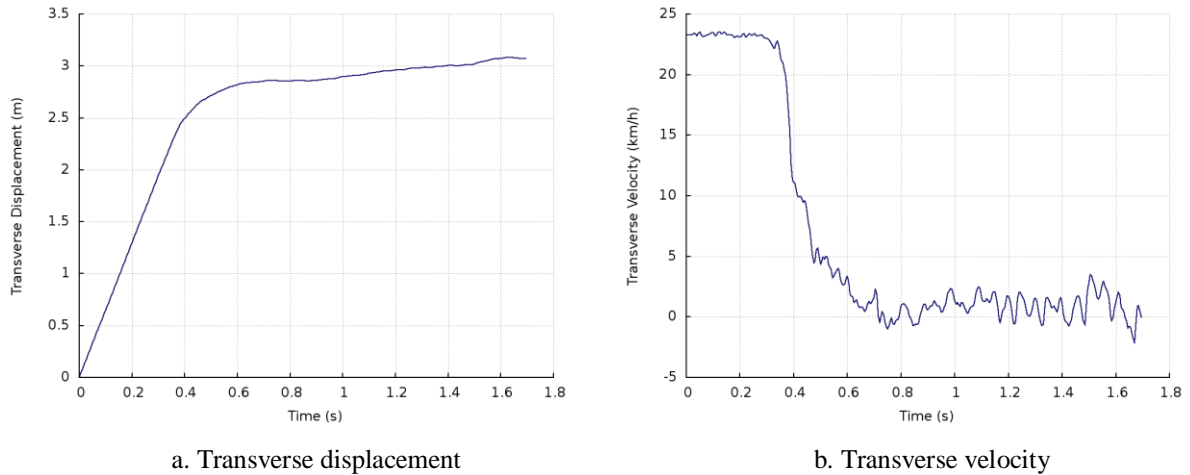


Fig. 4.16: Transverse displacement and velocity of the single-unit truck impacting the double-faced 29-inch W-beam guardrail at 56 mph (90 km/h) and 15°.

4.1.4 Tractor-trailer Impact at MASH TL-5 Conditions

Figure 4.17 shows the top view vehicle trajectory of the tractor-trailer impacting the double-faced 29-inch W-beam guardrail at 50 mph (80 km/h) and 15°. The W-beam guardrail is shown in its deformed state with the vehicle tire tracks outlined in white. The MASH exit box, placed at the last point of contact of the vehicle's tire tracks to the initial guardrail face, is shown by the yellow dotted rectangle. In this case, the tractor-trailer traveled the length of the exit box and thus passed the MASH exit box criterion.

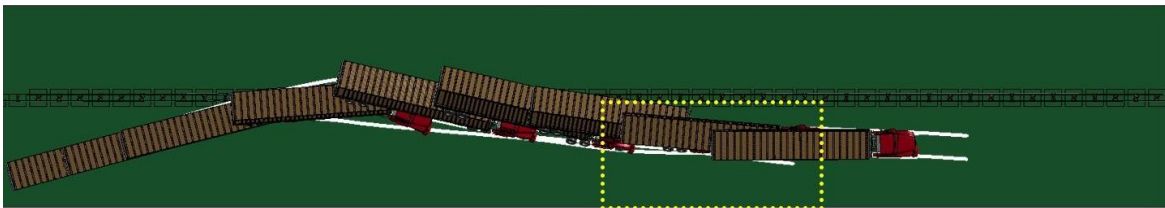


Fig. 4.17: A tractor-trailer impacting the double-faced 29-inch W-beam guardrail at 50 mph (80 km/h) and 15°.

The yaw, pitch, and roll angles of the tractor and the trailer in this impact case are shown in Fig. 4.18. The exit angle was determined to be -6° adding the impact angle (i.e., 15°) to the yaw angle (i.e., -21°) of the tractor at 2.57 seconds, when the tractor-trailer had the last contact with the guardrail. It can be seen from Fig. 4.18a that the yaw angle changes its direction at one second, indicating the beginning of the redirection of the tractor away from the guardrail. The constant yaw angle of the tractor from 1.5 to 2 seconds corresponded to the impact and initiation of the redirection of the trailer at 1.6 seconds, as shown in Fig. 4.18b. The maximum roll angles of the tractor and trailer were, 30.1° and 35.9° , respectively. Although these roll angles were relatively large, they were still below the rollover tipping point of 45° . The pitch angles in this impact were less than 8 degrees in both positive and negative directions and thus passed the MASH evaluation criterion F , which specified a maximum 75° roll or pitch angle.

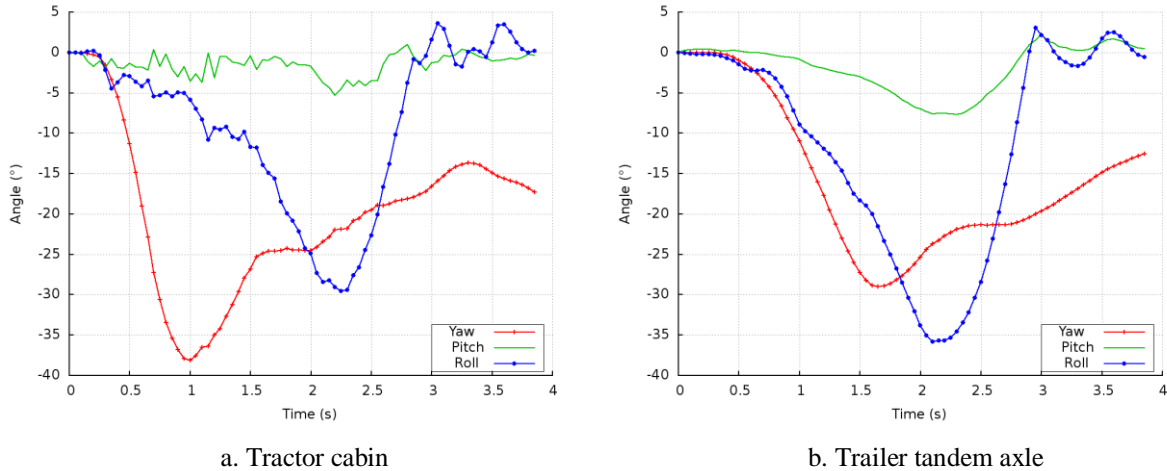


Fig. 4.18: Yaw, pitch, and roll angles of the tractor’s (a) cabin and trailer’s (b) tandem axle impacting the double-faced 29-inch W-beam guardrail at 50 mph (80 km/h) and 15°.

Figure 4.19 shows the maximum dynamic deflection of the double-faced 29-inch W-beam guardrail impacted by the tractor-trailer at 50 mph (80 km/h) and 15°. The maximum dynamic deflection of the guardrail was 8.1 ft (2.47 m), which occurred at 1.54 seconds. This deflection state coincided with the redirection of the articulating trailer as it rotated towards the guardrail after the tractor was redirected. The guardrail deflection was rather severe in this impact, with 13 posts and 7 double-faced guardrail segments severely deformed. Figure 4.20 shows the detailed views of vehicle-guardrail interactions at 0.6 and 1.54 seconds.

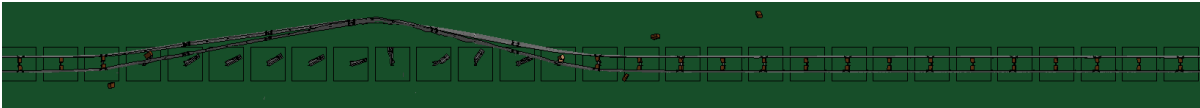
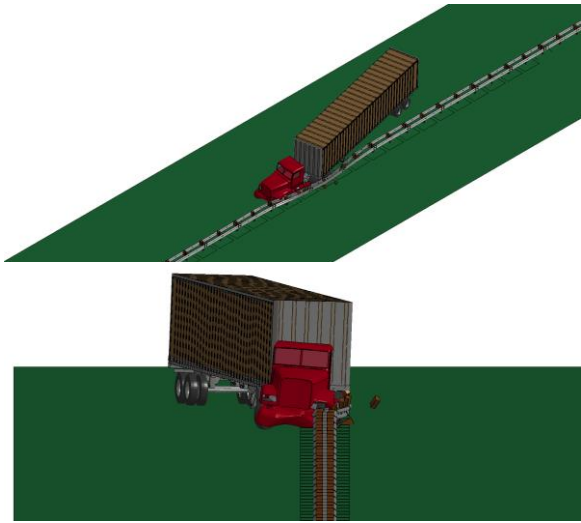
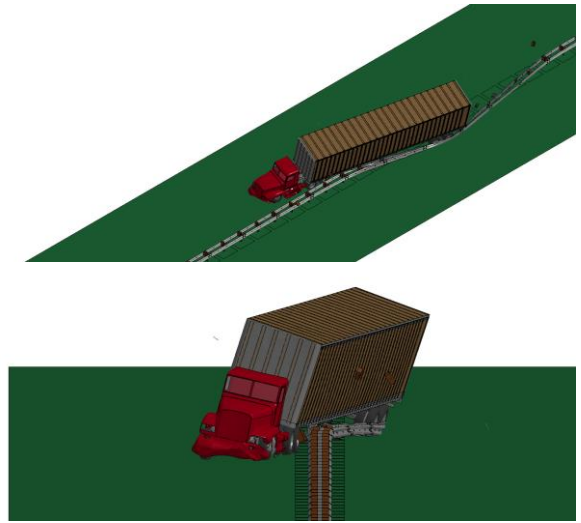


Fig. 4.19: Maximum dynamic deflection of the double-faced 29-inch W-beam guardrail at 50 mph (80 km/h) and 15° and impacted by a tractor-trailer.

Figure 4.21 show the time histories of transverse displacements and velocity measured at the CG point of the tractor and at the trailer tandem axle in the 50 mph (90 km/h) at 15° impact. Figure 4.21a shows the tractor’s transverse displacement throughout the impact. The maximum transverse displacement occurred at 0.6 seconds and corresponded to the impact state seen in Fig. 4.20a. Similarly in Fig. 4.21c, the point of maximum displacement of the trailer tandem axle’s transverse displacement occurred at 1.54 seconds that corresponded to the impact state illustrated in Fig. 4.20b. The transverse velocity of the tractor and the trailer was approximately 2.5 mph (4 km/h) towards the travel lane at the end of the impact scenario. Considering the exit box criterion, exit angle, and transverse velocity, the tractor-trailer had a low potential of reentering into the travel lane and causing a secondary collision.

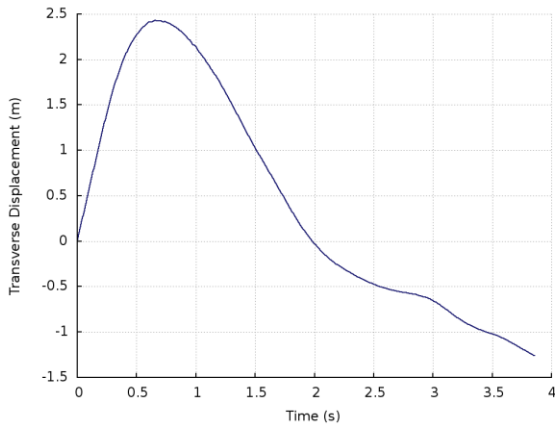


a. Impact at 0.6 seconds

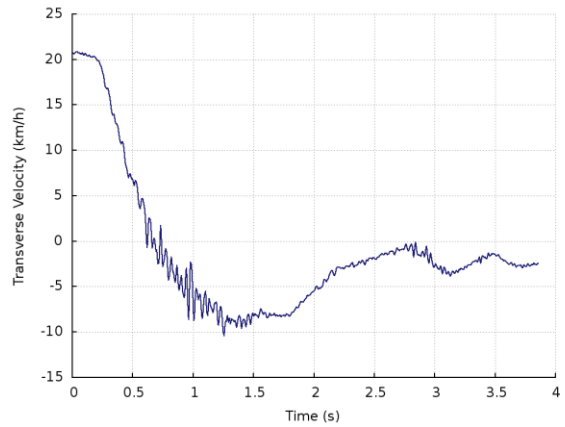


b. Impact at 1.54 seconds

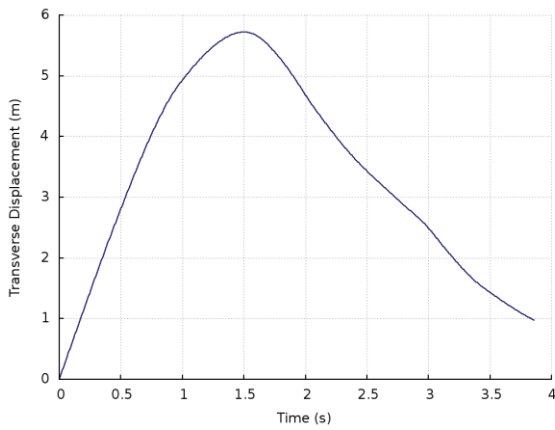
Fig. 4.20: A tractor-trailer impacting the double-faced 29-inch W-beam guardrail at 50 mph (80 km/h) and 15°.



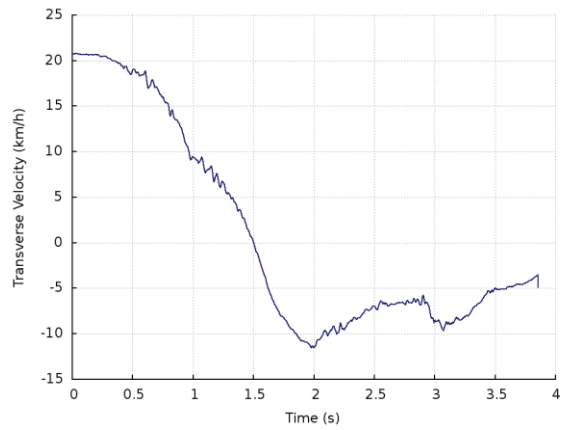
a. Tractor transverse displacement



b. Tractor transverse velocity



c. Trailer axle transverse displacement



d. Trailer axle transverse velocity

Fig. 4.21: Transverse displacements and velocities of the tractor-trailer impacting the double-faced 29-inch W-beam guardrail at 50 mph (80 km/h) and 15°.

4.2 Case 2: Double-faced 31-inch W-beam Guardrail

In this case, the double-faced 31-inch W-beam guardrail was evaluated under MASH TL-4 and TL-5 impact conditions with impacts from a small sedan, pickup truck, single-unit truck, and a tractor-trailer. The double-faced 31-inch W-beam guardrail design in this case is the same as that of Case 1, exception for the guardrail height being raised an additional two inches. The impact velocities and impact angles for MASH TL-4 and TL-5 are identical to those in Case 1. Table 4.4 gives a summary of the simulation’s guardrail performance for Case 2 in terms of vehicular responses.

Table 4.4: Simulation results of Case 2 (31-inch double-faced W-beam guardrail)

Test Vehicle	MASH Level	Impact Angle	Impact Velocity	Simulation Results
Dodge Neon	TL-4 & TL-5	25°	62 mph (100 km/h)	The vehicle failed the exit box criterion caused by vehicle spin-out and a large exit angle
Ford F250	TL-4 & TL-5	25°	62 mph (100 km/h)	The vehicle passed the exit box criterion and was safely redirected
Single-Unit Truck	TL-4	15°	56 mph (90 km/h)	The vehicle failed to remain upright and rolled onto the guardrail
Tractor-Trailer	TL-5	15°	50 mph (80 km/h)	The vehicle passed the exit box criterion and was safely redirected

4.2.1 Dodge Neon Impact at MASH TL-4 & TL-5 Conditions

Figure 4.22 shows the top view of vehicle trajectory of the Dodge Neon impacting the double-faced 31-inch W-beam guardrail at 62 mph (100 km/h) and 25°. The W-beam guardrail is shown in its deformed state with the vehicle’s tire tracks outlined in white. The exit box, shown by the yellow dotted rectangle, is placed at the last point of contact of the vehicle’s tire tracks with the initial guardrail face. It was observed that the Dodge Neon partially underrode the guardrail due to its relatively low profile, causing tire snagging on the guardrail post and resulting in a spin-out with a large exit angle. According to the MASH exit box criterion, since the vehicle’s trajectory was primarily transverse away from the guardrail and would not travel the length of the exit box, the impact scenario failed the MASH exit box criterion.

Figure 4.23 shows the yaw, pitch, and roll angles of the Dodge Neon impacting the double-faced 31-inch W-beam guardrail at 62 mph (100 km/h) and 25°. The exit angle was determined to be 63° by adding the 25° impact angle to the 38° yaw angle at the point of last contact with the guardrail at 0.62 seconds. The vehicle was not safely redirected due to the counterclockwise rotation after leaving the exit box as indicated by the steadily increasing positive yaw angle. It can be seen from Fig. 4.23 that the Dodge Neon was first redirected during the first 0.1 seconds, as indicated by the negative yaw angles, and then began to rotate in the opposite direction while losing contact with the guardrail. The counterclockwise rotation (indicated by the positive yaw angle) continued after the vehicle lost contact with the guardrail, resulting in a large exit angle. It was observed from the simulation results that the Dodge Neon partially under-rode the 31-inch W-beam guardrail and directly contacted the post, causing

pocketing and snagging on the front left tire of the vehicle. The roll and pitch angles in this impact were less than ten degrees in both positive and negative directions and thus passed the MASH evaluation criterion F , which specified a maximum 75° roll or pitch angle.

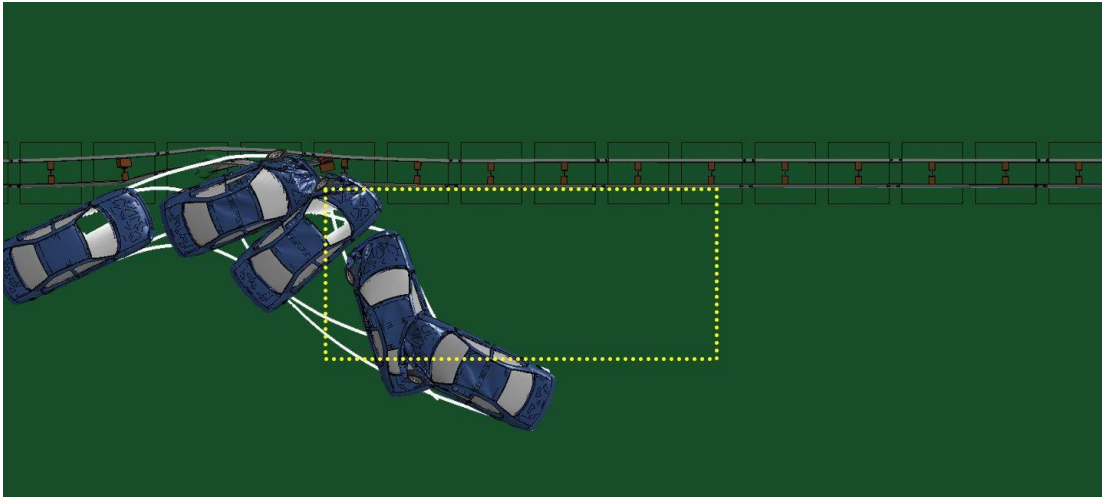


Fig. 4.22: A Dodge Neon impacting the double-faced 31-inch W-beam guardrail at 62 mph (100 km/h) and 25° .

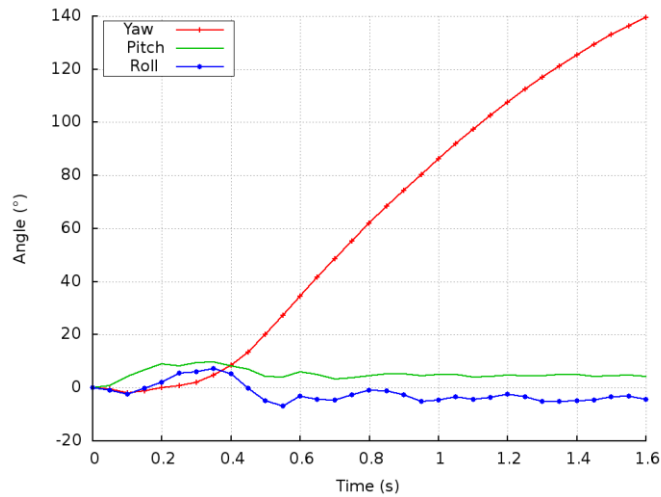


Fig. 4.23: Yaw, pitch, and roll angles of Dodge Neon impacting the double-faced 31-inch W-beam guardrail at 62 mph (100 km/h) and 25° .

Figure 4.24 shows the maximum dynamic deflection of the double-faced 31-inch W-beam guardrail under impact of the Dodge Neon at 62 mph (100 km/h) and 25° . The maximum dynamic deflection of the guardrail was 2.63 ft (0.8 m) that occurred at 0.2 seconds. The deformed section of the guardrail is relatively small and localized for the Dodge Neon impact. The damage caused by the impact affected six posts across three double-faced guardrail segments. Compared to the double-faced 29-inch W-beam guardrail impacted by the Dodge Neon (see Fig. 4.4), the double-faced 29-inch W-beam guardrail had a significantly lower maximum dynamic deflection by 0.525 ft (0.16 m). At the 31-inch rail height, the guardrail had very little engagement with the vehicle's bumper cover and fender. The Dodge Neon

intruded under the rail, engaged with the rail on the hood of the vehicle, and dragged the rail forward, resulting in a localized deflection of the guardrail.

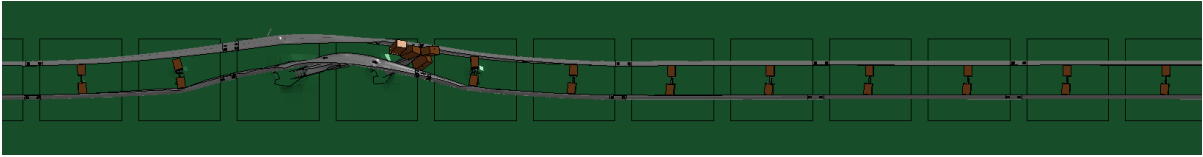


Fig. 4.24: Maximum dynamic deflection of the double-faced 31-inch W-beam guardrail at 62 mph (100 km/h) and 25° and impacted by a Dodge Neon.

Figure 4.25 shows detailed views of the vehicle-barrier interaction at the point of maximum rail deflection at 0.22 seconds in the Dodge Neon impact. Figure 4.26 shows the time histories of transverse displacement and velocity measured at the CG point of the vehicle for this impact. The maximum deflection at 0.22 seconds directly corresponded to the change in direction of the transverse displacement shown in Fig. 4.26a. In this case, the Dodge Neon impacting the double-faced 31-inch W-beam guardrail, had a transverse velocity of approximately 8 mph (13 km/h), indicating a moderate chance of moving towards the travel lane. The results in Figs. 4.22 to 4.26 indicated that the double-faced 31-inch W-beam guardrail could safely retain the Dodge Neon on the impacting side, with the possibility of causing a secondary collision, because the MASH exit box criterion was not met.



Fig. 4.25: Simulations of Dodge Neon impacting the double-faced 31-inch W-beam guardrail at 62 mph (100 km/h) and 25°.

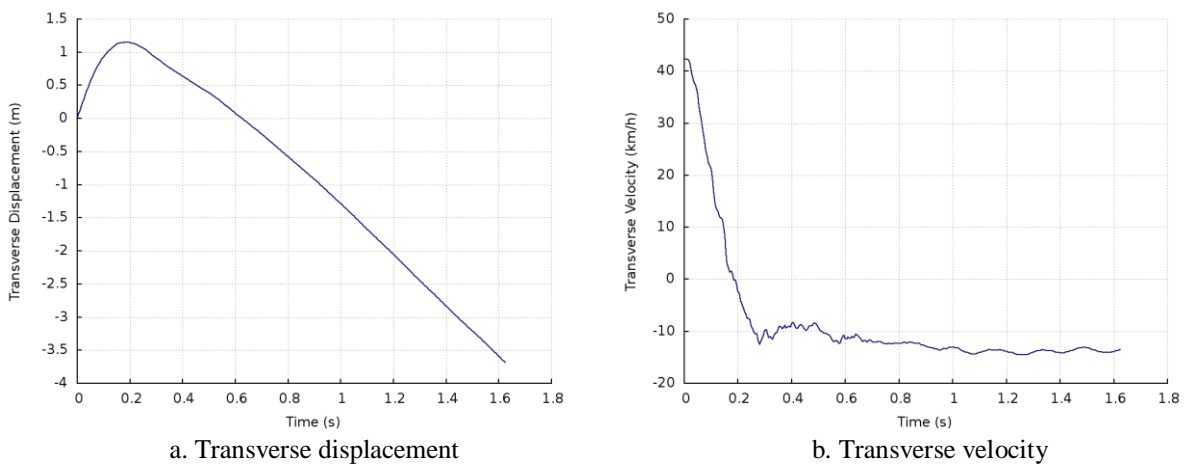


Fig. 4.26: Transverse displacement and velocity of the Dodge Neon impacting the double-faced 31-inch W-beam guardrail at 62 mph (100 km/h) and 25°.

4.2.2 Ford F250 Impact at MASH TL-4 & TL-5 Conditions

Figure 4.27 shows the top view of the vehicle trajectory for the Ford F250 while impacting the double-faced 31-inch W-beam guardrail at 62 mph (100 km/h) and 25°. The Ford F250 was redirected by the guardrail with a slightly large exit angle compared to the case of impacting the 29-inch W-beam guardrail. The vehicle's tire tracks are outlined in white and the exit box was shown by the yellow dotted rectangle. Due to the relatively small exit angle, the vehicle traversed the length of the exit box with the tire tracks exiting along the right side of the exit box. This post impact trajectory is defined as a safe redirect as per the MASH exit box criterion.

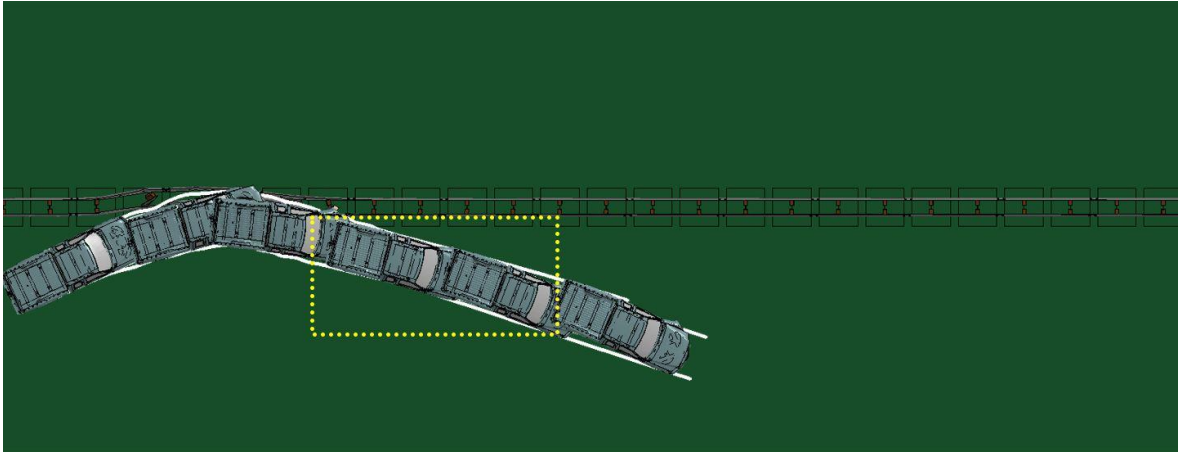


Fig. 4.27: A Ford F250 impacting the double-faced 31-inch W-beam guardrail at 62 mph (100 km/h) and 25°.

The yaw, pitch, and roll angles of the Ford F250 for Case 2 is shown in Fig. 4.28. The exit angle of the impact was determined to be -13° by adding the 25° impact angle to the -38° yaw angle at last contact with the guardrail at 0.86 seconds. The roll and pitch angles of the Ford F250 in this case were less than five degrees in both positive and negative directions and thus passed the MASH evaluation criterion F , which specified a maximum 75° roll or pitch angle.

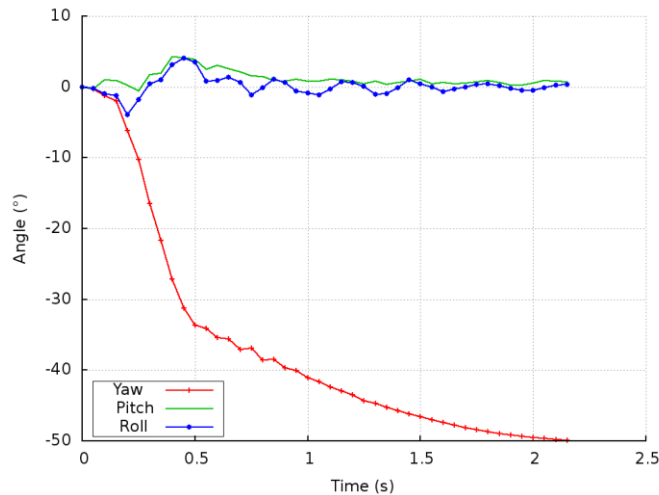


Fig. 4.28: Yaw, pitch, and roll angles of Ford F250 impacting the double-faced 31-inch W-beam guardrail at 62 mph (100 km/h) and 25°.

Figure 4.29 shows the maximum dynamic deflection of the double-faced 31-inch W-beam guardrail impacted by the Ford F250 at 62 mph (100 km/h) and 25°. The maximum dynamic deflection of the guardrail for this case was 3.86 ft (1.18 m) occurring at 0.2 seconds during the impact. The transverse deflection of the guardrail was slightly larger than that of the double-faced 29-inch W-beam guardrail impacted by the Ford F250. This was because the Ford F250's bumper height matched the median height of the 31-inch guardrail, allowing more direct and prolonged interaction with the guardrail. The damaged section of the double-faced 31-inch W-beam guardrail consisted of five posts spanning four guardrail segments. Figure 4.30 shows detailed views of vehicle-barrier interactions at the point of max deflection at 0.2 seconds.

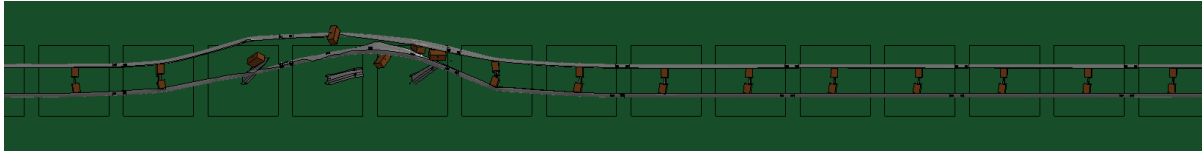


Fig. 4.29: Maximum dynamic deflection of the double-faced 31-inch W-beam guardrail at 62 mph (100 km/h) and 25° and impacted by a Ford F250.



Fig. 4.30: Simulations of Ford F250 impacting the double-faced 31-inch W-beam guardrail at 62 mph (100 km/h) and 25°.

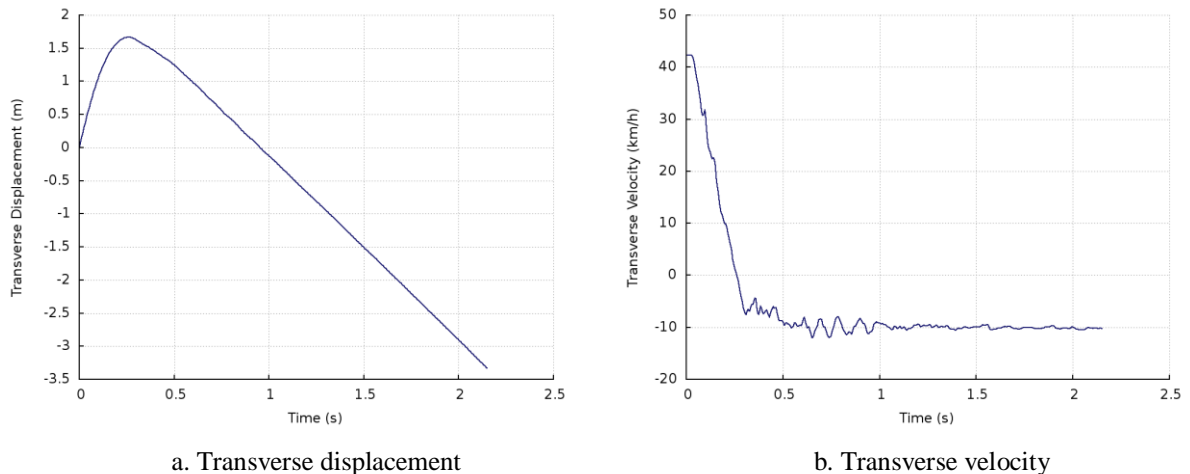


Fig. 4.31: Transverse displacement and velocity of the Ford F250 impacting the double-faced 31-inch W-beam guardrail at 62 mph (100 km/h) and 25°.

Figure 4.31 show the time histories of transverse displacement and velocity measured at the CG point of the Ford F250 impacting the double-faced 31-inch W-beam guardrail. The

maximum transverse displacement at 0.2 seconds (see Fig. 4.31a) coincides with the state of maximum deflection and the point where the vehicle began to redirect away from the guardrail. At 0.86 seconds, the vehicle lost contact with the guardrail with a transverse velocity of approximately 6.2 mph (10 km/h). In this case, the Ford F250 had a relatively small chance of being involved in a secondary collision based on the results from Figs. 4.27 through 4.30.

4.2.3 Single-unit Truck Impact at MASH TL-4 Conditions

Figure 4.32 shows the top view of vehicle trajectory of the single-unit truck impacting the double-faced 31-inch W-beam guardrail at 56 mph (90 km/h) and 15°. The guardrail is shown in its deformed state with the tire tracks outlined in white. Upon impacting the guardrail, the vehicle failed to remain upright and rolled onto the guardrail. For this impact behavior, the exit angle and exit box were not required. The vehicle's rollover onto the guardrail can be attributed to the higher center of gravity and long rigid wheelbase that does not allow the tail end to articulate and rotate around the guardrail. The rotation of the rigid wheelbase increased the likelihood of larger roll angles as the tail end of the truck impacted the guardrail. It should be noted that, although the single-unit truck failed to remain upright in this case, it was acceptable as per the MASH statement, "although it is preferable all vehicles remain upright, this requirement is not applicable for tests involving the 10000S (i.e., single-unit truck) and 36000V (i.e., tractor-trailer) vehicles." This exception of allowing a 90° roll angle for heavy vehicle impacts was based on the fact that the primary goal of this impact test is to demonstrate the guardrail's ability to contain and redirect the vehicle.

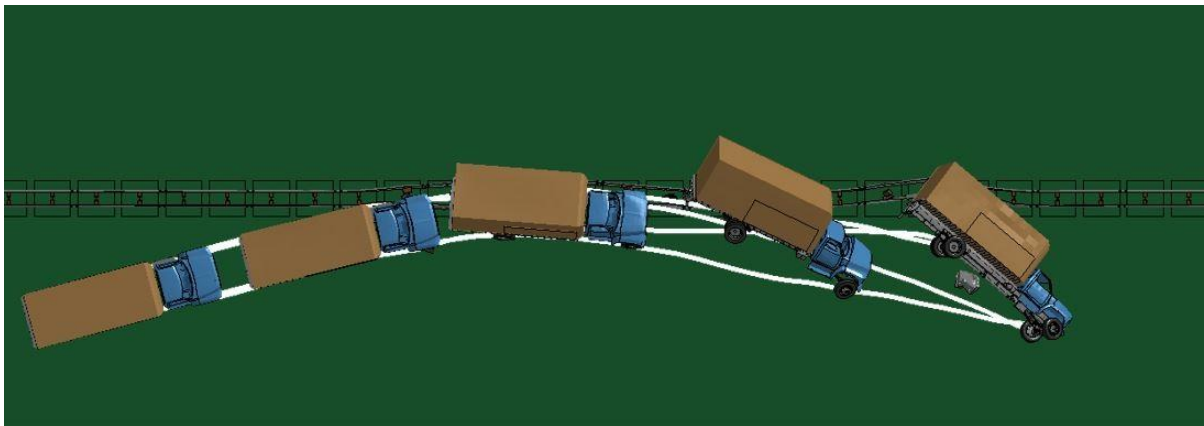


Fig. 4.32: A single-unit truck impacting the double-faced 31-inch W-beam guardrail at 56 mph (90 km/h) and 15°.

The yaw, pitch, and roll angles of the single-unit truck is shown in Fig. 4.33 for its impact on the double-faced 31-inch W-beam guardrail at 56 mph (90 km/h) and 15°. Due to the increased height of the CG point of the single-unit truck, the vehicle's roll angle surpassed 45°, resulting an imminent rollover. Since the vehicle failed to remain upright, the impact did not pass the MASH evaluation criterion F for the roll angle, which specified a maximum 75° roll or pitch angle.

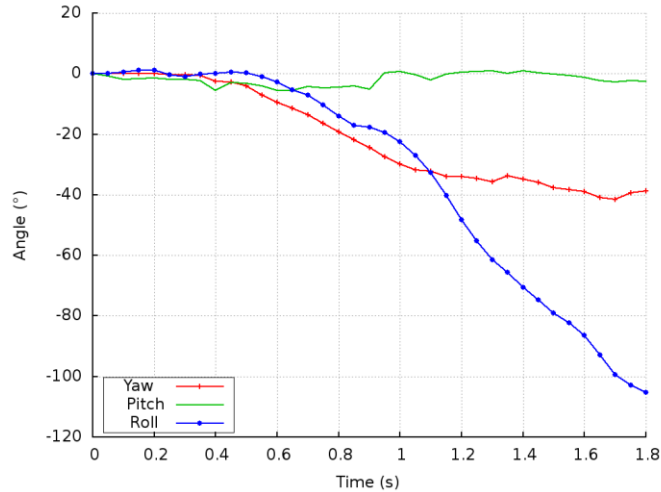


Fig. 4.33: Yaw, pitch, and roll angles of a single-unit truck impacting the double-faced 31-inch W-beam guardrail at 56 mph (90 km/h) and 15°.

Figure 4.34 shows the maximum dynamic deflection of the double-faced 31-inch W-beam guardrail impacted by the single-unit truck at 56 mph (90 km/h) and 15°. The maximum dynamic deflection of the guardrail in this impact was determined to be 3.85 ft (1.17 m) at 0.86 seconds. Due to the vehicle’s impact behavior, the guardrail damage was severe. The damaged guardrail spanned 15 posts on eight double-faced guardrail segments. The maximum dynamic deflection the 31-inch W-beam guardrail was 20.1 inches (0.51 m) more than that of the double-faced 29-inch W-beam guardrail. At the 31-inch guardrail height, the guardrail had very small engagement with the vehicle due to its higher ride height. The vehicle-barrier interaction was limited to mainly the vehicle’s tires and wheels as seen in Fig. 4.35.

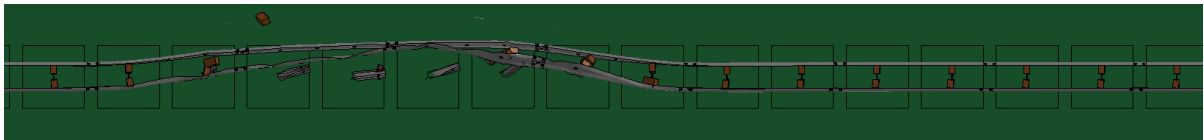


Fig. 4.34: Maximum dynamic deflection of the double-faced 31-inch W-beam guardrail at 56 mph (90 km/h) and 15° and impacted by a single-unit truck.



Fig. 4.35: Simulations of a single-unit truck impacting the double-faced 31-inch W-beam guardrail at 56 mph (90 km/h) and 15°.

Figure 4.36 shows the time histories of transverse displacements and velocities measured at the CG point of the truck cabin while impacting the double-faced 31-inch W-beam guardrail at 56 mph (90 km/h) and 15°. In Fig. 4.36a, the transverse displacements of the single-unit truck transitioned from an increasing trend to a decreasing one after the point of maximum guardrail deflection shown in Fig. 4.34. Unlike the case of the double-faced 29-inch W-beam guardrail, the single-unit truck impacting the double-faced 31-inch W-beam guardrail experienced a large yaw rotation while rolling on the guardrail. The increasing yaw angle explains the presence of the transverse displacement away from the guardrail in this case. The transverse velocity of the single-unit truck (Fig. 4.36b) was approximately 11 mph (18 km/h) at the end of the impact scenario, which would normally indicate a possibility of further displacement towards the travel lane. However, since the vehicle rolled over, the chance at which the vehicle would travel back to the travel lane was significantly reduced.

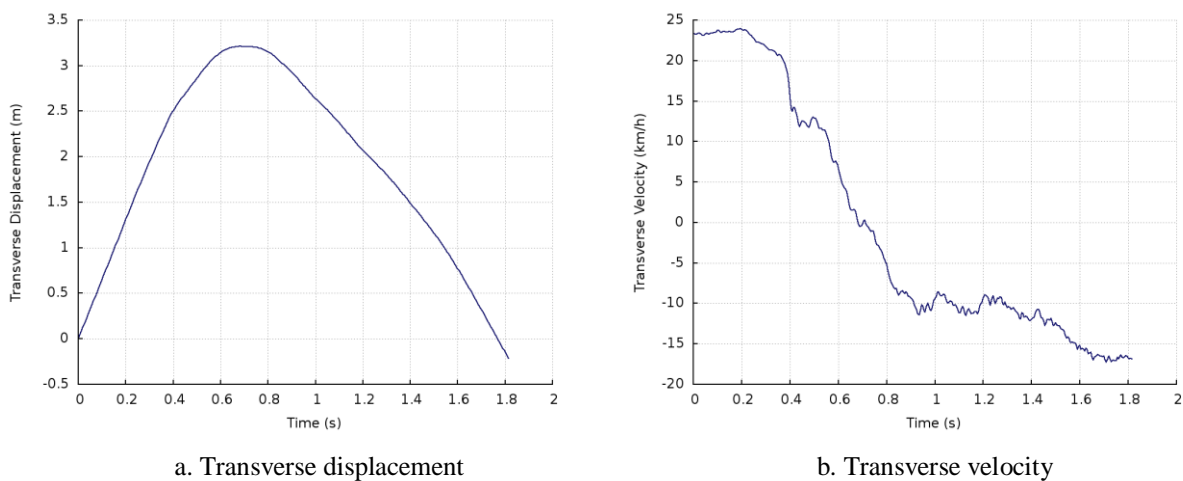


Fig. 4.36: Transverse displacement and velocity of the single-unit truck impacting the double-faced 31-inch W-beam guardrail at 56 mph (90 km/h) and 15°.

4.2.4 Tractor-trailer Impact at MASH TL-5 Conditions

Figure 4.37 shows the top view vehicle overlay trajectory of the tractor-trailer impacting the double-faced 31-inch W-beam guardrail at 50mph (80 km/h) and 15°. The W-beam guardrail is shown in its deformed state with the vehicle tire tracks outlined in white. The MASH exit box is shown by the yellow dotted rectangle. In this case, the tractor-trailer was redirected by the guardrail with a low exit angle and traveled the entire length of the exit box, thus meeting the MASH exit box criterion.

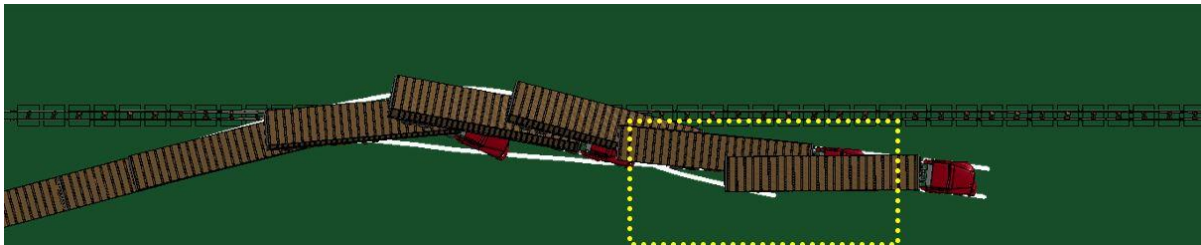


Fig. 4.37: A tractor-trailer impacting the double-faced 31-inch W-beam guardrail at 50 mph (80 km/h) and 15°.

The yaw, pitch, and roll angles of the tractor and trailer during the impact are shown in Fig. 4.38. The exit angle was determined to be -7° by adding the 15° impact angle to the -22° yaw angle at the trailer's last contact point with the guardrail at 2.4 seconds. In Fig. 4.38a, the transition of the tractor yaw angle at 1.05 seconds indicates the beginning of redirection away from the guardrail between 1.1-1.8 seconds. The redirection of the trailer tandem axle is seen at 1.7 seconds from the transition to positive roll and yaw angles, as seen in Fig. 4.18b. The maximum roll angles of the tractor and trailer were, 10.9° and 14.5° , respectively. In addition to these small roll angles, the pitch angles in this impact were less than five degrees in both positive and negative directions and thus passed the MASH evaluation criterion F , which specified a maximum roll or pitch angle of 75° .

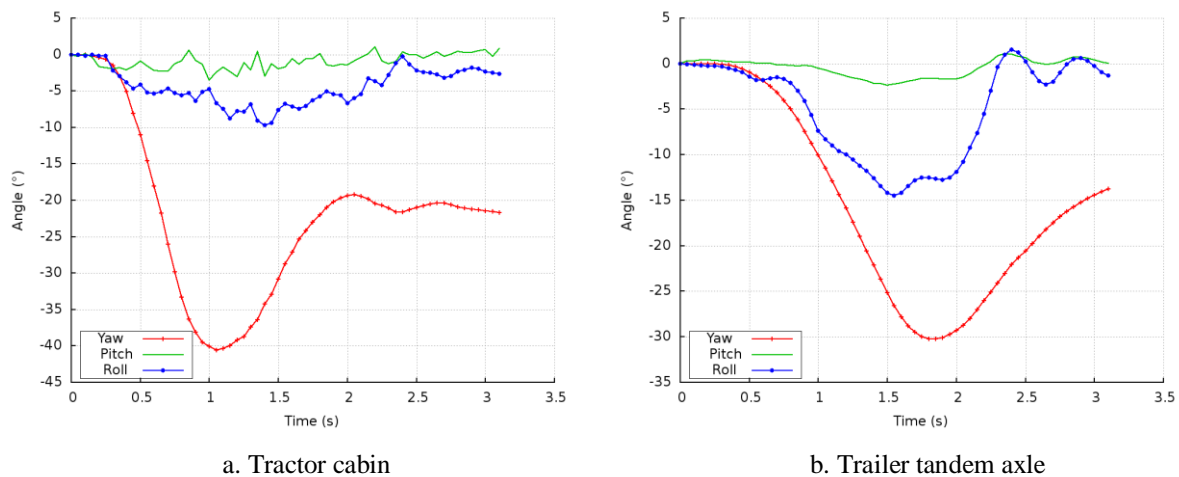


Fig. 4.38: Yaw, pitch, and roll angles of the tractor's (a) cabin and trailer's (b) tandem axle impacting the double-faced 31-inch W-beam guardrail at 50 mph (80 km/h) and 15° .

The maximum dynamic deflection of the double-faced 31-inch W-beam guardrail impacted by the tractor-trailer at 50 mph (80 km/h) and 15° is shown in Fig. 4.39. The maximum dynamic deflection of the guardrail was 8.6 ft (2.63 m), which occurred at 1.7 seconds. This deflection state coincided with the redirection of the trailer articulating about the kingpin joint as it rotated towards the guardrail after the tractor was redirected. The guardrail deflection is rather large, severely deforming 14 posts and 8 double-faced guardrail segments throughout the impact.



Fig. 4.39: Maximum dynamic deflection of the double-faced 31-inch W-beam guardrail at 50 mph (80 km/h) and 15° and impacted by a tractor-trailer.

Figure 4.40 shows detailed views of two different states of vehicle-barrier interaction throughout the tractor-trailer impact against the double-faced 31-inch W-beam guardrail at 50 mph (80 km/h) and 15° . Figure 4.20a illustrate the impact of the tractor at 0.6 seconds while Fig. 4.20b illustrate the trailer impact at the state of maximum dynamic deflection, which occurred at 1.7 seconds.

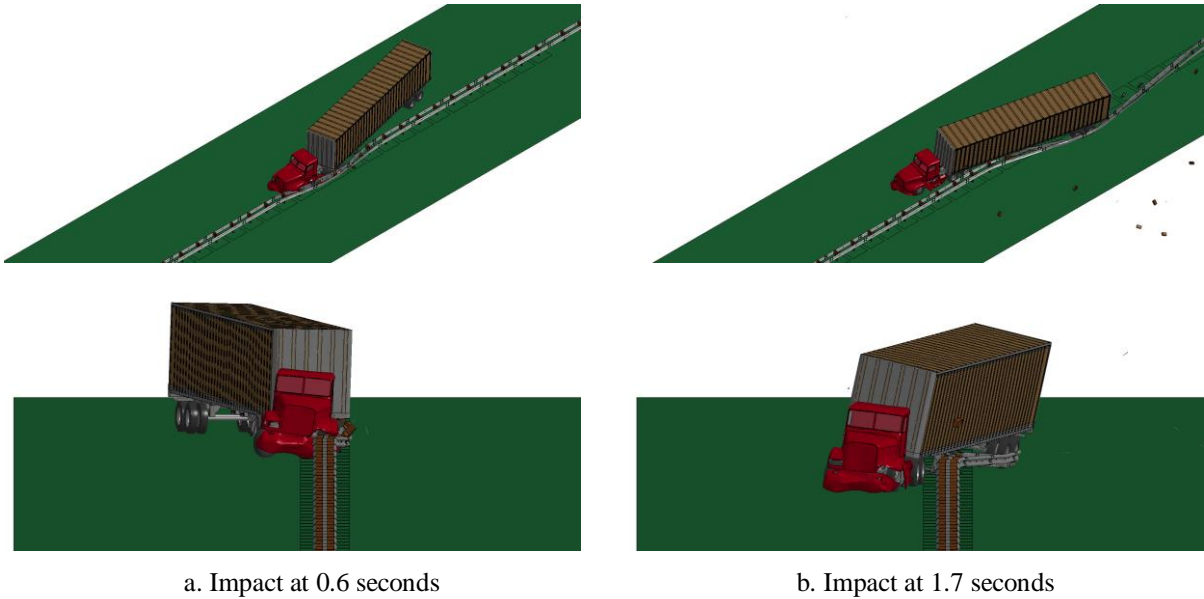
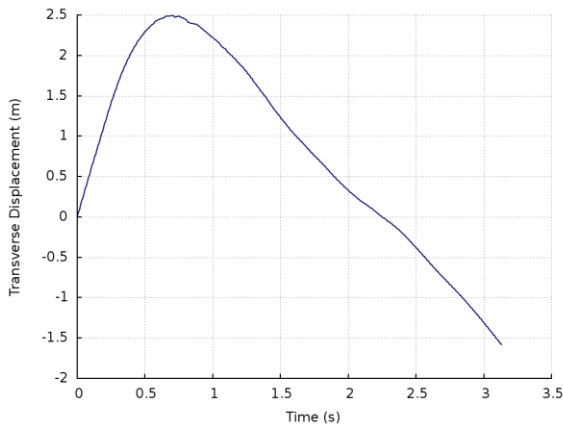
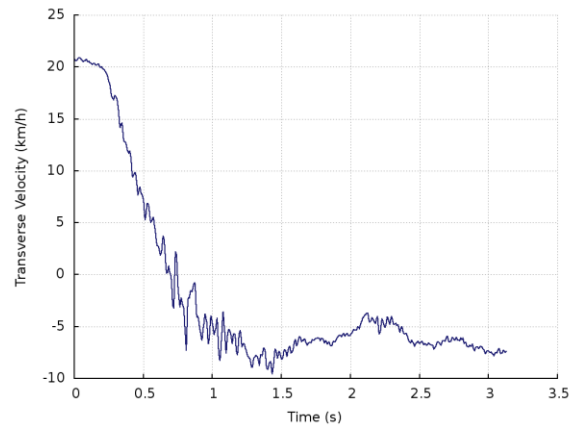


Fig. 4.40: Simulations of a tractor-trailer impacting the double-faced 31-inch W-beam guardrail at 50 mph (80 km/h) and 15°.

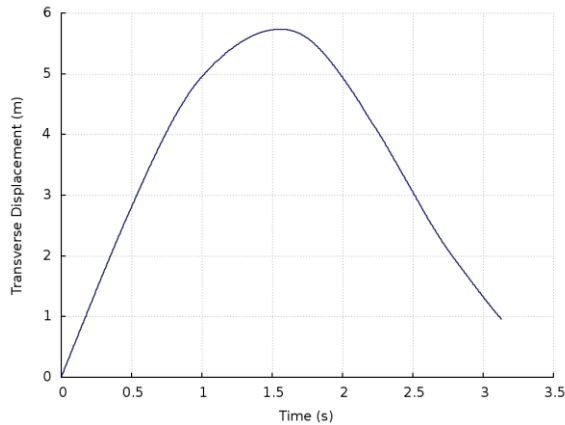
Figure 4.41 show the time histories of transverse displacements and velocities measured at the CG point of the tractor and at the trailer tandem axle in this impact case. Figure 4.41a shows the tractor's transverse displacements throughout the impact. The maximum positive transverse displacement occurred at 0.7 seconds, which immediately followed the impact state seen in Fig. 4.40a. Similarly in Fig. 4.41c, the maximum displacement of the trailer tandem axle's occurred at 1.6 seconds, which corresponded to the impact state illustrated in Fig. 4.40b. The transverse velocity of the tractor, as shown in Fig. 4.41b, was approximately 4.3 mph (7 km/h) towards the travel lane at the end of the impact scenario, while the trailer's transverse velocity was approximately 6.2 mph (10 km/h) as seen in Fig. 4.41d. Considering the exit box criterion, exit angle, and transverse velocity, the tractor-trailer had a low potential of reentering into the travel lane and being involved in a secondary collision.



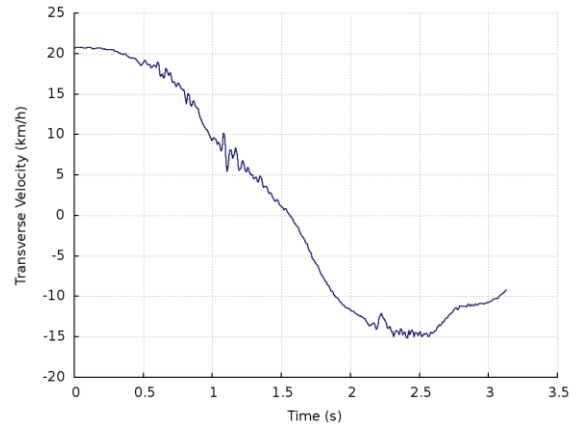
a. Tractor transverse displacement



b. Tractor transverse velocity



c. Trailer axle transverse displacement



d. Trailer axle transverse velocity

Fig. 4.41: Transverse displacement and velocities of the tractor-trailer impacting the double-faced 31-inch W-beam guardrail at 50 mph (80 km/h) and 15°.

4.3 Case 3: Double-faced 29-inch Thrie-beam Guardrails

In this case, the double-faced 29-inch wood- and steel-blockout Thrie-beam guardrails were evaluated under impacts by a small sedan, pickup truck, single-unit truck, and tractor-trailer (i.e., MASH TL-4 and TL-5 conditions). An impact angle of 25° was used for impacts by the small sedan (i.e., Dodge Neon) and pickup truck (i.e., Ford F250), and an impact angle of 15° was used for impacts of the single-unit truck and tractor-trailer. The impact speeds were 62 mph (100 km/h) for the Dodge Neon and Ford F250, 56 mph (90 km/h) for the single-unit truck, and 50 mph (80 km/h) for the tractor-trailer, respectively. Since the impacts by Dodge Neon and Ford F250 are identical in MASH TL-4 and TL-5 impact conditions, the simulation results are only listed and discussed once. Table 4.5 gives a summary of simulation results for Case 3 on the guardrail performance in terms of vehicular responses.

4.3.1 Dodge Neon Impact at MASH TL-4 & TL-5 Conditions

Figure 4.42 shows the top view vehicle trajectory of the Dodge Neon impacting the double-faced 29-inch wood-blockout Thrie-beam guardrail at 62 mph (100 km/h) and 25°. The wood-blockout Thrie-beam guardrail is shown in its deformed state with the vehicle tire tracks outlined in white and the exit box, placed at the last point of contact of the vehicle's tire tracks to the initial guardrail face, is shown by the yellow dotted rectangle. Upon impacting the Thrie-beam guardrail, the Dodge Neon was redirected by the guardrail and lost contact with the guardrail with an exit angle small enough to pass the MASH exit box criterion. Figure 4.43 shows the top view vehicle trajectory of the Dodge Neon impacting the double-faced 29-inch steel-blockout Thrie-beam guardrail at 62 mph (100 km/h) and 25°. The steel-blockout Thrie-beam guardrail is shown in its deformed state and the exit box shown by the yellow dotted rectangle. Compared to the wood-blockout Thrie-beam guardrail, the steel-blockout Thrie-beam guardrail had a more rigid response and thus redirected the Dodge Neon with a large exit angle that failed the MASH exit box criterion.

Table 4.5: Simulation results of Case 3 (Double-faced 29-inch Wood- and Steel-blockout Thrie-beam Guardrails)

Test Vehicle	MASH Level	Impact Angle	Impact Velocity	Blockout Type	Simulation Results
Dodge Neon	TL-4 & TL-5	25°	62 mph (100 km/h)	Wood	The vehicle passed the exit box criterion and was safely redirected
				Steel	The vehicle was redirected by the guardrail with a large exit angle and failed the exit box criterion
Ford F250	TL-4 & TL-5	25°	62 mph (100 km/h)	Wood	The vehicle was redirected by the guardrail with a large exit angle and failed the exit box criterion
				Steel	The vehicle was redirected after vaulting up the guardrail and passed the exit box criterion
Single-Unit Truck	TL-4	15°	56 mph (90 km/h)	Wood	The vehicle failed to remain upright and rolled onto the guardrail
				Steel	The vehicle failed to remain upright and rolled onto the guardrail
Tractor-Trailer	TL-5	15°	50 mph (80 km/h)	Wood	The vehicle failed to remain upright and rolled onto the guardrail
				Steel	The vehicle failed to remain upright and rolled onto the guardrail

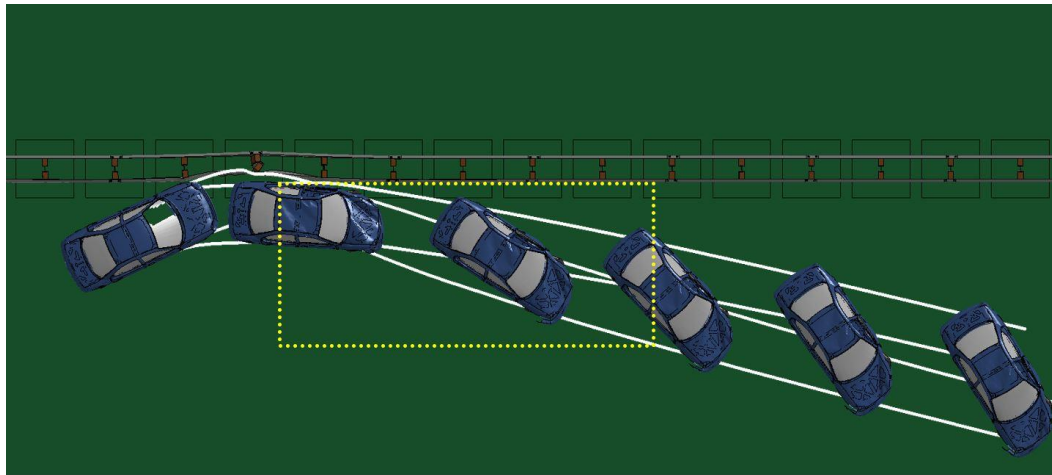


Fig. 4.42: A Dodge Neon impacting the double-faced 29-inch wood-blockout Thrie-beam guardrail at 62 mph (100 km/h) and 25°.

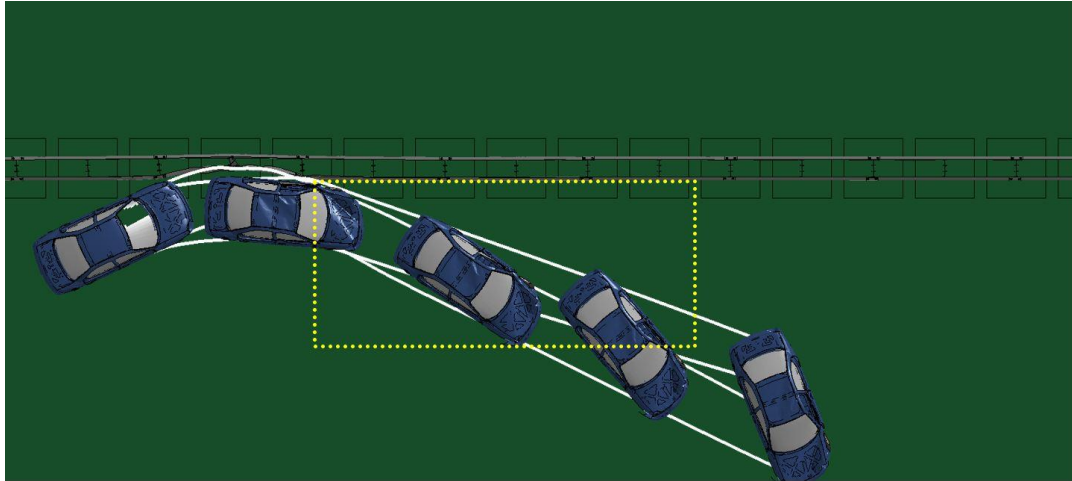


Fig. 4.43: A Dodge Neon impacting the double-faced 29-inch steel-blockout Thrie-beam guardrail at 62 mph (100 km/h) and 25°.

The yaw, pitch, and roll angles of the Dodge Neon impacting the double-faced 29-inch wood- and steel-blockout Thrie-beam guardrails are shown in Figs. 4.44a and 4.44b, respectively. In both cases, the vehicle was redirected with an exit angle of -22.5° for impact on the 29-inch wood-blockout Thrie-beam guardrail, and -24° for impact on the steel-blockout Thrie-beam guardrail. The exit angle was determined by adding the 25° impact angle to the yaw angle at the point of last contact with the guardrail, at 0.42 seconds (i.e., -47.5°) and 0.4 seconds (i.e., -49°) for the wood-blockout and steel-blockout Thrie-beam guardrails, respectively.

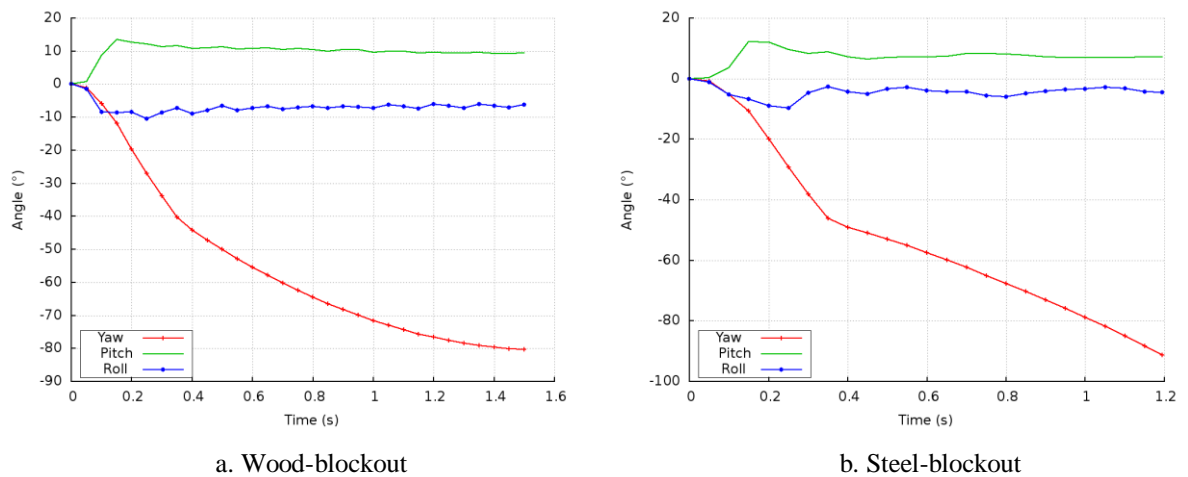


Fig. 4.44: Yaw, pitch, and roll angles of Dodge Neon impacting the double-faced 29-inch (a) wood- (b) steel-blockout Thrie-beam guardrail at 62 mph (100 km/h) and 25°.

Comparing the wood- and steel-blockout guardrails, both redirected the Dodge Neon in the same amount of time, but the steel-blockout Thrie-beam guardrail redirected the vehicle with a two-degree larger exit angle than the wood-blockout guardrail and failed the MASH exit box criterion. From the time histories of the yaw angles in Figs. 4.44a and 4.44b, it can be seen that the Dodge Neon was redirected almost immediately and then started to rotate away from the

guardrail as indicated by the steadily increasing negative yaw angles. The roll and pitch angles in both impacts were less than fifteen degrees in both positive and negative directions and thus passed the MASH evaluation criterion F , which specified a maximum 75° roll or pitch angle.

Figures 4.45 and 4.46 show the maximum dynamic deflections of the double-faced 29-inch wood- and steel-blockout Thrie-beam guardrails impacted by the Dodge Neon at 62 mph (100 km/h) and 25° . The maximum dynamic deflection of the wood-blockout Thrie-beam guardrail was 1.45 ft (0.44 m) at 0.085 seconds and the maximum dynamic deflection of the steel-blockout Thrie-beam guardrail was 1.53 ft (0.47 m) at 0.09 seconds. Under impacts by the Dodge Neon, the double-faced 29-inch steel-blockout Thrie-beam guardrails had a slightly larger deflection than the wood-blockout guardrail, yet the damaged sections of both guardrails were relatively small and localized; the damaged sections affected three posts across two double-faced guardrail segments.

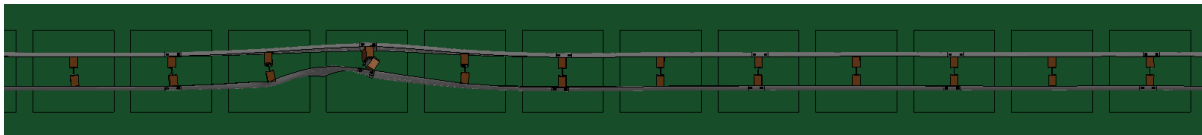


Fig. 4.45: Maximum dynamic deflection of the double-faced 29-inch wood-blockout Thrie-beam guardrail at 62 mph (100 km/h) and 25° and impacted by a Dodge Neon.

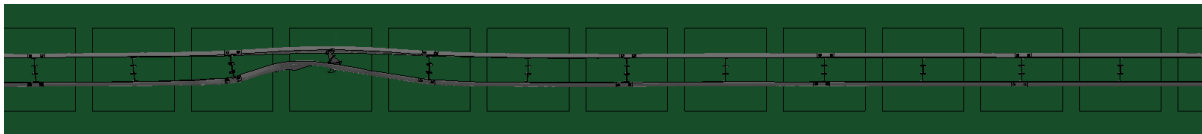


Fig. 4.46: Maximum dynamic deflection of the double-faced 29-inch steel-blockout Thrie-beam guardrail at 62 mph (100 km/h) and 25° and impacted by a Dodge Neon.

Figures 4.47 and 4.48 show detailed views of the vehicle-barrier interactions at the point of maximum dynamic deflections while the Dodge Neon impacts the double-faced 29-inch wood- and steel-blockout Thrie-beam guardrails, respectively, at 62 mph (100 km/h) and 25° . Since the rail face of the double-faced 29-inch Thrie-beam guardrails extended lower than the W-beam guardrails, Dodge Neon was prevented from underriding the Thrie-beam guardrail.

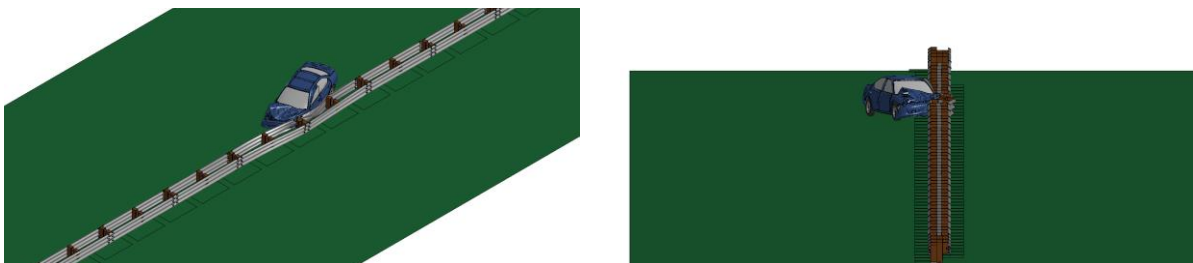


Fig. 4.47: Simulations of Dodge Neon impacting the double-faced 29-inch wood-blockout Thrie-beam guardrail at 62 mph (100 km/h) and 25° .

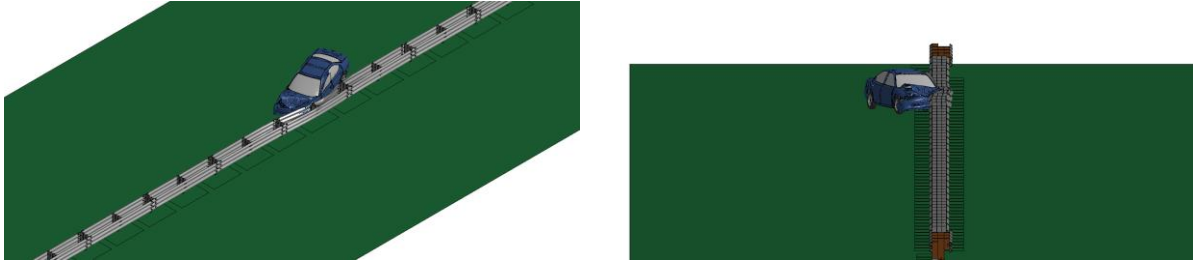
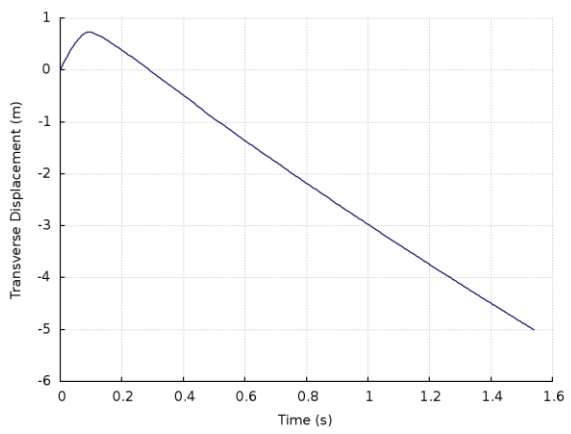
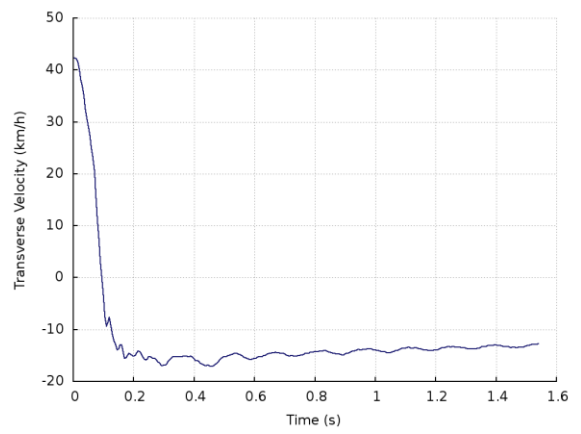


Fig. 4.48: Simulations of Dodge Neon impacting the double-faced 29-inch steel-blockout Thrie-beam guardrail at 62 mph (100 km/h) and 25°.

Figures 4.49 and 4.50 show the time histories of transverse displacements and velocities measured at the CG point of the Dodge Neon during impacts on the double-faced 29-inch wood- and steel-blockout Thrie-beam guardrails at 62 mph (100 km/h) and 25°. In Fig. 4.49a, the maximum positive transverse displacement of the Dodge Neon occurred at 0.085 seconds, which corresponded with the state of maximum guardrail deflection as seen in Fig. 4.45. Similarly, in Fig. 4.50a, the maximum positive transverse displacement of the Dodge Neon occurred at 0.09 seconds, correlating with the state of maximum guardrail deflection as seen in Fig. 4.46. Comparing these two 29-inch Thrie-beam guardrails, the steel-blockout Thrie-beam guardrail redirected the Dodge Neon more gradually over a longer period of time but deflected more than the wood-block one. The more abrupt redirection by the wood-blockout Thrie-beam guardrail is confirmed by the steep slope of the transverse velocity curve from 0 to 0.2 seconds in Fig 4.49b, compared to that of the steel-blockout Thrie-beam guardrail in Fig. 4.50b. At the end of the impact scenarios, the transverse velocities of the Dodge Neon were approximately 7.5 mph (12 km/h) for the wood-block guardrail and 13 mph (21 km/h) for the steel-blockout guardrail. This increased transverse velocity towards the travel lane on the double-faced 29-inch steel-blockout Thrie-beam guardrail, along with the failure of the MASH exit box criterion, denoted a relatively high change of the vehicle reentering the travel lane and the potential of causing a secondary collision.

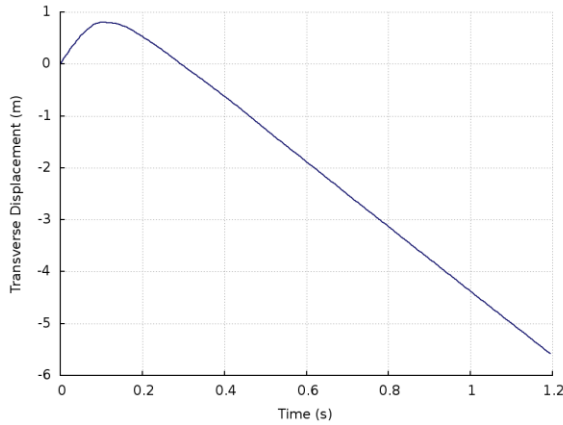


a. Transverse displacement

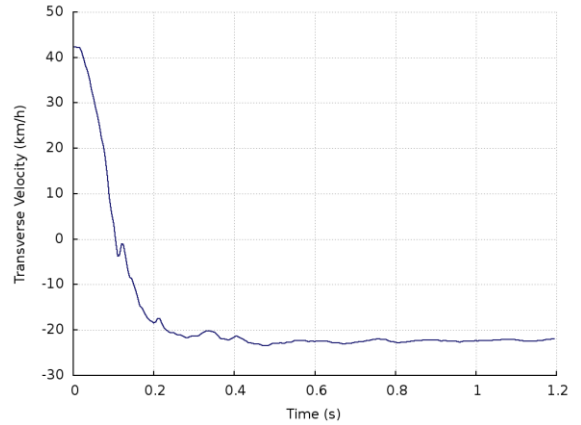


b. Transverse velocity

Fig. 4.49: Transverse displacement and velocity of the Dodge Neon impacting the double-faced 29-inch wood-blockout Thrie-beam guardrail at 62 mph (100 km/h) and 25°.



a. Transverse displacement



b. Transverse velocity

Fig. 4.50: Transverse displacement and velocity of the Dodge Neon impacting the double-faced 29-inch steel-blockout Thrie-beam guardrail at 62 mph (100 km/h) and 25°.

4.3.2 Ford F250 Impact at MASH TL-4 & TL-5 Conditions

Figure 4.51 shows the top view vehicle trajectory of the Ford F250 impacting the double-faced 29-inch wood-blockout Thrie-beam guardrail at 62 mph (100 km/h) and 25°. The wood-blockout Thrie-beam guardrail is shown in its deformed state with the vehicle's tire tracks outlined in white and the exit box shown by the yellow dotted rectangle. Upon impacting the double-faced 29-inch wood-blockout Thrie-beam guardrail, the Ford F250 was redirected by the guardrail and lost contact with the guardrail with a large negative exit angle and the vehicle traveled transversely away from the guardrail, failing to pass the MASH exit box criterion.

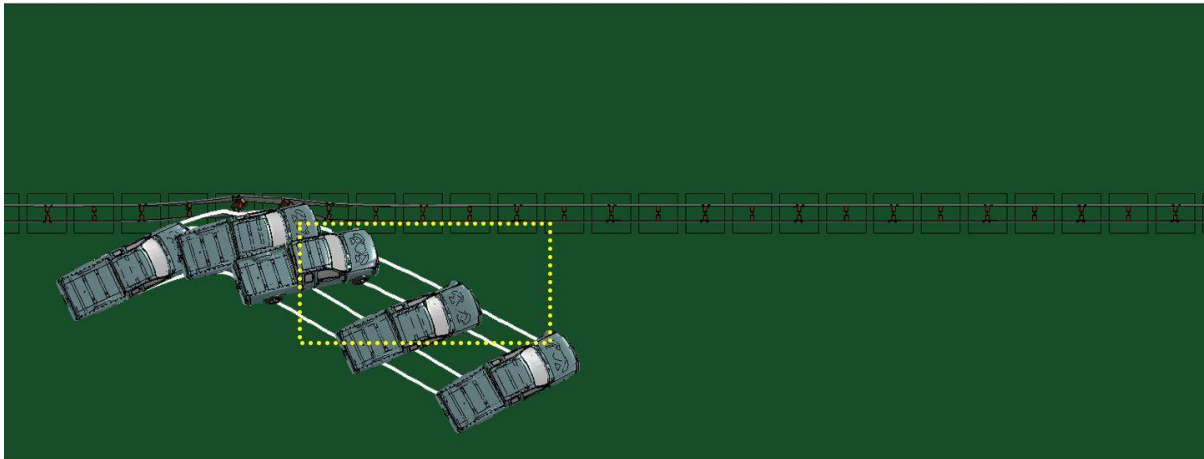


Fig. 4.51: A Ford F250 impacting the double-faced 29-inch wood-blockout Thrie-beam guardrail at 62 mph (100 km/h) and 25°.

Figure 4.52 shows the top view vehicle trajectory of the Ford F250 impacting the double-faced 29-inch steel-blockout Thrie-beam guardrail at 62 mph (100 km/h) and 25°. The steel-blockout Thrie-beam guardrail is shown in its deformed state and the exit box is shown by the yellow dotted rectangle. Upon impacting the steel-blockout Thrie-beam guardrail, the Ford F250 deflected the rails and posts, turned the guardrail's face into a makeshift slope, and became

partially airborne while being redirected on the impacting side of the guardrail. The vehicle remained upright and was successfully redirected with a small exit angle, thus passing the MASH exit box criterion. Compared to the double-faced wood-blockout Thrie-beam guardrail at 29-inch placement height, the steel-blockout Thrie-beam guardrail had a more rigid response, which caused the Ford F250 to lose contact with the guardrail with a small exit angle.

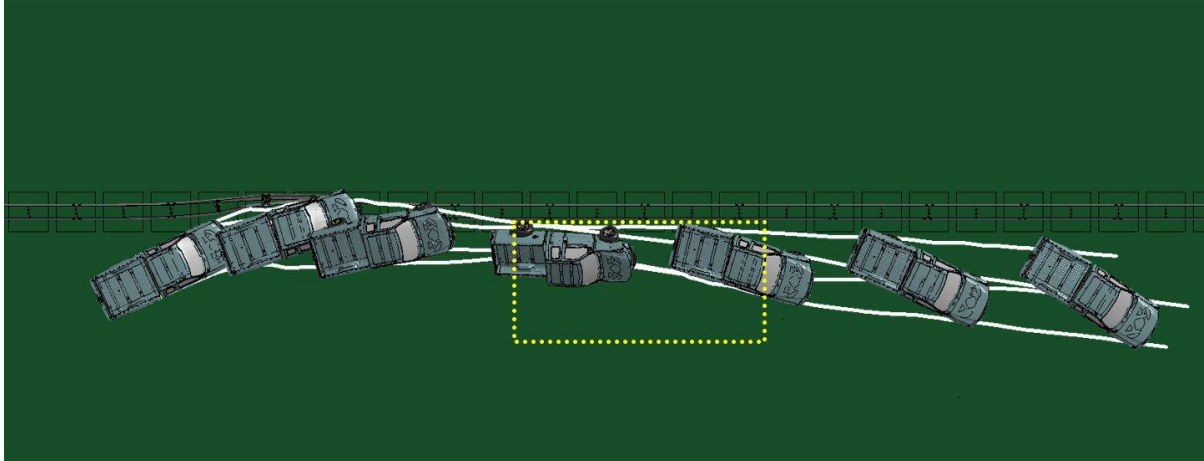


Fig. 4.52: A Ford F250 impacting the double-faced 29-inch steel-blockout Thrie-beam guardrail at 62 mph (100 km/h) and 25°.

The yaw, pitch, and roll angles of the Ford F250 in the impacts against the double-faced 29-inch wood- and steel-blockout Thrie-beam guardrails are shown in Figs. 4.53a and 4.53b. For the impact against the wood-blockout Thrie-beam guardrail, the vehicle was redirected with an exit angle of 14° by adding the 25° impact angle to the -11° yaw angle at the point of last contact with the guardrail at 0.45 seconds. This exit angle can be seen in Fig. 4.51 where the vehicle's orientation at the end of contact with the guardrail is comparable to its impact angle. For the impact against the steel-blockout Thrie-beam guardrail, the vehicle was safely redirected with an exit angle of -1.5° by adding the 25° impact angle to the -26.5° yaw angle at the point of last contact with the guardrail at 1.22 seconds.

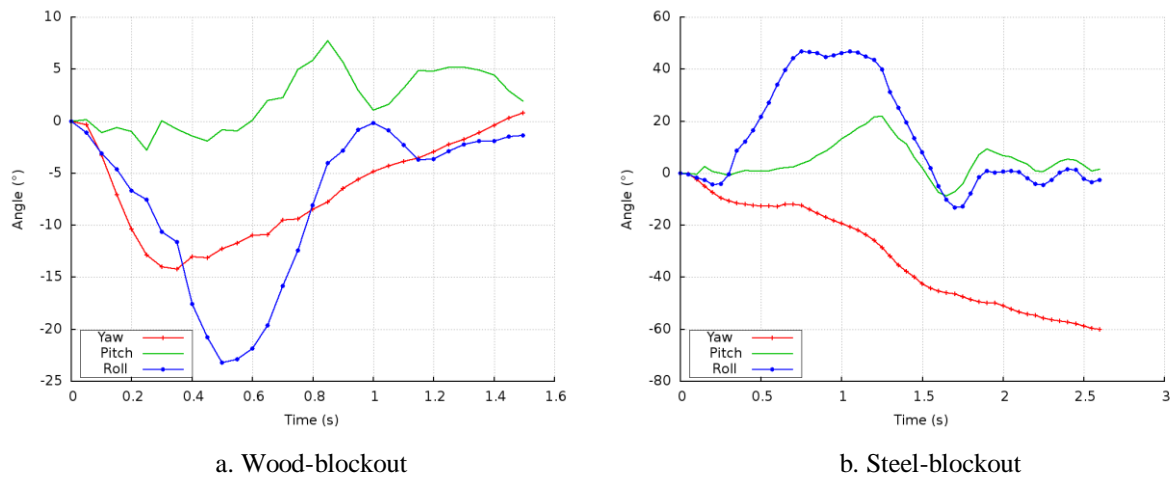


Fig. 4.53: Yaw, pitch, and roll angles of Ford F250 impacting the double-faced 29-inch (a) wood- (b) steel-blockout Thrie-beam guardrail at 62 mph (100 km/h) and 25°.

From the time histories of roll angles in Figs. 4.53a and 4.53b, it can be seen that in both impact cases, the Ford F250 experienced substantially higher roll angles compared to impacts on the W-beam guardrail. For impacts on the wood- and steel-blockout Thrie-beam guardrails, the largest roll angles were -24° and 47° , respectively. The pitch angles in both impacts was less than 24 degrees in both positive and negative directions. Although these roll and pitch angles were larger than those in previous cases, they still passed the MASH evaluation criterion F , which specified a maximum 75° roll or pitch angle.

Figures 4.54 and 4.55 shows the maximum dynamic deflections of the double-faced 29-inch wood- and steel-blockout Thrie-beam guardrails impacted by the Ford F250 at 62 mph (100 km/h) and 25° . The maximum dynamic deflections of the wood- and steel-blockout Thrie-beam guardrails were 2.75 ft (0.84 m) occurred at 0.125 seconds and 3.4 ft (1.04 m) occurred at 0.185 seconds, respectively. Comparing the two double-faced 29-inch Thrie-beam guardrails impacted by the Ford F250, the steel-blockout guardrail deformed 0.65 ft (0.2 m) further and resulted in a larger damaged section than the wood-blockout guardrail. Although the damaged sections of both guardrails were relatively small and localized, the steel-blockout Thrie-beam damage spanned four posts and two double-faced guardrail segments while the wood-blockout Thrie-beam damage only spanned three posts across two double-faced guardrail segments.

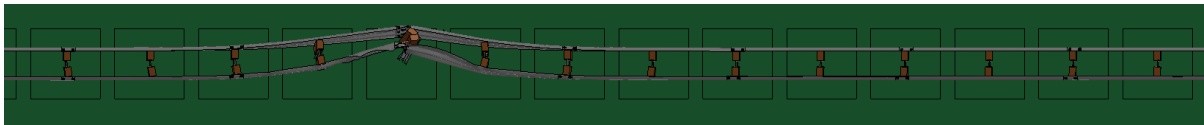


Fig. 4.54: Maximum dynamic deflection of the double-faced 29-inch wood-blockout Thrie-beam guardrail at 62 mph (100 km/h) and 25° and impacted by a Ford F250.



Fig. 4.55: Maximum dynamic deflection of the double-faced 29-inch steel-blockout Thrie-beam guardrail at 62 mph (100 km/h) and 25° and impacted by a Ford F250.

Figures 4.56 and 4.57 show detailed views of the vehicle-guardrail interactions at the point of maximum dynamic deflections while the Ford F250 impacts the double-faced 29-inch wood- and steel-blockout Thrie-beam guardrails at 62 mph (100 km/h) and 25° . Compared to the W-beam guardrails, the W-beam rail face of the Thrie-beam guardrails extended lower than that of the W-beam guardrail, and thus allowed for more direct contact with the vehicle's components on the impacting side, leading to quicker redirections with less deformations.

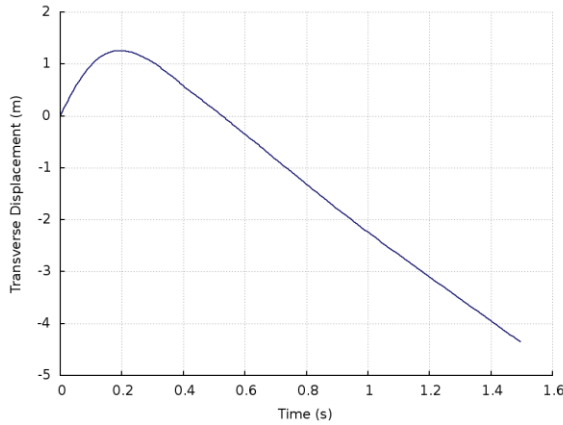


Fig. 4.56: Simulations of Ford F250 impacting the double-faced 29-inch wood-blockout Thrie-beam guardrail at 62 mph (100 km/h) and 25°.

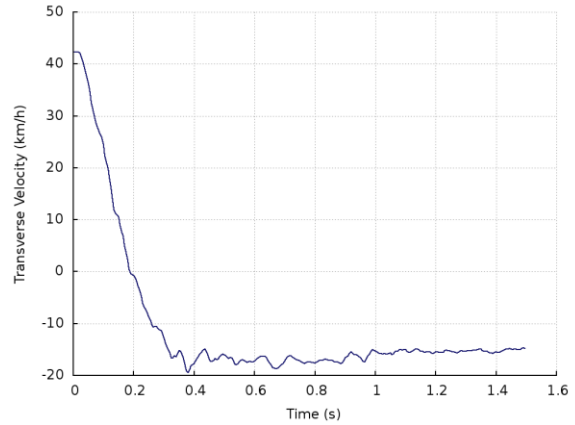


Fig. 4.57: Simulations of Ford F250 impacting the double-faced 29-inch steel-blockout Thrie-beam guardrail at 62 mph (100 km/h) and 25°.

Figures 4.58 and 4.59 show the time histories of transverse displacements and velocities measured at the CG point of the Ford F250 during impacts against the double-faced 29-inch wood- and steel-blockout Thrie-beam guardrails at 62 mph (100 km/h) and 25°. In Fig. 4.58a, the maximum positive transverse displacement of the Ford F250 occurred at 0.18 seconds, which corresponded to the state of maximum guardrail deflection seen in Fig. 4.56. Similarly, in Fig. 4.59a, the maximum positive transverse displacement of the Ford F250 occurred at 0.23 seconds, which also corresponded to the state of maximum guardrail deflection as seen in Fig. 4.57. Comparing the two double-faced 29-inch Thrie-beam guardrail under impacts from Ford F250 impacts, the steel-blockout Thrie-beam guardrail redirected the vehicle quicker, over a shorter period of time, but deflected more throughout the impact scenario. The more abrupt redirection from the steel-blockout Thrie-beam guardrail impact was confirmed by the steep slope on the transverse velocity curve from 0 to 0.4 seconds in Fig 4.59b. Towards the end of the impact against the wood-blockout Thrie-beam guardrail, the transverse velocity of the vehicle (see Fig. 4.58b) approximately 8.7 mph (14 km/h). Comparatively, the transverse velocity of the vehicle impacting the steel-blockout Thrie-beam guardrail was only 3.4 mph (5.5 km/h) at the end of the impact scenario. The increased transverse velocity towards the travel lane in the impact on the wood-blockout Thrie-beam guardrail, along with the failure to pass the MASH exit box criterion, denoted a relatively high potential of the vehicle reentering the travel lane and causing a secondary collision.

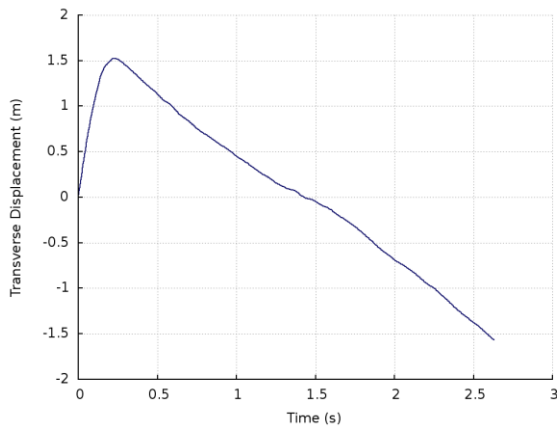


a. Transverse displacement

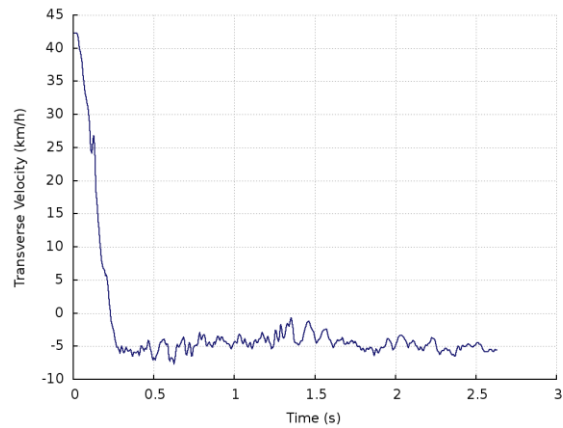


b. Transverse velocity

Fig. 4.58: Transverse displacement and velocity of the Ford F250 impacting the double-faced 29-inch wood-blockout Thrie-beam guardrail at 62 mph (100 km/h) and 25°.



a. Transverse displacement



b. Transverse velocity

Fig. 4.59: Transverse displacement and velocity of the Ford F250 impacting the double-faced 29-inch steel-blockout Thrie-beam guardrail at 62 mph (100 km/h) and 25°.

4.3.3 Single-unit Truck Impact at MASH TL-4 Conditions

Figure 4.60 shows the top view vehicle trajectory of the single-unit truck impacting the double-faced 29-inch wood-blockout Thrie-beam guardrail at 56 mph (90 km/h) and 15°. The wood-blockout Thrie-beam guardrail is shown in its deformed state with the vehicle tire tracks outlined in white. Upon impacting the wood-blockout Thrie-beam guardrail, the vehicle failed to remain upright and rolled onto the guardrail. For this vehicular response, the exit box was not required and the MASH exit box criterion was not applied. Figure 4.61 shows the top view vehicle trajectory of the single-unit truck impacting the double-faced 29-inch steel-blockout Thrie-beam guardrail at 56 mph (90 km/h) and 15°. The steel-blockout Thrie-beam guardrail is shown in its deformed state with the vehicle tire tracks outlined in white. Similar to the impact on the wood-blockout guardrail, the single-unit truck failed to remain upright and rolled onto the guardrail upon impacting the steel-blockout Thrie-beam guardrail; therefore, the MASH exit box criterion was not used in this impact scenario.

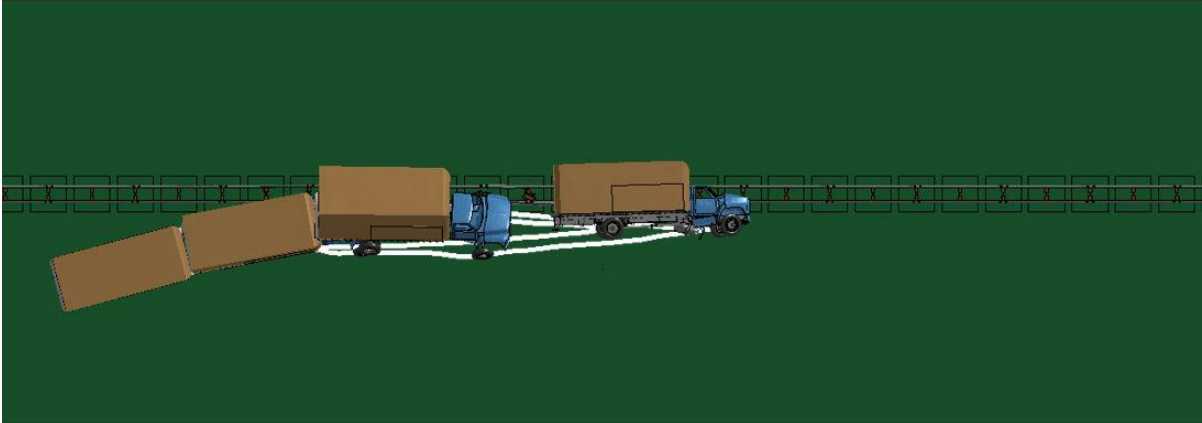


Fig. 4.60: A single-unit truck impacting the double-faced 29-inch wood-blockout Thrie-beam guardrail at 56 mph (90 km/h) and 15°.

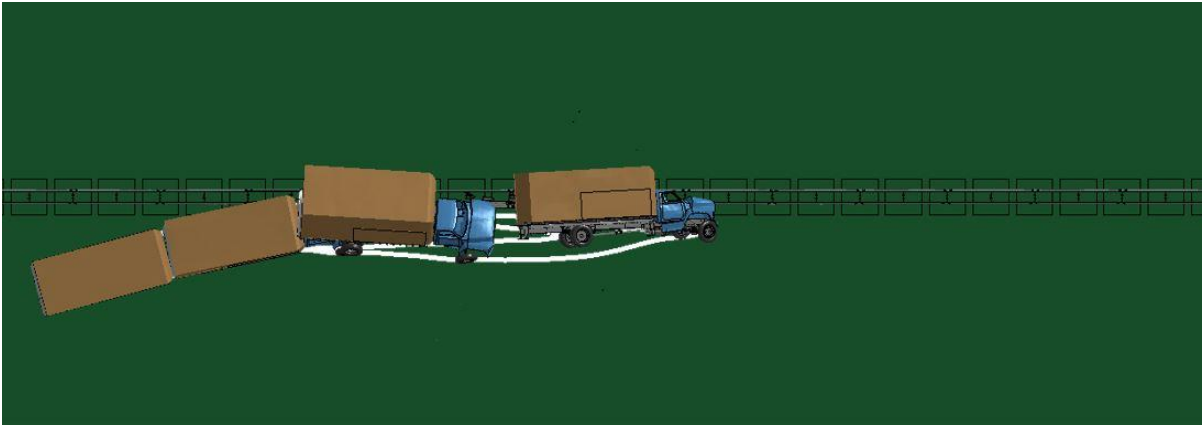


Fig. 4.61: A single-unit truck impacting the double-faced 29-inch steel-blockout Thrie-beam guardrail at 56 mph (90 km/h) and 15°.

It should be noted that, although the single-unit truck failed to remain upright in the impacts on both wood- and steel-blockout guardrails, it was not required to remain upright as per MASH, “although it is preferable all vehicles remain upright, this requirement is not applicable for tests involving the 10000S (i.e., single-unit truck) and 36000V (i.e., tractor-trailer) vehicles.” This exception of allowing a roll for heavy vehicle impacts was based on that the primary goal of the impact scenario was to demonstrate the guardrails ability to contain and redirect the vehicle.

The yaw, pitch, and roll angles of the single-unit truck in the impacts against the double-faced 29-inch wood- and steel-blockout Thrie-beam guardrails are shown in Figs. 4.62a and 4.62b. Due to the increased height of the single-unit truck’s CG point, the vehicle had an imminent rollover once its roll angle surpassed 45°. Since the single-unit truck failed to remain upright in both impacts against the 29-inch wood- and steel-blockout Thrie-beam guardrail, these two impacts did not pass the MASH evaluation criterion *F*, because the roll angles exceeded the 75° maximum allowable roll angle. Nevertheless, the single-unit truck was not required to remain upright according to MASH.

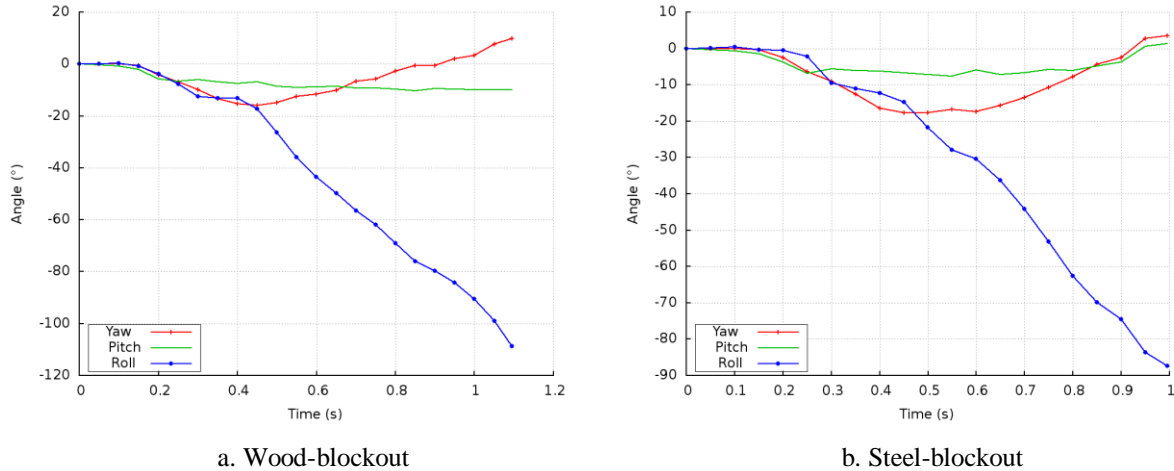


Fig. 4.62: Yaw, pitch, and roll angles of single-unit trucks impacting the double-faced 29-inch (a) wood- (b) steel-blockout Thrie-beam guardrail at 62 mph (100 km/h) and 25°.

Figures 4.63 and 4.64 show the maximum dynamic deflections of the double-faced 29-inch wood- and steel-blockout Thrie-beam guardrails impacted by the single-unit truck at 56 mph (90 km/h) and 15°. The maximum dynamic deflection was 0.9 ft (0.28 m) occurred at 1.1 seconds for the wood-blockout Thrie-beam guardrail and 1.1 ft (0.34 m) occurred at 0.61 seconds for the steel-blockout Thrie-beam guardrail. Under impacts by the single-unit truck, both the double-faced 29-inch Thrie-beam guardrails had nonlocalized, long damaged sections with the damage spreading between the impact point and the point where the vehicle rolled onto the guardrails. The damage on the wood-blockout Thrie-beam guardrail spanned eleven posts and six double-faced guardrail segments while the damage on the steel-blockout Thrie-beam guardrail spanned ten posts across five double-faced guardrail segments.

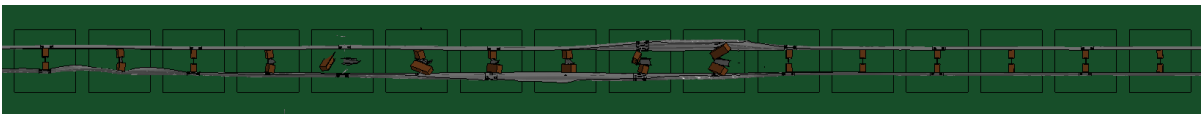


Fig. 4.63: Maximum dynamic deflection of the double-faced 29-inch wood-blockout Thrie-beam guardrail at 56 mph (90 km/h) and 15° and impacted by a single-unit truck.

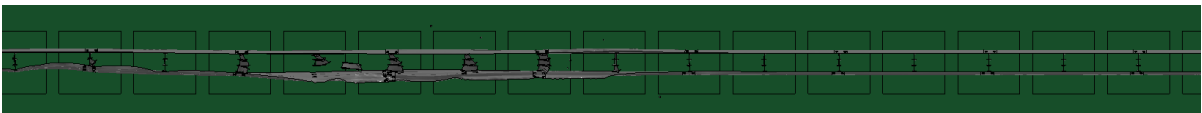


Fig. 4.64: Maximum dynamic deflection of the double-faced 29-inch steel-blockout Thrie-beam guardrail at 56 mph (90 km/h) and 15° and impacted by a single-unit truck.

Figures 4.65 and 4.66 show detailed views of the vehicle-barrier interactions at 0.4 seconds shortly after the single-unit truck impacts the double-faced 29-inch wood- and steel-blockout Thrie-beam guardrails at 56 mph (90 km/h) and 15°. Although the rail of Thrie-beam guardrails extended lower than the W-beam guardrail, the single-unit truck did not engage with more of the guardrail face due to the elevated ride height of the vehicle.



Fig. 4.65: Simulations of single-unit truck impacting the double-faced 29-inch wood-blockout Thrie-beam guardrail at 56 mph (90 km/h) and 15°.



Fig. 4.66: Simulations of single-unit truck impacting the double-faced 29-inch steel-blockout Thrie-beam guardrail at 56 mph (90 km/h) and 15°.

Figures 4.67 and 4.68 show the time histories of transverse displacements and velocities measured at the CG point of the single-unit truck impacting the double-faced 29-inch wood- and steel-blockout Thrie-beam guardrails at 56 mph (90 km/h) and 15°. In both Fig. 4.67a and 4.68a, the maximum positive transverse displacements of the single-unit truck occurred at the end of the impact scenarios due to the rollover behavior.

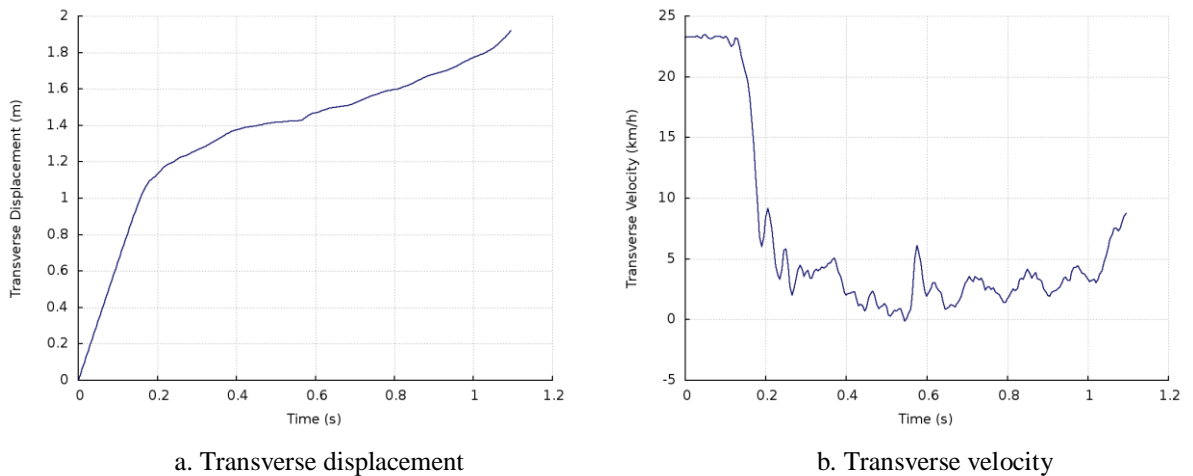


Fig. 4.67: Transverse displacement and velocity of the single-unit truck impacting the double-faced 29-inch wood-blockout Thrie-beam guardrail at 56 mph (90 km/h) and 15°.

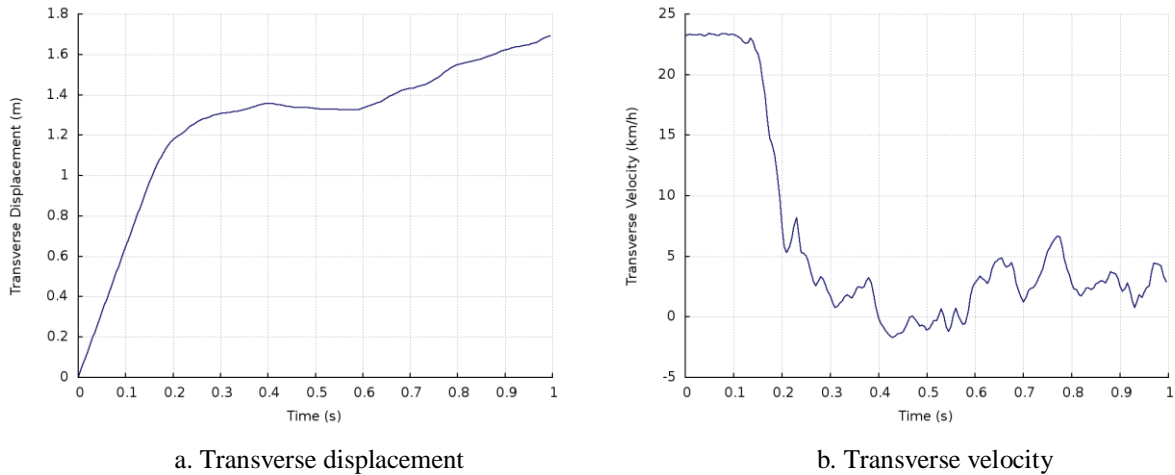


Fig. 4.68: Transverse displacement and velocity of the single-unit truck impacting the double-faced 29-inch steel-blockout Thrie-beam guardrail at 56 mph (90 km/h) and 15°.

4.3.4 Tractor-trailer Impact at MASH TL-5 Conditions

Figure 4.69 shows the top view vehicle trajectory of the tractor-trailer impacting the double-faced 29-inch wood-blockout Thrie-beam guardrail at 50 mph (80 km/h) and 15°. The wood-blockout Thrie-beam guardrail is shown in its deformed state with the vehicle tire tracks outlined in white. Upon impacting the wood-blockout Thrie-beam guardrail, the tractor-trailer failed to remain upright and rolled onto the guardrail. For this type of vehicular response, there was no determinable exit angle, an exit box was not required, and the MASH exit box criterion was not used. Figure 4.70 shows the top view vehicle trajectory of the tractor-trailer impacting the double-faced 29-inch steel-blockout Thrie-beam guardrail at 50 mph (80 km/h) and 15°. The steel-blockout Thrie-beam guardrail is shown in its deformed state with the vehicle tire tracks outlined in white. Similar to the impact on the wood-blockout Thrie-beam guardrail, upon impacting the steel-blockout Thrie-beam guardrail, the tractor-trailer failed to remain upright and rolled onto the guardrail. Therefore, the MASH exit box criterion was not used in this impact scenario. It should be noted that, although the tractor-trailer failed to remain upright in both impacts of this case, it was not required by MASH as per the statement, “although it is preferable all vehicles remain upright, this requirement is not applicable for tests involving the 10000S (i.e., single-unit truck) and 36000V (i.e., tractor-trailer) vehicles.” This exception of allowing a 90° roll for heavy vehicle impacts was based on the fact that the primary goal of this impact was to demonstrate the guardrails ability to contain and redirect heavy vehicles.



Fig. 4.69: A tractor-trailer impacting the double-faced 29-inch wood-blockout Thrie-beam guardrail at 50 mph (80 km/h) and 15°.



Fig. 4.70: A tractor-trailer impacting the double-faced 29-inch steel-blockout Thrie-beam guardrail at 50 mph (80 km/h) and 15°.

The yaw, pitch, and roll angles of the tractor and trailer are shown in Figs. 4.71 and 4.72 for impacts on the double-faced 29-inch wood- and steel-blockout Thrie-beam guardrails, respectively, at 50 mph (80 km/h) and 15°.

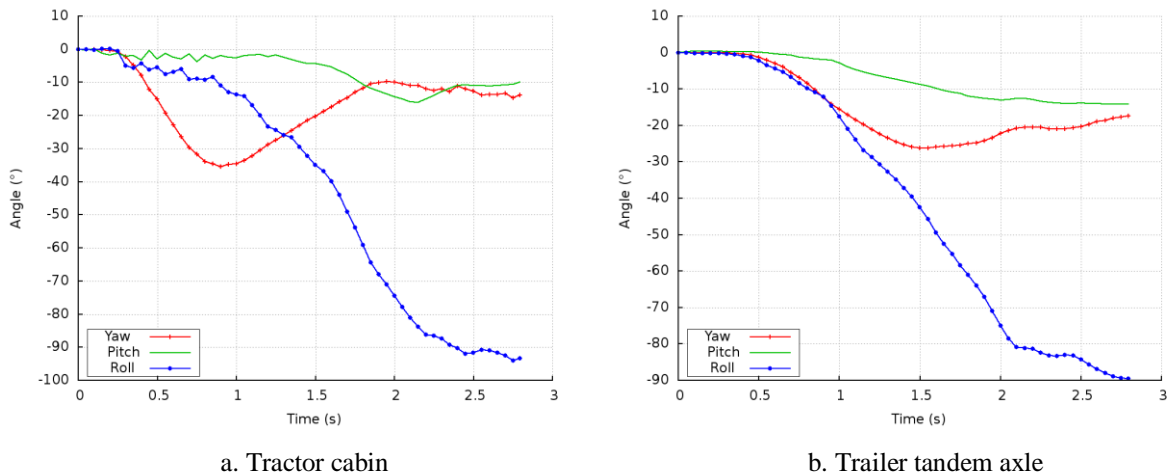


Fig. 4.71: Yaw, pitch, and roll angles of the tractor's (a) cabin and trailer's (b) tandem axle impacting the double-faced 29-inch wood-blockout Thrie-beam guardrail at 50 mph (80 km/h) and 15°.

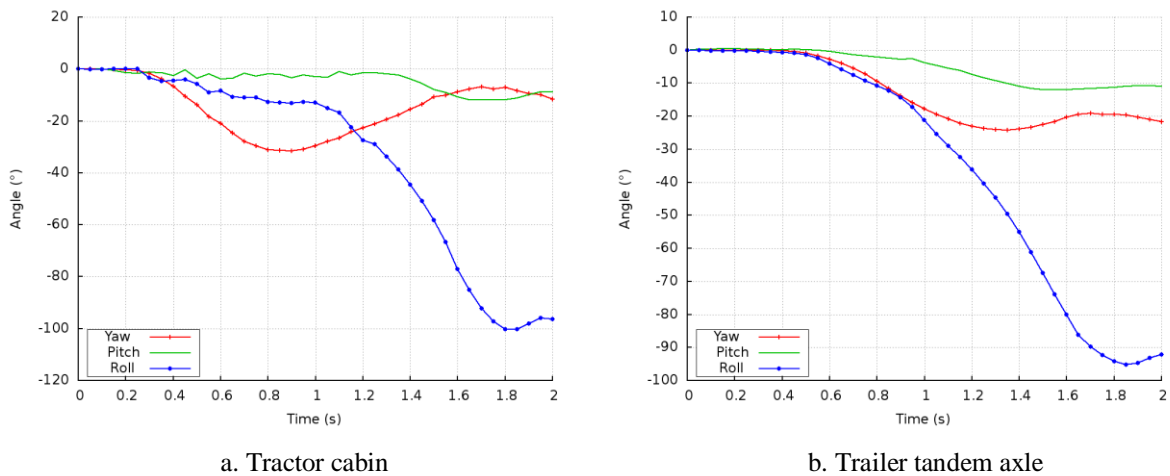


Fig. 4.72: Yaw, pitch, and roll angles of the tractor's (a) cabin and trailer's (b) tandem axle impacting the double-faced 29-inch steel-blockout Thrie-beam guardrail at 50 mph (80 km/h) and 15°.

The roll angles in these impact scenarios also failed the MASH evaluation criterion F , which specified a maximum 75° roll or pitch angle, though it was not a requirement for the tractor-trailer to remain upright according to MASH. The steadily increasing roll angle signified the vehicle's flipping about the longitudinal axis of the tractor-trailer (i.e., a "barrel roll"). It can be seen from Figs. 4.71a and 4.72a that the tractor was initially redirected by the guardrails, but began to roll when the trailer impacted the guardrail at about 1.2 seconds. The tractor rolled with the trailer as they are rigidly connected through the fifth wheel-kingpin connection.

Figures 4.73 and 4.74 show the maximum dynamic deflections of the double-faced 29-inch wood- and steel-blockout Thrie-beam guardrails impacted by the tractor-trailer at 50 mph (80 km/h) and 15° . The maximum dynamic deflection of the wood-blockout Thrie-beam guardrail was 4.75 ft (1.45 m) occurred at 1.37 seconds and the maximum dynamic deflection of the steel-blockout Thrie-beam guardrail was 3.8 ft (1.17 m) occurred at 1.28 seconds. The damaged sections of the two double-faced 29-inch Thrie-beam guardrail impacted by the tractor-trailer were not localized due to the vehicles rolling onto the guardrail. The damage of the wood-blockout Thrie-beam guardrail spanned nine posts and five double-faced guardrail segments, while the damage of the steel-blockout Thrie-beam guardrail spanned nine posts across five double-faced guardrail segments.

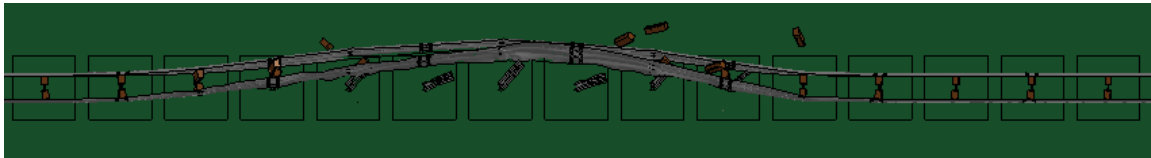


Fig. 4.73: Maximum dynamic deflection of the double-faced 29-inch wood-blockout Thrie-beam guardrail at 50 mph (80 km/h) and 15° and impacted by a tractor-trailer.

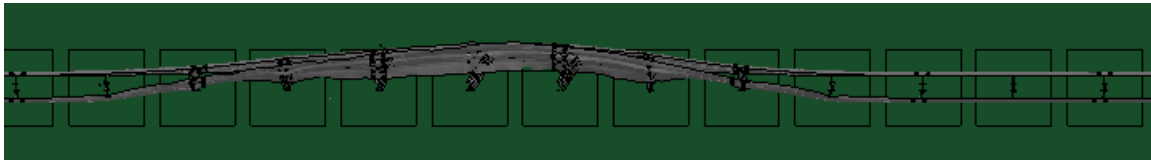


Fig. 4.74: Maximum dynamic deflection of the double-faced 29-inch steel-blockout Thrie-beam guardrail at 50 mph (80 km/h) and 15° and impacted by a tractor-trailer.

Figures 4.75 and 4.76 show detailed views of two different states of vehicle-barrier interaction throughout the tractor-trailer impacts against the double-faced 29-inch wood- and steel-blockout Thrie-beam guardrails at 50 mph (80 km/h) and 15° . Figures 4.75a and 4.76a illustrate the redirection of the tractor at 0.6 seconds during the impacts on the wood- and steel-blockout Thrie-beam guardrails. Figure 4.75b illustrate the state of maximum dynamic deflection of the trailer occurred at 1.37 seconds during impact on the wood-blockout Thrie-beam guardrail. Similarly, Fig. 4.76b shows the state of maximum dynamic deflection of the trailer occurred at 1.28 seconds during impact on the steel-blockout Thrie-beam guardrail.

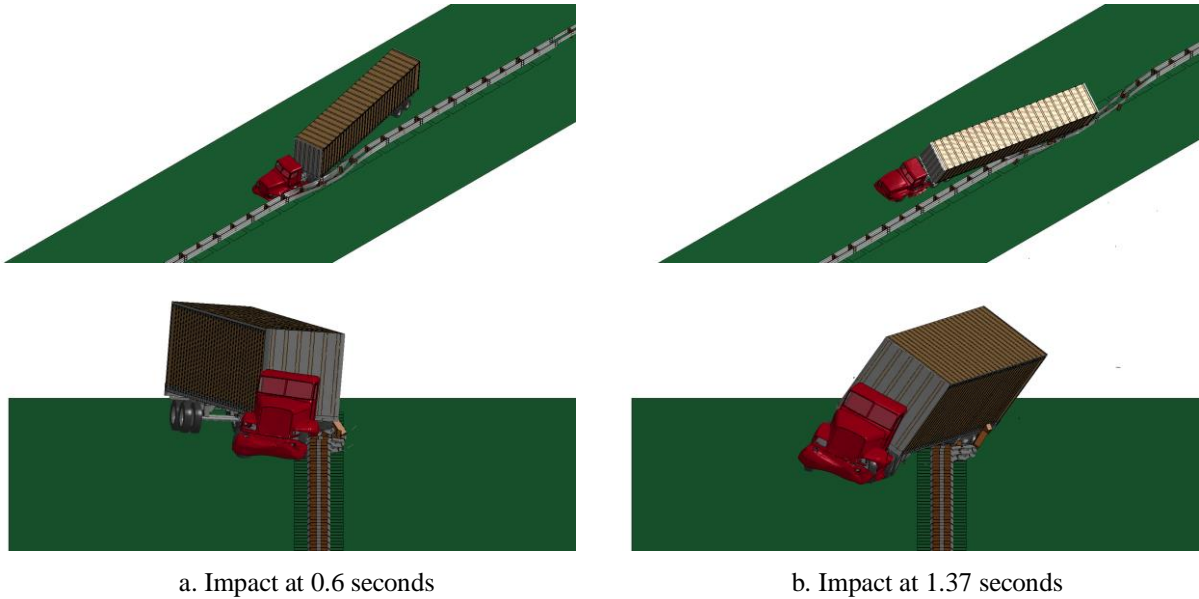


Fig. 4.75: Simulations of tractor-trailer impacting the double-faced 29-inch wood-blockout Thrie-beam guardrail at 50 mph (80 km/h) and 15°.

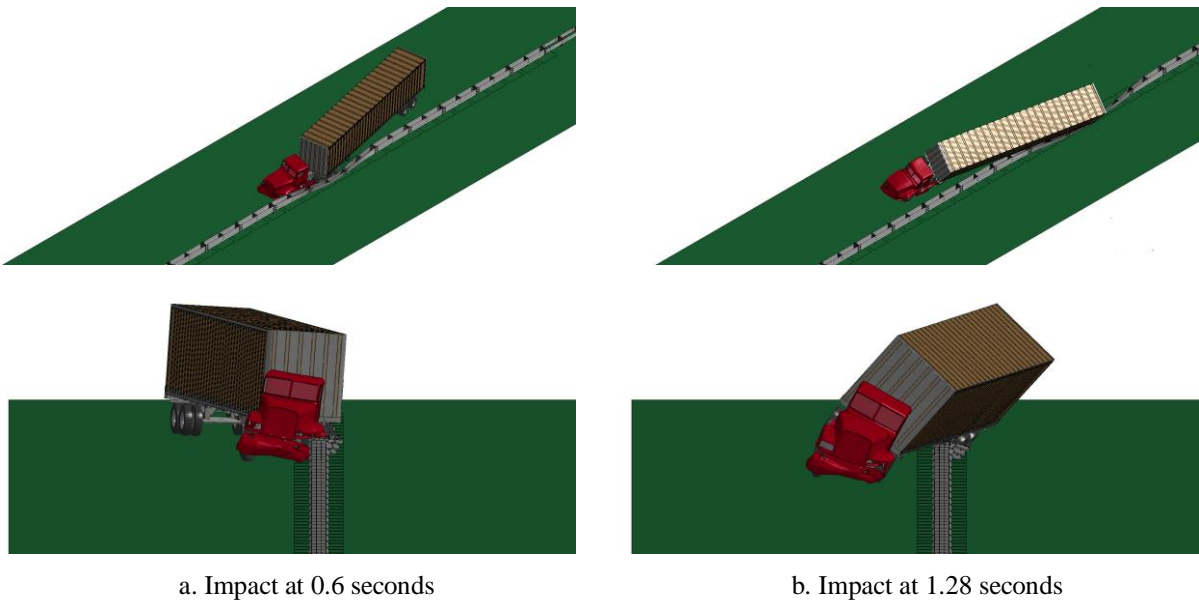
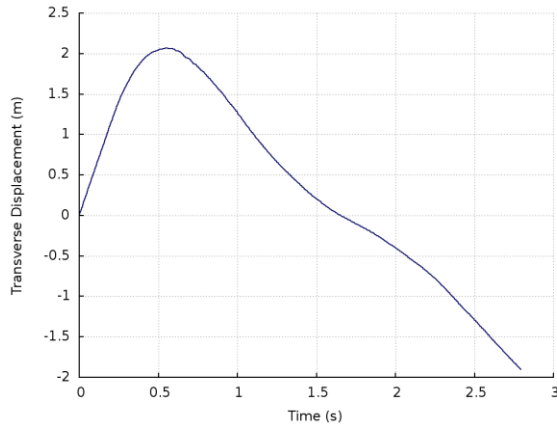


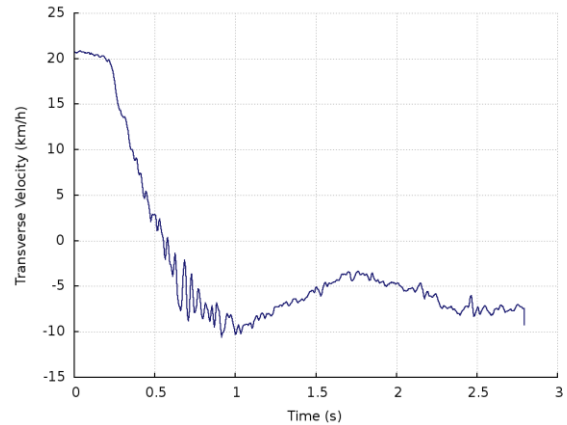
Fig. 4.76: Simulations of tractor-trailer impacting the double-faced 29-inch steel-blockout Thrie-beam guardrail at 50 mph (80 km/h) and 15°.

Figures 4.77 and 4.78 show the time histories of transverse displacements and velocities measured at the CG points of the tractor cabin and at the trailer tandem axle in the impact on the double-faced 29-inch wood- and steel-blockout Thrie-beam guardrails. In both impacts, the maximum positive transverse displacements occurred at 0.6 seconds, as seen in Figs. 4.77a and 4.78a, which corresponded to the impact states seen in Figs. 4.75a and 4.76a, respectively. Similarly in Fig. 4.77c, the maximum positive transverse displacement of the trailer tandem axle occurred at 1.37 seconds, which corresponded to the impact state illustrated in Fig. 4.75b.

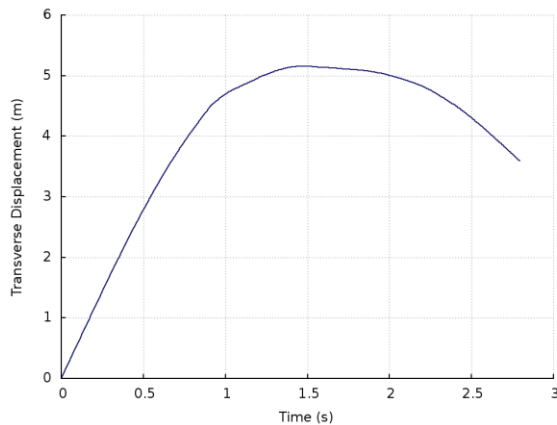
During the impact on the double-faced 29-inch steel-blockout Thrie-beam guardrail, the maximum positive displacement of the trailer tandem axle's transverse displacement (see Fig. 4.78c) occurred at 1.28 seconds and it corresponded to the impact state illustrated in Fig. 4.76b. The absence of a constant negative transverse displacement in the trailer tandem axle, as seen in Figs. 4.77c and 4.78c, corresponded to the presence of a rollover in both impact cases.



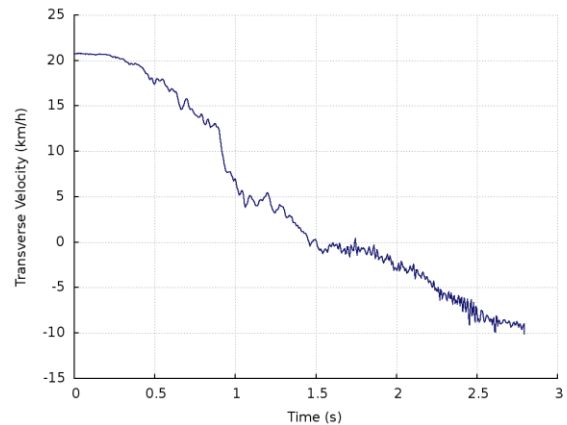
a. Tractor transverse displacement



b. Tractor transverse velocity

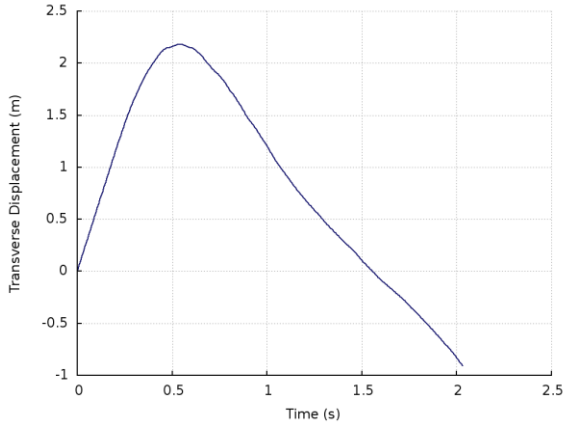


c. Trailer axle transverse displacement

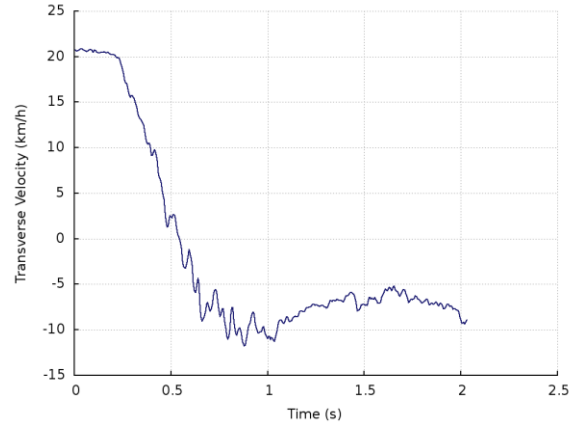


d. Trailer axle transverse velocity

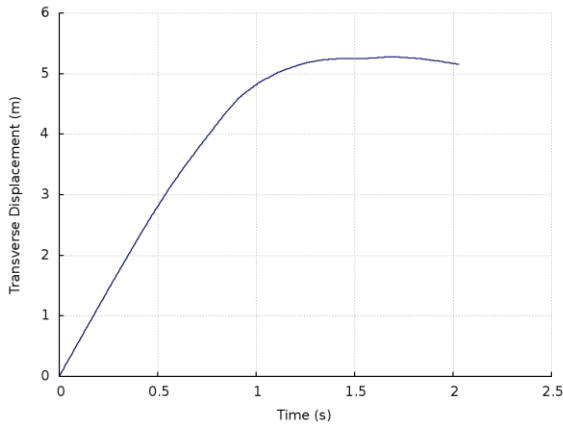
Fig. 4.77: Transverse displacement and velocities of the tractor-trailer impacting the double-faced 29-inch wood-blockout Thrie-beam guardrail at 50 mph (80 km/h) and 15°.



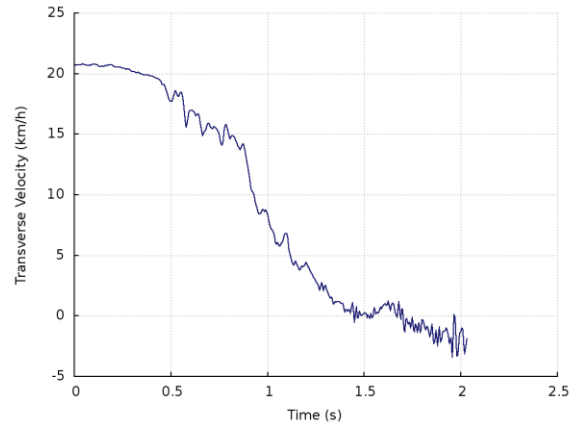
a. Tractor transverse displacement



b. Tractor transverse velocity



c. Trailer axle transverse displacement



d. Trailer axle transverse velocity

Fig. 4.78: Transverse displacement and velocities of the tractor-trailer impacting the double-faced 29-inch steel-blockout Thrie-beam guardrail at 50 mph (80 km/h) and 15°.

4.4 Case 4: Double-faced 31-inch Thrie-beam Guardrails

In this case, the double-faced 31-inch wood- and steel-blockout Thrie-beam guardrails were evaluated under MASH TL-4 and TL-5 impact conditions, i.e., impacted by a small sedan, pickup truck, single-unit truck, and tractor-trailer. For impacts by the small sedan (i.e., Dodge Neon) and pickup truck (i.e., Ford F250), an impact speed of 62 mph (100 km/h) and an impact angle of 25° were used. For impacts by the single-unit truck, an impact speed of 56 mph (90 km/h) and an impact angle of 15° were used. For impacts by the tractor-trailer, an impact speed of 50 mph (80 km/h) and an impact angle of 15° were used. Since the impacts by the Dodge Neon and Ford F250 are identical in MASH TL-4 and TL-5 impact conditions, the simulation results are only listed and discussed once. Table 4.6 gives a summary of simulation results for Case 4 on the guardrail performance in terms of vehicular responses.

Table 4.6: Simulation results of Case 4 (Double-faced 31-inch Wood- and Steel-blockout Thrie-beam Guardrails)

Test Vehicle	MASH Level	Impact Angle	Impact Velocity	Blockout Type	Simulation Results
Dodge Neon	TL-4 & TL-5	25°	62 mph (100 km/h)	Wood	The vehicle passed the exit box criterion and was safely redirected
				Steel	The vehicle was redirected by the guardrail with a large exit angle and failed the exit box criterion
Ford F250	TL-4 & TL-5	25°	62 mph (100 km/h)	Wood	The vehicle was redirected by the guardrail with a large exit angle and failed the exit box criterion
				Steel	The vehicle was redirected after vaulting up the guardrail and passed the exit box criterion
Single-unit Truck	TL-4	15°	56 mph (90 km/h)	Wood	The vehicle failed to remain upright and rolled onto the guardrail
				Steel	The vehicle failed to remain upright and rolled onto the guardrail
Tractor-Trailer	TL-5	15°	50 mph (80 km/h)	Wood	The vehicle failed to remain upright and rolled onto the guardrail
				Steel	The vehicle failed to remain upright and rolled onto the guardrail

4.4.1 Dodge Neon Impact at MASH TL-4 & TL-5 Conditions

Figure 4.79 shows the top view vehicle trajectory of the Dodge Neon impacting the double-faced 31-inch wood-blockout Thrie-beam guardrail at 62 mph (100 km/h) and 25°. The wood-blockout Thrie-beam guardrail is shown in its deformed state with the vehicle tire tracks outlined in white and the exit box is shown by the yellow dotted rectangle. Upon impacting the wood-blockout Thrie-beam guardrail, the Dodge Neon was redirected by the guardrail with an exit angle allowing to pass the MASH exit box criterion. It was also noted that the Dodge Neon maintained a clockwise rotation after losing contact and moving away from the guardrail. Figure 4.80 shows the top view vehicle trajectory of the Dodge Neon impacting the double-

31-inch steel-blockout Thrie-beam guardrail at 62 mph (100 km/h) and 25°. The steel-blockout Thrie-beam guardrail is shown in its deformed state and the exit box is shown by the yellow dotted rectangle. It can be seen from Fig. 4.80 that the double-faced 31-inch steel-blockout Thrie-beam guardrail was more rigid than the wood-blockout Thrie-beam guardrail, caused a large exit angle on the Dodge Neon and failed to pass the MASH exit box criterion.

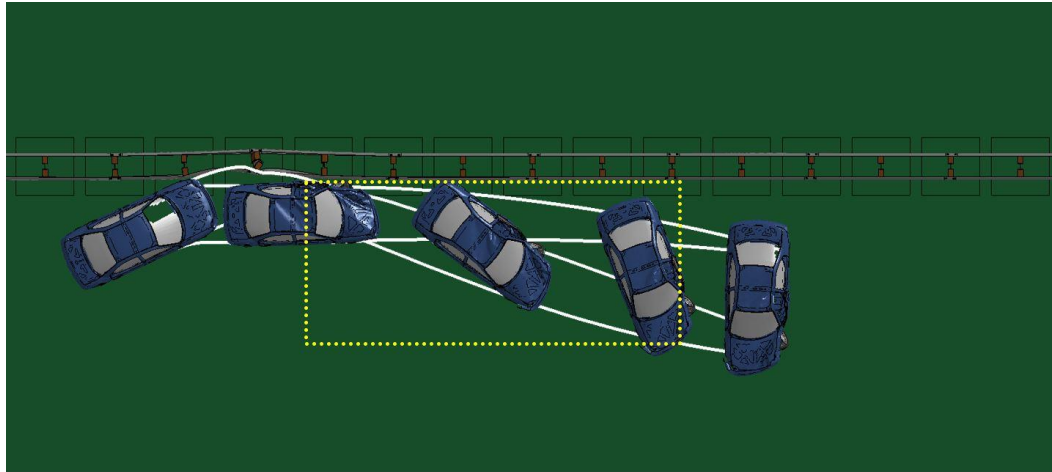


Fig. 4.79: A Dodge Neon impacting the double-faced 31-inch wood-blockout Thrie-beam guardrail at 62 mph (100 km/h) and 25°.

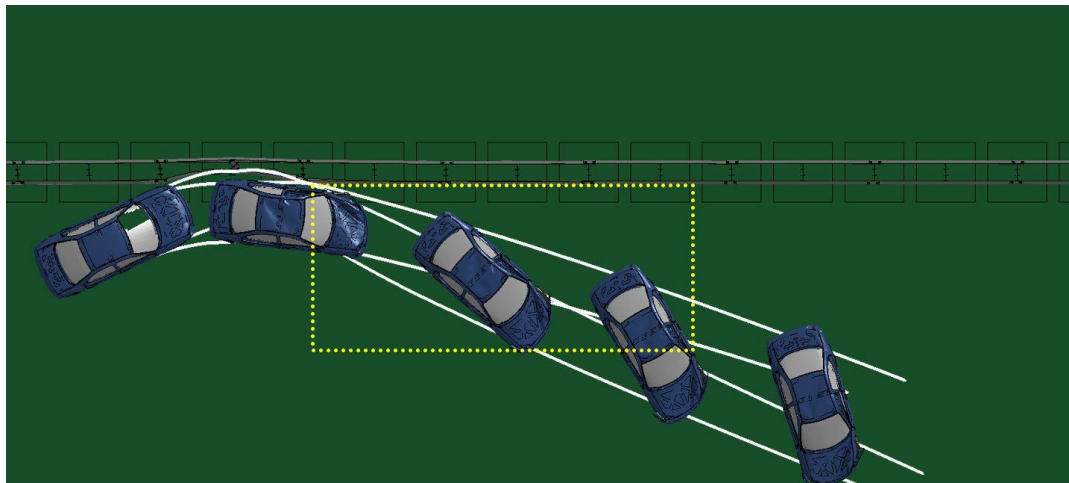


Fig. 4.80: A Dodge Neon impacting the double-faced 31-inch steel-blockout Thrie-beam guardrail at 62 mph (100 km/h) and 25°.

The yaw, pitch, and roll angles of the Dodge Neon in the impacts against the double-faced 31-inch wood- and steel-blockout Thrie-beam guardrails are shown in Figs. 4.81a and 4.81b. The exit angles of the Dodge Neon in these two impacts were determined to be 7.1° occurred at 0.245 seconds for the wood-blockout Thrie-beam guardrail and -28.5° occurred at 0.41 seconds for the steel-blockout Thrie-beam guardrail. In the case of impacting the wood-blockout Thrie-beam guardrail, the exit angle was determined at the instant when the vehicle had last contact with the guardrail. Although the exit angle was small, the vehicle continued to rotate away

from the guardrail after losing contact with the guardrail, as indicated by the decreasing yaw angle in Fig. 4.81a.

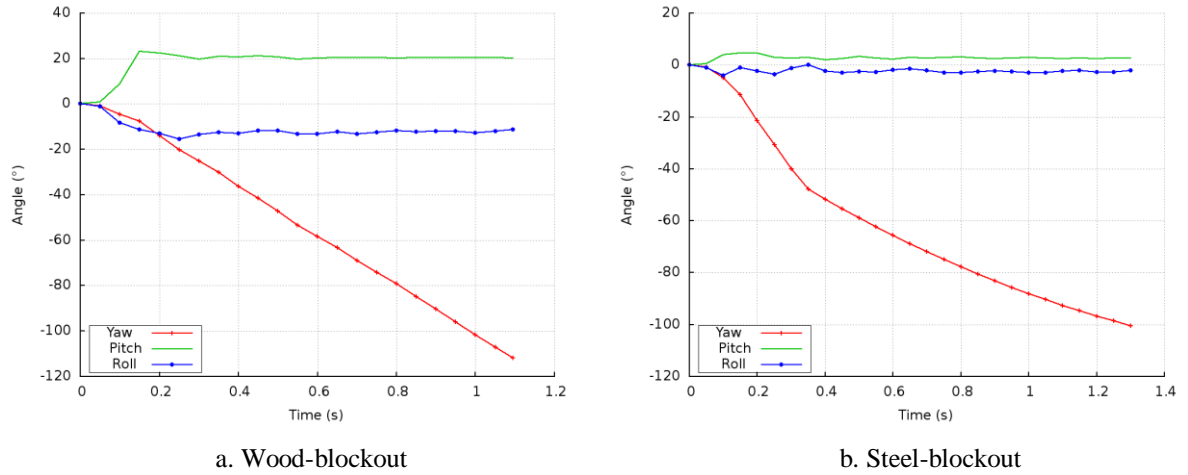


Fig. 4.81: Yaw, pitch, and roll angles of Dodge Neon impacting the double-faced 31-inch (a) wood- (b) steel-blockout Thrie-beam guardrail at 62 mph (100 km/h) and 25°.

Figures 4.82 and 4.83 show the maximum dynamic deflections of the double-faced 31-inch wood- and steel-blockout Thrie-beam guardrails impacted by the Dodge Neon at 62 mph (100 km/h) and 25°. The maximum dynamic deflections were 1.49 ft (0.45 m) occurred at 0.09 seconds for the wood-blockout Thrie-beam guardrail and 1.61 ft (0.49 m) occurred at 0.12 seconds for the double-faced 31-inch steel-blockout Thrie-beam guardrail. Comparing the two double-faced 31-inch Thrie-beam guardrails under impacts by the Dodge Neon, the steel-blockout guardrail had 0.12 ft (0.036 m) more in deflection than the wood-blockout guardrail, and the damaged sections of both guardrails were contained to the impact locations. The damaged sections of both Thrie-beam guardrails spanned three posts across two double-faced guardrail segments.

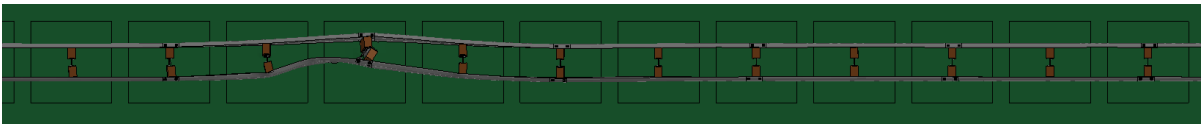


Fig. 4.82: Maximum dynamic deflection of the double-faced 31-inch wood-blockout Thrie-beam guardrail at 62 mph (100 km/h) and 25° and impacted by a Dodge Neon.

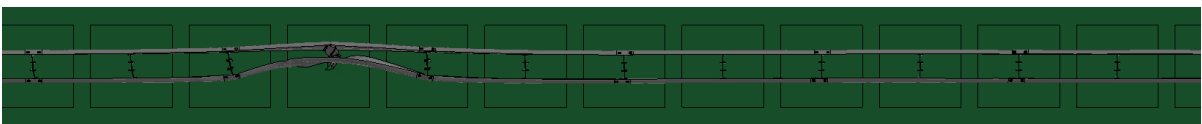


Fig. 4.83: Maximum dynamic deflection of the double-faced 31-inch steel-blockout Thrie-beam guardrail at 62 mph (100 km/h) and 25° and impacted by a Dodge Neon.

Figures 4.84 and 4.85 show the detailed views of the vehicle-barrier interactions at the point of maximum dynamic deflections of the double-faced 31-inch wood- and steel-blockout Thrie-

beam guardrails impacted by the Dodge Neon at 62 mph (100 km/h) and 25°. The impact state shown in Fig. 4.84 corresponded to the maximum guardrail deflection state seen in Fig. 4.82. Similarly, the impact state in Fig. 4.85 corresponded to the maximum guardrail deflection state seen in Fig. 4.83. Even with the increased rail height compared to the 29-inch Thrie-beam guardrails, the 31-inch guardrails were capable of preventing the Dodge Neon from underriding the guardrails due to the rail face extended lower than the W-beam guardrails.

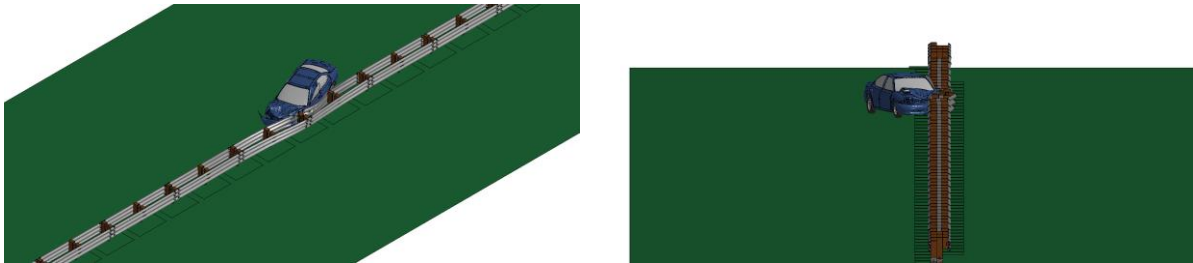


Fig. 4.84: Simulations of Dodge Neon impacting the double-faced 31-inch wood-blockout Thrie-beam guardrail at 62 mph (100 km/h) and 25°.

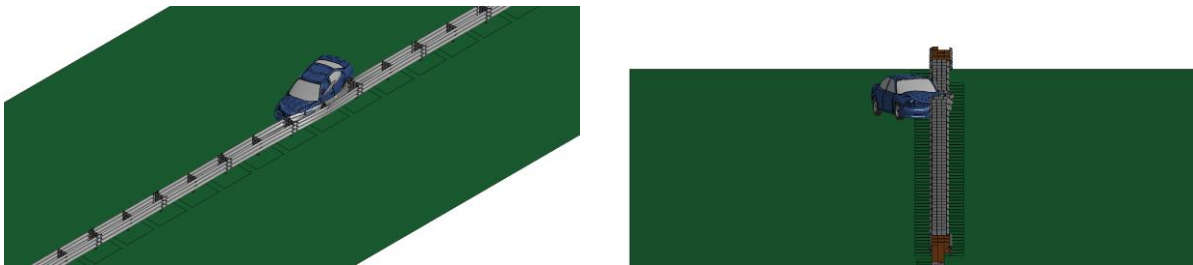


Fig. 4.85: Simulations of Dodge Neon impacting the double-faced 31-inch steel-blockout Thrie-beam guardrail at 62 mph (100 km/h) and 25°.

Figures 4.86 and 4.87 show the time histories of transverse displacements and velocities measured at the CG point of the Dodge Neon impacting the double-faced 31-inch wood- and steel-blockout Thrie-beam guardrails at 62 mph (100 km/h) and 25°. The maximum positive transverse displacement of the wood-blockout Thrie-beam guardrail occurred at 0.09 seconds (see Fig. 4.86a), which corresponded with the state of maximum guardrail deflection as seen in Figs. 4.82 and 4.84. Similarly, the maximum positive transverse displacement of the steel-blockout Thrie-beam guardrail occurred at 0.12 seconds, which corresponded with the state of maximum guardrail deflection as seen in Figs. 4.83 and 4.85. Under impacts of the Dodge Neon, the double-faced 31-inch steel-blockout Thrie-beam guardrail redirected the vehicle more gradually, over a longer period of time, but experienced more deflection than the 31-inch wood-block Thrie-beam guardrail. The more abrupt redirection by the wood-blockout Thrie-beam guardrail was confirmed by the steeper slope of the transverse velocity curve between 0 and 0.2 seconds in Fig 4.86b compared to that of the steel-blockout Thrie-beam guardrail in Fig. 4.87b. At the end of the impact scenario for the wood-blockout Thrie-beam guardrail, the transverse velocity of the Dodge Neon was approximately 6.8 mph (11 km/h), seen in Fig. 4.86b. Comparatively, the Dodge Neon had a residual transverse velocity of 12.4 mph (20 km/h) at the end of the impact scenario impacting the steel-blockout Thrie-beam guardrail. The increased transverse velocity towards the travel lane in the impact on the double-faced 31-inch

steel-blockout Thrie-beam guardrail, combined with the failure of the MASH exit box criterion, denotes a relatively high chance of the vehicle reentering the travel lane and causing a secondary collision.

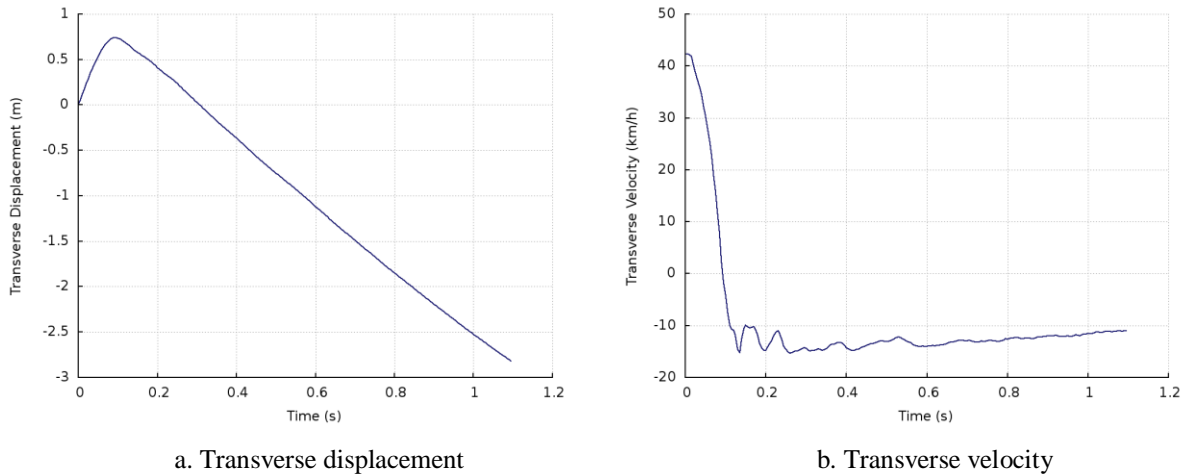


Fig. 4.86: Transverse displacement and velocity of the Dodge Neon impacting the double-faced 31-inch wood-blockout Thrie-beam guardrail at 62 mph (100 km/h) and 25°.

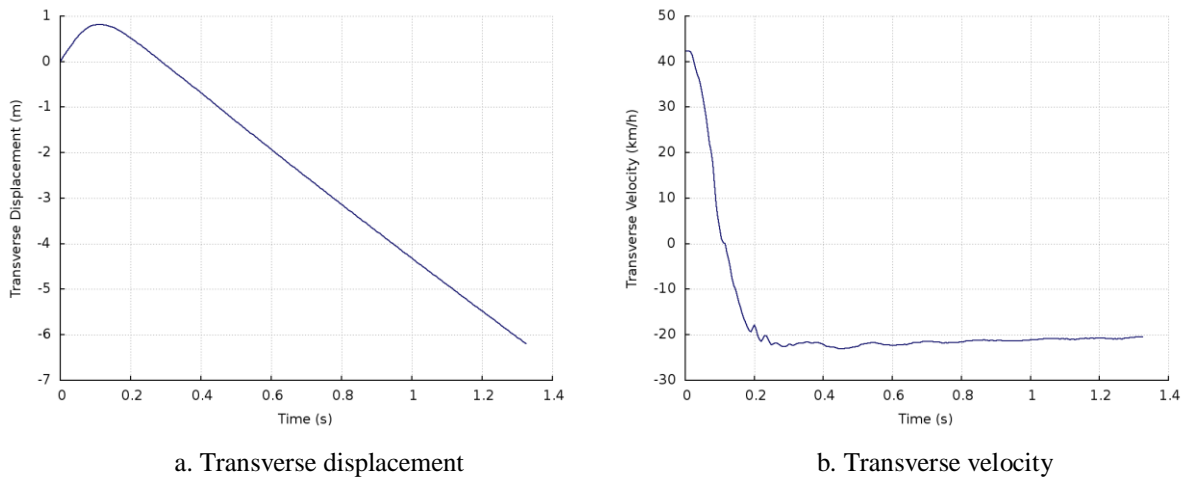


Fig. 4.87: Transverse displacement and velocity of the Dodge Neon impacting the double-faced 31-inch steel-blockout Thrie-beam guardrail at 62 mph (100 km/h) and 25°.

4.4.2 Ford F250 Impact at MASH TL-4 & TL-5 Conditions

Figure 4.88 shows the top view vehicle trajectory of the Ford F250 impacting the double-faced 31-inch wood-blockout Thrie-beam guardrail at 62 mph (100 km/h) and 25°. The wood-blockout Thrie-beam guardrail is shown in its deformed state with the vehicle tire tracks outlined in white and the exit box is shown by the yellow dotted rectangle. Upon impacting the wood-blockout Thrie-beam guardrail, the Ford F250 was redirected by the guardrail with a large exit angle, resulting in a failure to pass the MASH exit box criterion. Figure 4.89 shows the top view vehicle trajectory of the Ford F250 impacting the double-faced 31-inch steel-blockout Thrie-beam guardrail at 62 mph (100 km/h) and 25°. The steel-blockout Thrie-beam

guardrail is shown in its deformed state and the exit box is shown by the yellow dotted rectangle. Upon impacting the steel-blockout Thrie-beam guardrail, the Ford F250 deflected the rails and posts, turning the guardrail face into a makeshift slope and became partially airborne as the vehicle was redirected on the impacting side of the guardrail. The vehicle remained upright and was successfully redirected with an exit angle that allowed to pass the MASH exit box criterion.

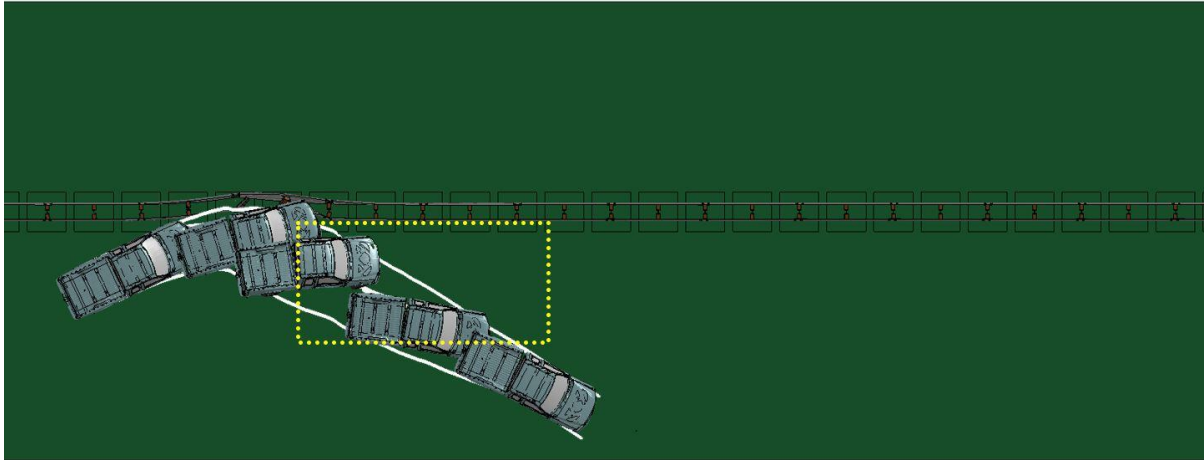


Fig. 4.88: A Ford F250 impacting the double-faced 31-inch wood-blockout Thrie-beam guardrail at 62 mph (100 km/h) and 25°.

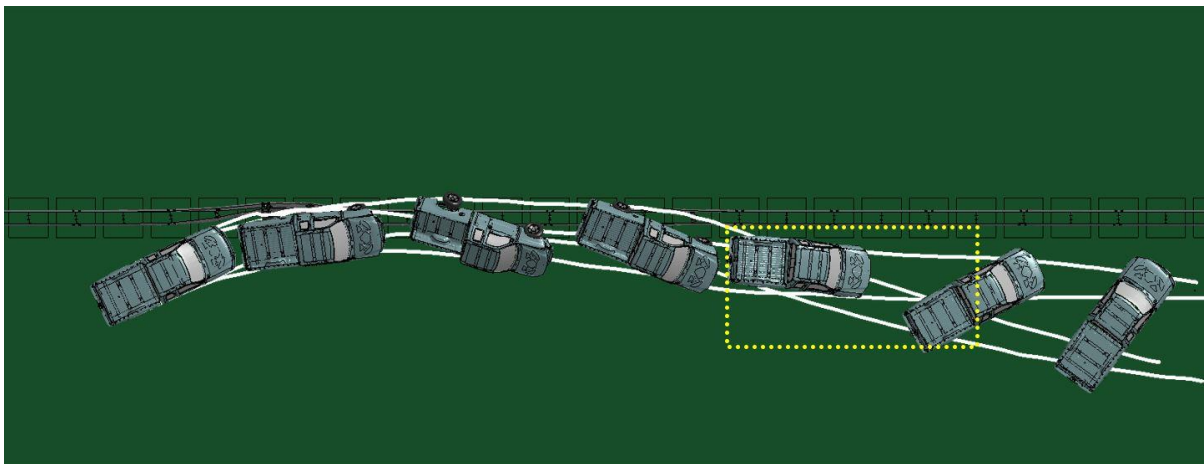


Fig. 4.89: A Ford F250 impacting the double-faced 31-inch steel-blockout Thrie-beam guardrail at 62 mph (100 km/h) and 25°.

The yaw, pitch, and roll angles of the Ford F250 impacting the double-faced 31-inch wood- and steel-blockout Thrie-beam guardrails are shown in Figs. 4.90a and 4.90b, respectively. The exit angles were determined by calculating the angle between the initial guardrail face and left (i.e., driver's side) longitudinal face of the vehicle. For the impact on the wood-blockout Thrie-beam guardrail, the vehicle was redirected with an exit angle of -7.2° , determined by adding the 25° impact angle to the -17.8° yaw angle at the point of last contact with the guardrail at 0.4 seconds. For impact on the steel-blockout Thrie-beam guardrail, the vehicle was safely

redirected with an exit angle of -14.8° . In this case, the last point of contact with the guardrail can be seen from the inflection point at 1.4 seconds on the roll-angle curve in Fig. 4.90b, which corresponded to the point where the vehicle's tail end contacted the guardrail. It can be seen from 4.90b that the Ford F250 had substantially higher roll angles impacting the steel-blockout Thrie-beam guardrail than the wood-blockout Thrie-beam guardrail. The largest roll angle in the impact on the steel-blockout Thrie-beam guardrail was 47.3° . The pitch angles in both impacts were less than 21 degrees in both positive and negative directions. Both impacts cases passed the MASH evaluation criterion F , which specified a maximum 75° roll or pitch angle.

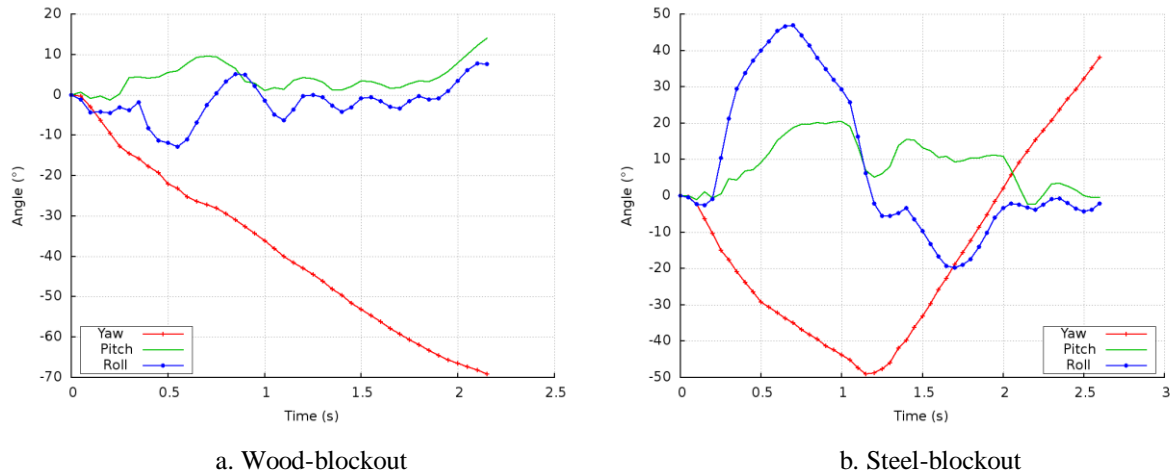


Fig. 4.90: Yaw, pitch, and roll angles of Ford F250 impacting the double-faced 31-inch (a) wood- (b) steel-blockout Thrie-beam guardrail at 62 mph (100 km/h) and 25° .

Figures 4.91 and 4.92 show the maximum dynamic deflections of the double-faced 31-inch wood- and steel-blockout Thrie-beam guardrails impacted by the Ford F250 at 62 mph (100 km/h) and 25° . The maximum dynamic deflections were 3.05 ft (0.93 m) at 0.175 seconds and 3.21 ft (0.98 m) at 0.165 seconds for the wood-blockout and steel-blockout Thrie-beam guardrails, respectively. Under impacts by the Ford F250, the steel-blockout guardrail deformed 0.16 ft (0.05 m) further and resulted in a larger damaged section than the wood-blockout guardrail. The damaged sections of both guardrails were relatively localized and spanned four posts and two double-faced guardrail segments.

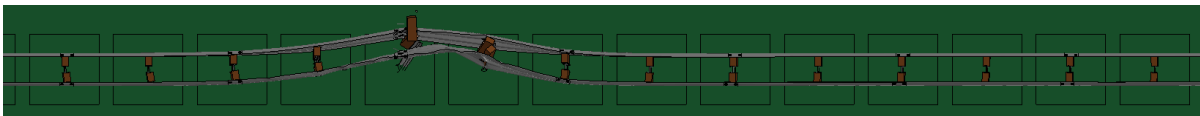


Fig. 4.91: Maximum dynamic deflection of the double-faced 31-inch wood-blockout Thrie-beam guardrail at 62 mph (100 km/h) and 25° and impacted by a Ford F250.

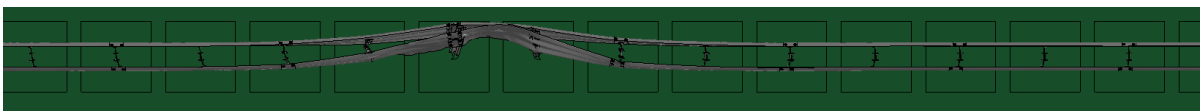


Fig. 4.92: Maximum dynamic deflection of the double-faced 31-inch steel-blockout Thrie-beam guardrail at 62 mph (100 km/h) and 25° and impacted by a Ford F250.

Figures 4.93 and 4.94 show detailed views of vehicle-barrier interactions of the Ford F250 impacting the double-faced 31-inch wood- and steel-blockout Thrie-beam guardrails at 62 mph (100 km/h) and 25°, respectively. The impact state in Fig. 4.93 corresponded to the maximum dynamic deflection at 0.175 seconds seen in Fig. 4.91. Similarly, for Fig. 4.94, the impact state corresponded to the state of maximum dynamic deflection at 0.165 seconds seen in Fig. 4.92.

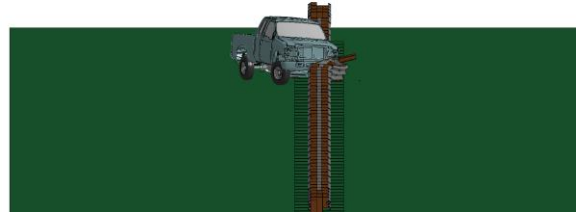
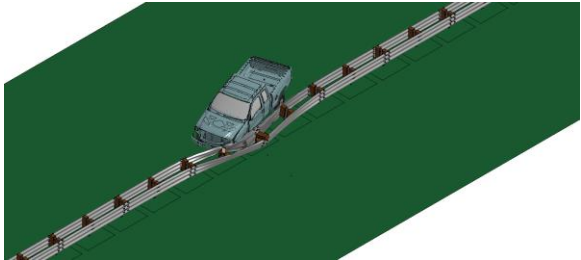


Fig. 4.93: Simulations of Ford F250 impacting the double-faced 31-inch wood-blockout Thrie-beam guardrail at 62 mph (100 km/h) and 25°.

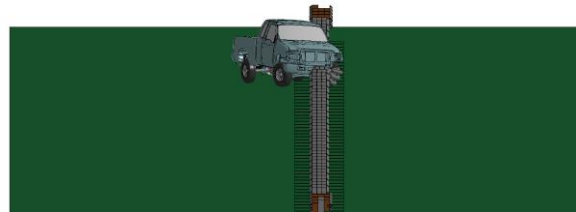
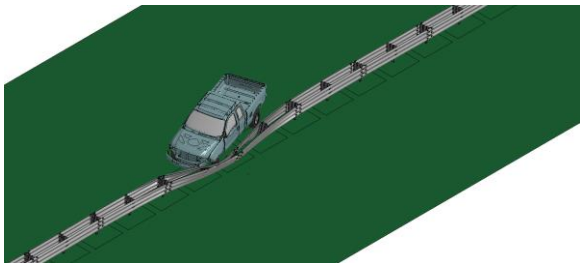


Fig. 4.94: Simulations of Ford F250 impacting the double-faced 31-inch steel-blockout Thrie-beam guardrail at 62 mph (100 km/h) and 25°.

Figures 4.95 and 4.96 show the time histories of transverse displacements and velocities measured at the CG point of the Ford F250 impacting the double-faced 31-inch wood- and steel-blockout Thrie-beam guardrails at 62 mph (100 km/h) and 25°. For impact on the wood-blockout Thrie-beam guardrail (see Fig. 4.95a), the maximum positive transverse displacement of the Ford F250 occurred at 0.195 seconds, which corresponded to the state immediately following the maximum guardrail deflection seen in Fig. 4.91. Similarly, for impact on the steel-blockout Thrie-beam guardrail (see Fig. 4.96a), the maximum positive transverse displacement of the Ford F250 occurred at 0.385 seconds that corresponded to the state when the vehicle became partially airborne after impacting the guardrail. It was observed that, under impacts by the Ford F250, the wood-blockout Thrie-beam guardrail redirected the vehicle quicker, over a shorter period of time, and deflected less throughout the impact course than the steel-blockout Thrie-beam guardrail. On the other hand, the steel-blockout Thrie-beam guardrail reduced the vehicle's transverse velocity quicker than the wood-blockout Thrie-beam guardrail; this is confirmed by the steep slope on the transverse velocity curve between 0 to 0.4 seconds in Fig 4.96b compared to that in Fig. 4.95b. Towards the end of the impact, the transverse velocity of the Ford F250 was approximately 11.1 mph (18 km/h) in the impact on the wood-blockout Thrie-beam guardrail seen in Fig. 4.95b. Comparatively, the residual transverse velocity of the Ford F250 was only 4.3 mph (7 km/h) in the impact on the steel-blockout Thrie-beam guardrail. The relatively high transverse velocity of the Ford F250 in the

impact on the double-faced 31-inch wood-blockout guardrail, combined with the failure to pass the MASH exit box criterion, denoted a relatively high chance of the vehicle reentering the travel lane and causing a secondary collision.

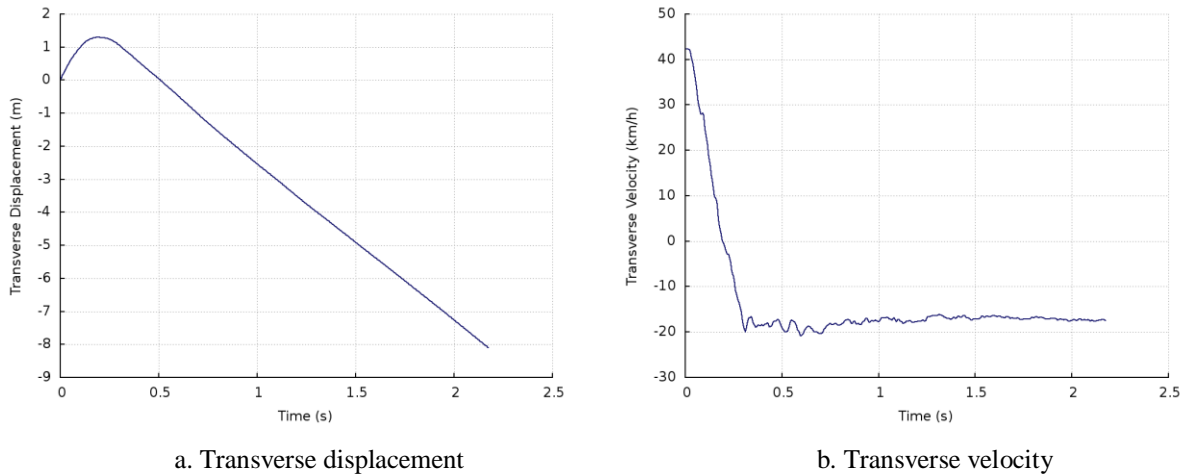


Fig. 4.95: Transverse displacement and velocity of the Ford F250 impacting the double-faced 31-inch wood-blockout Thrie-beam guardrail at 62 mph (100 km/h) and 25°.

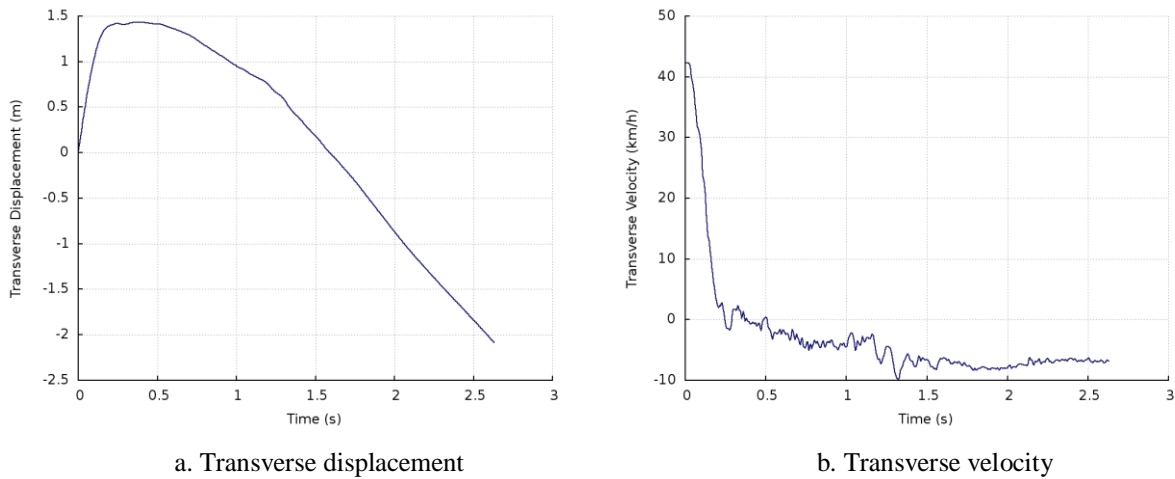


Fig. 4.96: Transverse displacement and velocity of the Ford F250 impacting the double-faced 31-inch steel-blockout Thrie-beam guardrail at 62 mph (100 km/h) and 25°.

4.4.3 Single-unit Truck Impact at MASH TL-4 Conditions

Figure 4.97 shows the top view vehicle trajectory of the single-unit truck impacting the double-faced 31-inch wood-blockout Thrie-beam guardrail at 56 mph (90 km/h) and 15°. The wood-blockout Thrie-beam guardrail is shown in its deformed state with the vehicle tire tracks outlined in white. Upon impacting the wood-blockout Thrie-beam guardrail, the vehicle failed to remain upright and rolled onto the guardrail. In this case, there was no determinable exit angle and the MASH exit box criterion was not used. Figure 4.98 shows the top view vehicle trajectory of the single-unit truck impacting the double-faced 31-inch steel-blockout Thrie-beam guardrail at 56 mph (90 km/h) and 15°. The steel-blockout Thrie-beam guardrail is shown

in its deformed state with the vehicle tire tracks outlined in white. Similar to the impact on the wood-blockout guardrail, the single-unit truck failed to remain upright and rolled onto the guardrail upon impacting the steel-blockout Thrie-beam guardrail. Therefore, the MASH exit box criterion was not used. It should be noted that the single-unit truck was not required to remain upright in both impacts, as per the statement in MASH, “although it is preferable all vehicles remain upright, this requirement is not applicable for tests involving the 10000S (i.e., single-unit truck) and 36000V (i.e., tractor-trailer) vehicles.” This exception allowing a 90° roll for heavy vehicle impacts relies on the fact that the primary goal of the impact scenarios is to demonstrate the guardrail’s ability to contain and redirect the vehicle.

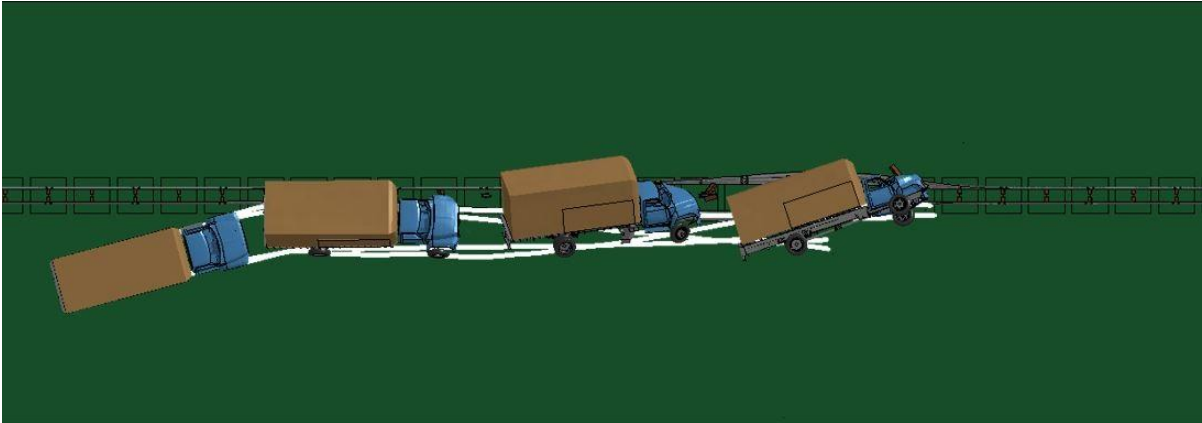


Fig. 4.97: A single-unit truck impacting the double-faced 31-inch wood-blockout Thrie-beam guardrail at 56 mph (90 km/h) and 15°.

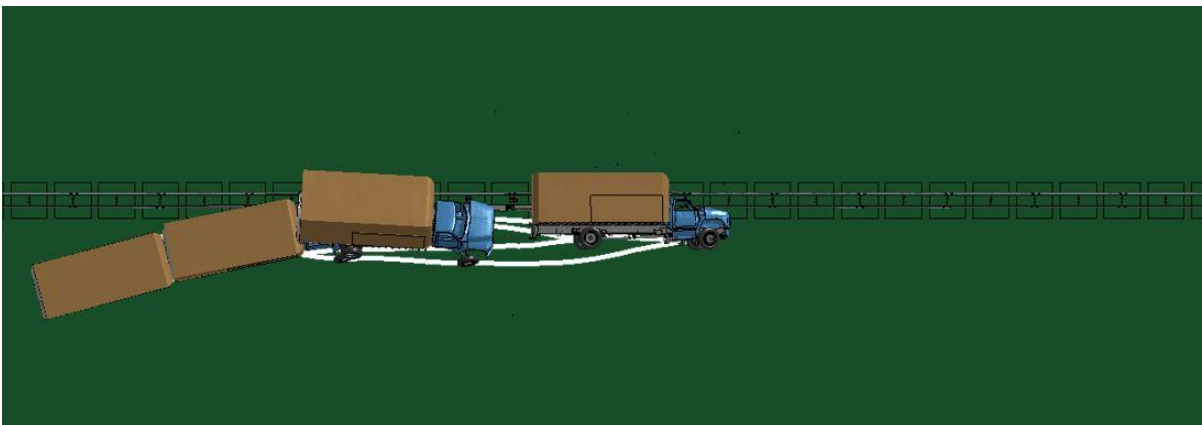


Fig. 4.98: A single-unit truck impacting the double-faced 31-inch steel-blockout Thrie-beam guardrail at 56 mph (90 km/h) and 15°.

Figures 4.99a and 4.99b show the yaw, pitch, and roll angles of the single-unit truck impacting the double-faced 31-inch wood- and steel-blockout Thrie-beam guardrails. Due to the relatively high CG point of the single-unit truck, a rollover was imminent once the vehicle’s roll angle surpassed 45°. Since the vehicles failed to remain upright in both impacts, it did not pass the MASH evaluation criterion *F*, which specified a maximum of 75° roll or pitch angle, though the single-unit truck was not required to remain upright by MASH.

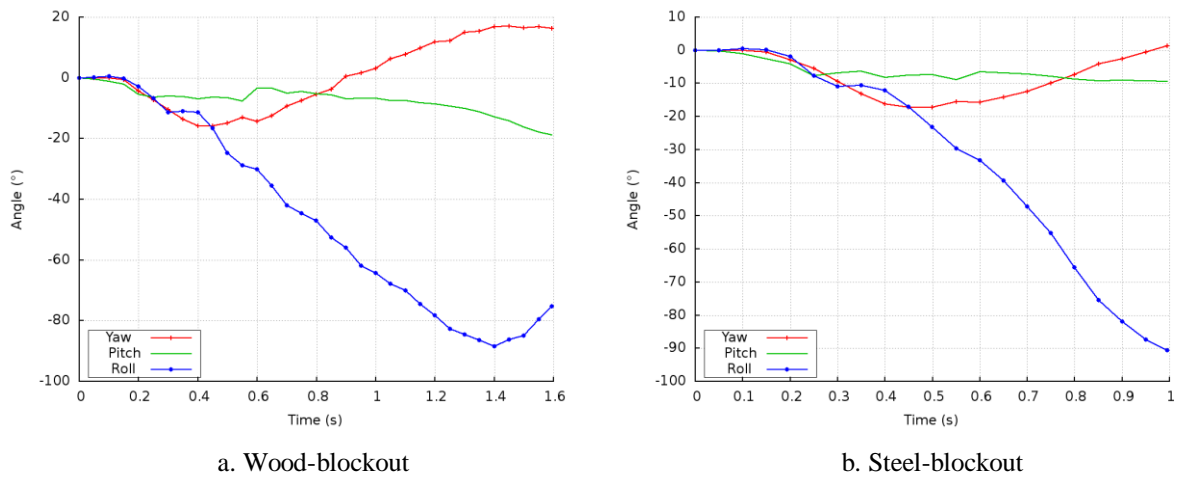


Fig. 4.99: Yaw, pitch, and roll angles of single-unit trucks impacting the double-faced 31-inch (a) wood- (b) steel-blockout Thrie-beam guardrail at 62 mph (100 km/h) and 25°.

The maximum dynamic deflections of the double-faced 31-inch wood- and steel-blockout Thrie-beam guardrails are shown in Figs. 4.100 and 4.101, respectively, for impacts by the single-unit truck at 56 mph (90 km/h) and 15°. The maximum dynamic deflections were -3.71 ft (-1.13 m) at 1.47 seconds and 1.1 ft (0.34 m) at 0.85 seconds for the wood- and steel-blockout Thrie-beam guardrails, respectively. Under impacts by the single-unit truck, the damaged sections of the two double-faced 31-inch Thrie-beam guardrail were not localized due to the the vehicle’s rollover onto the guardrails. The damage on the wood-blockout Thrie-beam guardrail spanned sixteen posts and eight double-faced guardrail segments, while the damage on the steel-blockout Thrie-beam guardrail spanned nine posts across five double-faced guardrail segments.

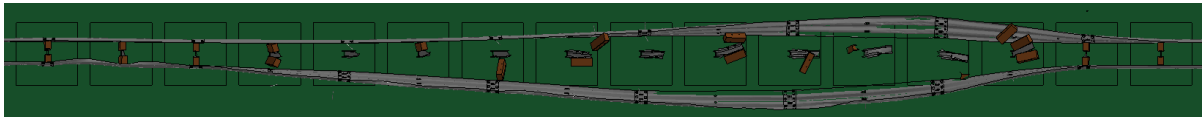


Fig. 4.100: Maximum dynamic deflection of the double-faced 31-inch wood-blockout Thrie-beam guardrail at 56 mph (90 km/h) and 15° and impacted by a single-unit truck.



Fig. 4.101: Maximum dynamic deflection of the double-faced 31-inch steel-blockout Thrie-beam guardrail at 56 mph (90 km/h) and 15° and impacted by a single-unit truck.

Figures 4.102 and 4.103 show detailed views of the vehicle-barrier interactions at 0.4 seconds, in the impacts on the double-faced 31-inch wood- and steel-blockout Thrie-beam guardrails by the single-unit truck at 56 mph (90 km/h) and 15°. Similar to the cases of W-beam and 29-inch Thrie-beam guardrails, the interactions with the double-faced 31-inch Thrie-beam guardrails resulted in the vehicle rolling onto the guardrails in both impact scenarios.



Fig. 4.102: Simulations of single-unit truck impacting the double-faced 31-inch wood-blockout Thrie-beam guardrail at 56 mph (90 km/h) and 15°.



Fig. 4.103: Simulations of single-unit truck impacting the double-faced 31-inch steel-blockout Thrie-beam guardrail at 56 mph (90 km/h) and 15°.

Figures 4.104 and 4.105 show the time histories of transverse displacements and velocities measured at the CG point of the single-unit truck impacting the double-faced 31-inch wood- and steel-blockout Thrie-beam guardrails at 56 mph (90 km/h) and 15°. In Figs. 4.104a and 4.105a, the maximum positive transverse displacements of the single-unit truck occurred towards the end of the impact scenarios due to the vehicle's rollover. The transverse velocities in both impacts were reduced to essentially zero at the end of the impact scenarios, eliminating the chance of reentering the travel lane and causing a secondary collision.

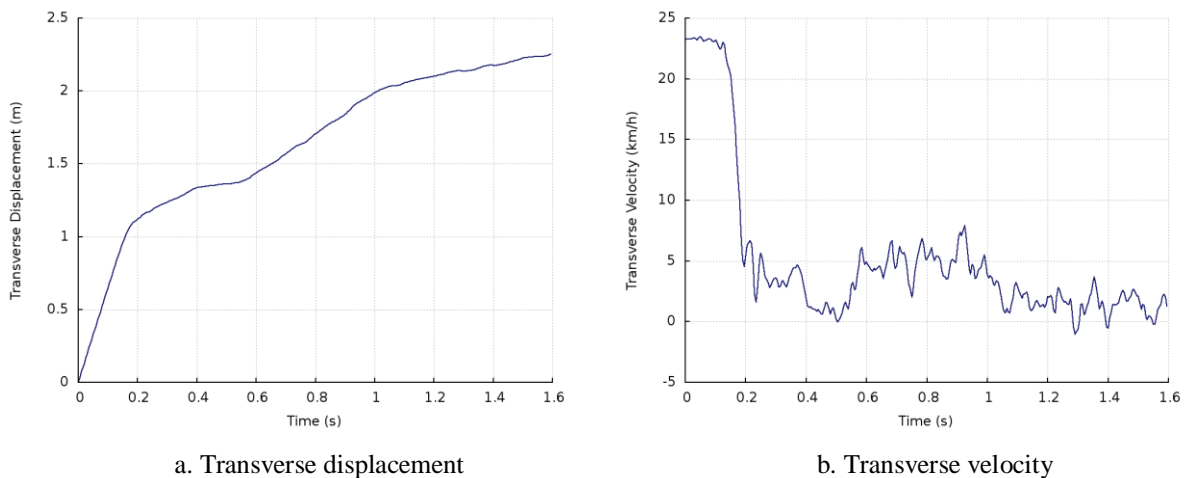


Fig. 4.104: Transverse displacement and velocity of the single-unit truck impacting the double-faced 31-inch wood-blockout Thrie-beam guardrail at 56 mph (90 km/h) and 15°.

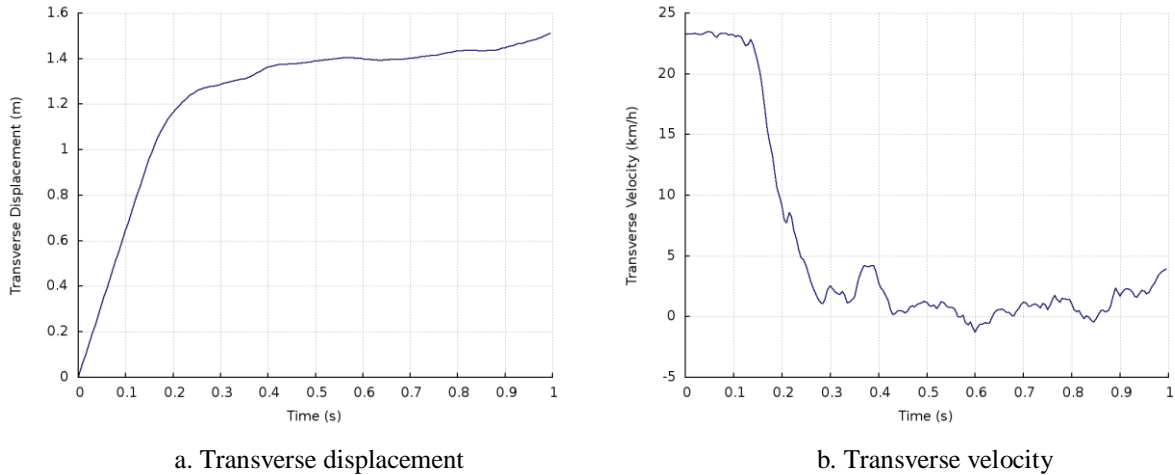


Fig. 4.105: Transverse displacement and velocity of the single-unit truck impacting the double-faced 31-inch steel-blockout Thrie-beam guardrail at 56 mph (90 km/h) and 15°.

4.4.4 Tractor-trailer Impact at MASH TL-5 Conditions

Figure 4.106 shows the top view vehicle trajectory of the tractor-trailer impacting the double-faced 31-inch wood-blockout Thrie-beam guardrail at 50 mph (80 km/h) and 15°. The wood-blockout Thrie-beam guardrail is shown in its deformed state with the vehicle tire tracks outlined in white. Upon impacting the wood-blockout Thrie-beam guardrail, the tractor-trailer failed to remain upright and rolled onto the guardrail. For this vehicular response, there was no determinable exit angle and the MASH exit box criterion was not used. Figure 4.107 shows the top view vehicle trajectory of the tractor-trailer impacting the double-faced 31-inch steel-blockout Thrie-beam guardrail at 50 mph (80 km/h) and 15°. The steel-blockout Thrie-beam guardrail is shown in its deformed state with the vehicle tire tracks outlined in white. Similar to the case of impacting the wood-blockout Thrie-beam guardrail, the tractor-trailer failed to remain upright and rolled onto the steel-blockout Thrie-beam guardrail. Therefore, the MASH exit box criterion was not used. It should be noted that the tractor-trailer was not required to remain upright as per the MASH statement, “although it is preferable all vehicles remain upright, this requirement is not applicable for tests involving the 10000S (i.e., single-unit truck) and 36000V (i.e., tractor-trailer) vehicles.” This exception of allowing a 90° roll for heavy vehicle impacts relies on the fact that the primary goal of the impact scenarios is to demonstrate the guardrails ability to contain and redirect the vehicle.



Fig. 4.106: A tractor-trailer impacting the double-faced 31-inch wood-blockout Thrie-beam guardrail at 50 mph (80 km/h) and 15°.



Fig. 4.107: A tractor-trailer impacting the double-faced 31-inch steel-blockout Thrie-beam guardrail at 50 mph (80 km/h) and 15°.

The yaw, pitch, and roll angles of the tractor-trailer during impacts on double-faced 31-inch wood- and steel-blockout Thrie-beam guardrails are shown in Figs. 4.108 and 4.109. The roll angles in these impacts also failed the MASH evaluation criterion F , which specified a maximum 75° roll or pitch angle, although it is not a requirement for the tractor-trailer to remain upright according to MASH. The steadily increasing roll angle signified the vehicle’s flipping about the longitudinal axis of the tractor-trailer, i.e., a “barrel roll”. It can be seen from Figs. 4.108a and 4.109a that the tractors were initially redirected by the guardrails, but rolled with the trailer upon the trailer impacting the guardrail at approximately 1.6 seconds, due to their rigid connection through the fifth wheel-kingpin.

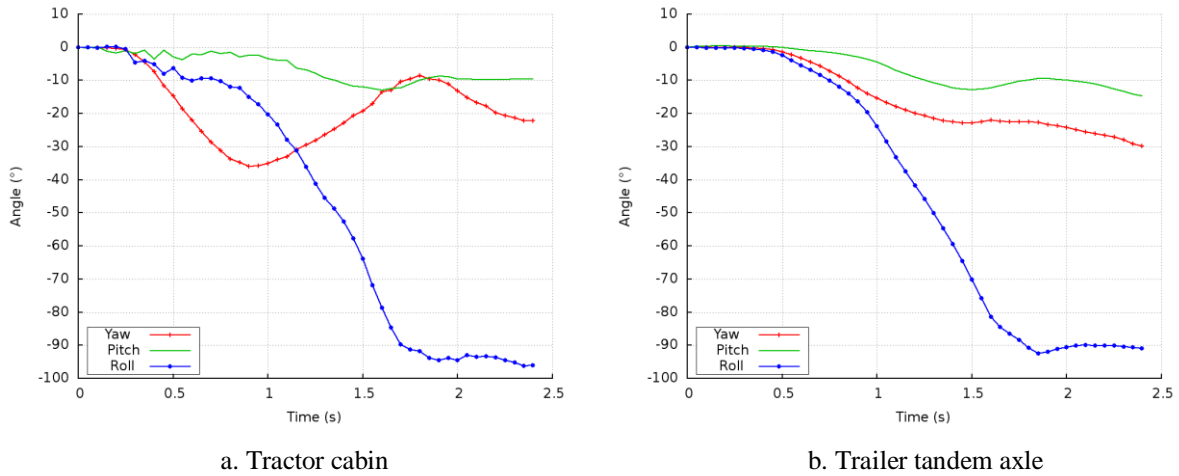


Fig. 4.108: Yaw, pitch, and roll angles of the tractor-trailer impacting the double-faced 31-inch wood-blockout Thrie-beam guardrail at 50 mph (80 km/h) and 15°.

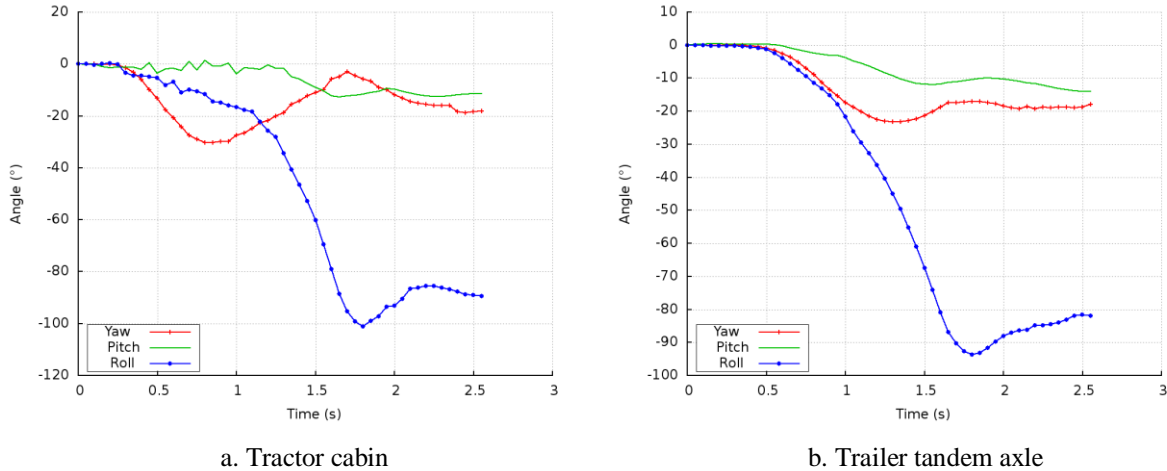


Fig. 4.109: Yaw, pitch, and roll angles of the tractor-trailer impacting the double-faced 31-inch steel-blockout Thrie-beam guardrail at 50 mph (80 km/h) and 15°.

The maximum dynamic deflections of the double-faced 31-inch wood- and steel-blockout Thrie-beam guardrails are shown in Figs. 4.110 and 4.111 for impacts by the tractor-trailer at 50 mph (80 km/h) and 15°. The maximum dynamic deflections were 4.02 ft (1.23 m) at 2.21 seconds and 3.68 ft (1.12 m) at 1.26 seconds for the wood-blockout and steel-blockout Thrie-beam guardrails, respectively. The damaged sections of the two double-faced 31-inch Thrie-beam guardrails were not localized due to the vehicles rolling onto the guardrail. The damage of the double-faced 31-inch wood-blockout Thrie-beam guardrail spanned eighteen posts and ten double-faced guardrail segments. The damage of the steel-blockout Thrie-beam guardrail spanned ten posts across six double-faced guardrail segments.



Fig. 4.110: Maximum dynamic deflection of the double-faced 31-inch wood-blockout Thrie-beam guardrail at 50 mph (80 km/h) and 15° and impacted by a tractor-trailer.



Fig. 4.111: Maximum dynamic deflection of the double-faced 31-inch steel-blockout Thrie-beam guardrail at 50 mph (80 km/h) and 15° and impacted by a tractor-trailer.

Figures 4.112 and 4.113 show the detailed views of two different states of vehicle-barrier interaction throughout the tractor-trailer impacts against the double-faced 31-inch wood- and steel-blockout Thrie-beam guardrails at 50 mph (80 km/h) and 15°. Figures 4.112a and 4.113a show the redirection of the tractor at 0.6 seconds. Figures 4.112b and 4.113b show the trailer impacting the wood-blockout guardrail at 1.5 seconds and the steel-blockout guardrail at 1.26 seconds, respectively.

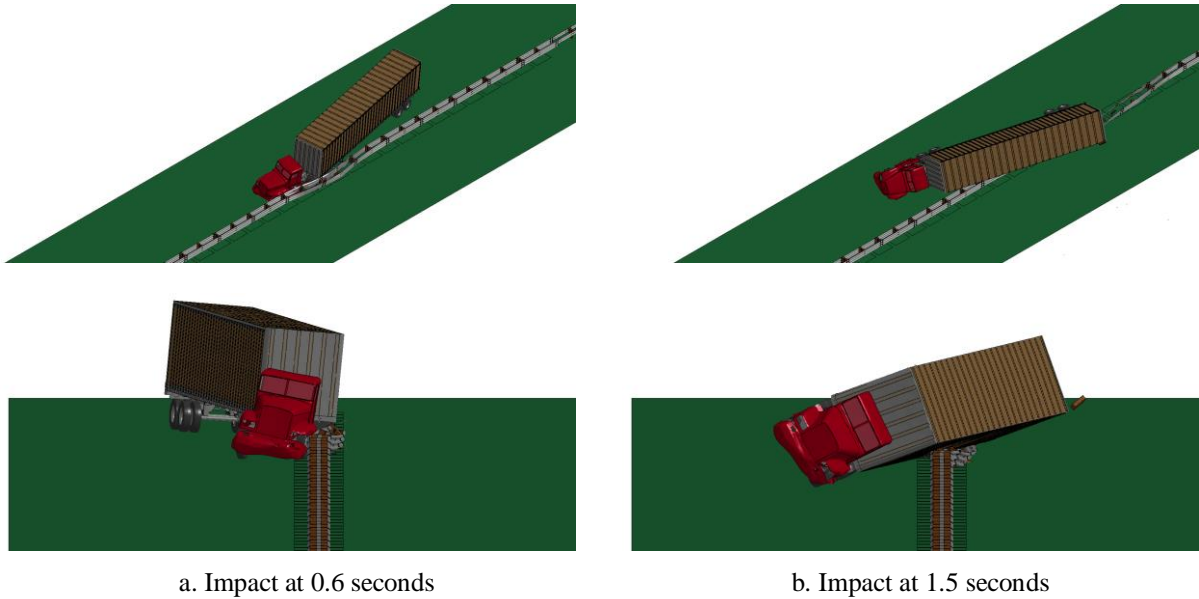


Fig. 4.112: Simulations of tractor-trailer impacting the double-faced 31-inch wood-blockout Thrie-beam guardrail at 50 mph (80 km/h) and 15°.

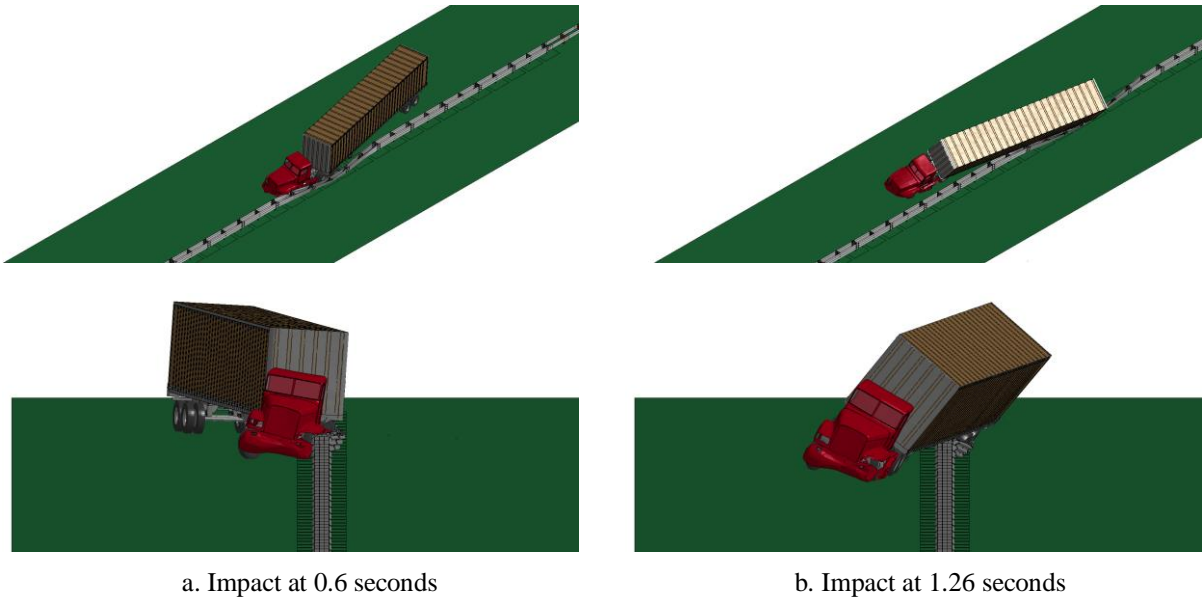
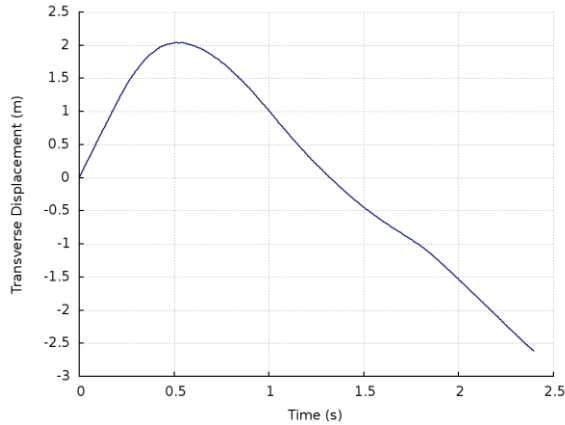


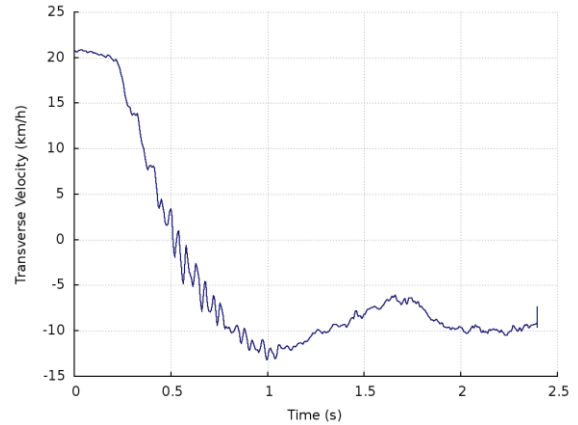
Fig. 4.113: Simulations of tractor-trailer impacting the double-faced 31-inch steel-blockout Thrie-beam guardrail at 50 mph (80 km/h) and 15°.

Figures 4.114 and 4.115 show the time histories of transverse displacements and velocities measured at the CG point of the tractor cabin and at the trailer tandem axle in the impacts against the double-faced 31-inch wood- and steel-blockout Thrie-beam guardrails at 50 mph (80 km/h) and 15°. It can be seen from Figure 4.114a that the maximum positive transverse displacement of the tractor occurred at 0.6 seconds, corresponding to the impact state seen in Fig. 4.112a. Similarly in Fig. 4.114c, the maximum positive transverse displacement of the trailer tandem axle occurred at 1.5 seconds and corresponded to the impact state illustrated in

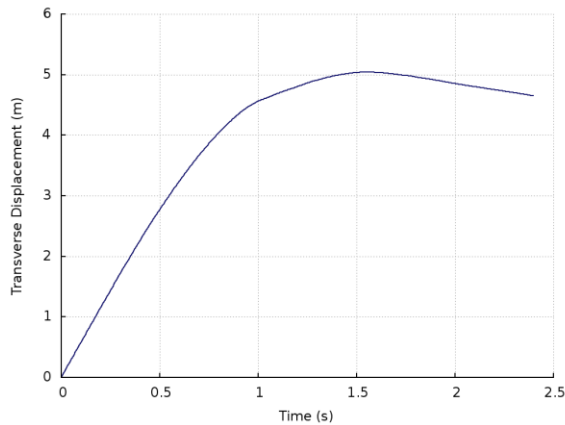
Fig. 4.112b. Figure 4.115a shows the transverse displacements of the tractor in the impact against the double-faced 31-inch steel-blockout Thrie-beam guardrail. The maximum positive transverse displacement of the tractor occurred at 0.6 seconds, corresponding to the impact state seen in Fig. 4.113a. Similarly in Fig. 4.115c, the maximum positive transverse displacement of the trailer tandem axle at 1.26 seconds, which corresponded to the impact state seen in Fig. 4.113b. In the two impacts against the wood- and steel-blockout Thrie-beam guardrails, the trailer rolled onto and stayed in contact with the guardrails; this was evidenced by the absence of a negative transverse displacements of the trailer tandem axle as seen in Figs. 4.114c and 4.115c.



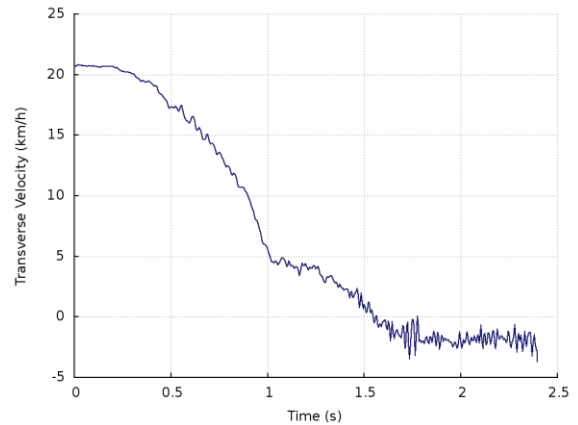
a. Tractor transverse displacement



b. Tractor transverse velocity

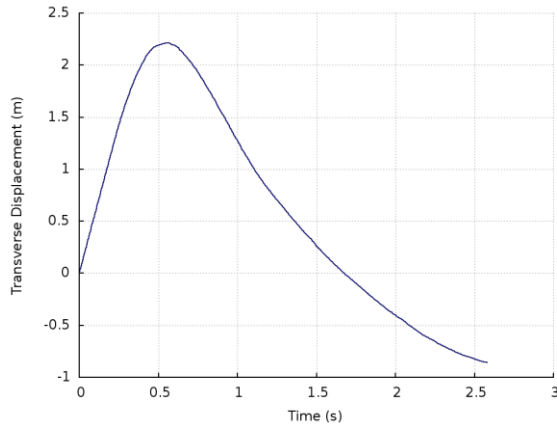


c. Trailer axle transverse displacement

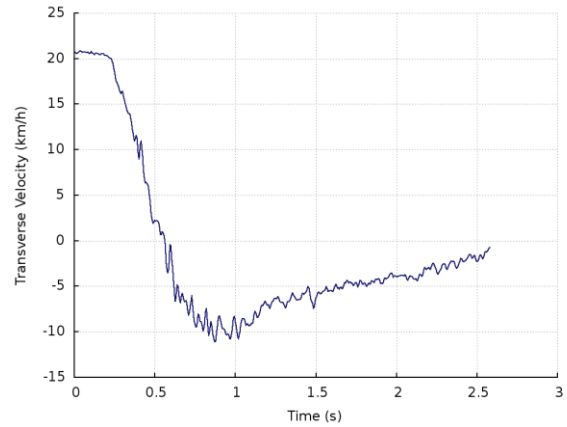


d. Trailer axle transverse velocity

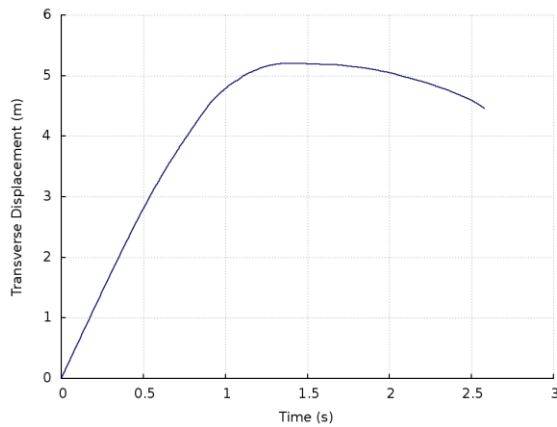
Fig. 4.114: Transverse displacement and velocities of the tractor-trailer impacting the double-faced 31-inch wood-blockout Thrie-beam guardrail at 50 mph (80 km/h) and 15°.



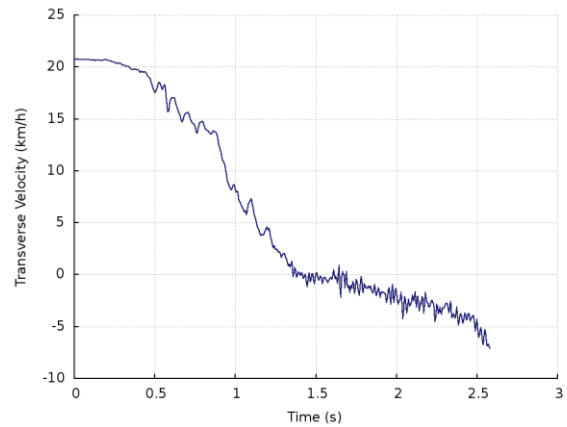
a. Tractor transverse displacement



b. Tractor transverse velocity



c. Trailer axle transverse displacement



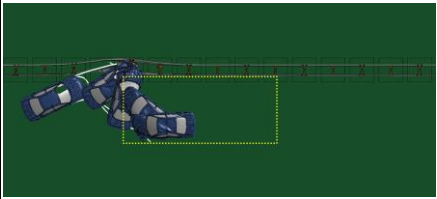
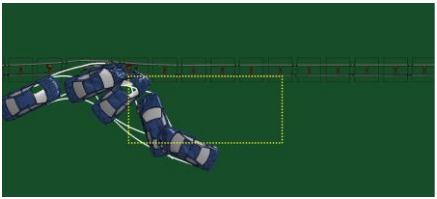
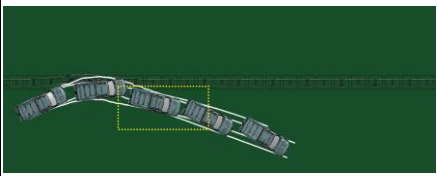
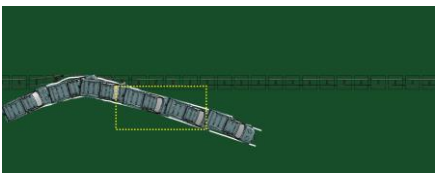
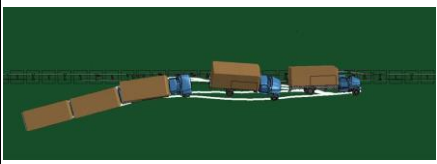
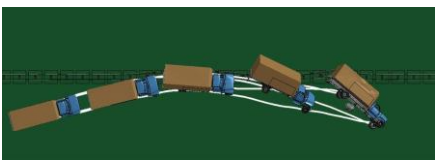
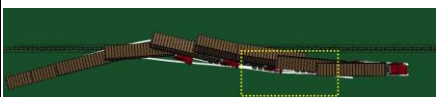

d. Trailer axle transverse velocity

Fig. 4.115: Transverse displacement and velocities of the tractor-trailer impacting the double-faced 31-inch steel-blockout Thrie-beam guardrail at 50 mph (80 km/h) and 15°.

4.5 Comparison of Guardrails at 29- and 31-inch Placement Heights

In Sections 4.1 to 4.4, the performance of double-faced W-beam and Thrie-beam guardrails with wood- and steel-blockouts were evaluated at 29- and 31-inch placement heights, under MASH TL-4 and TL-5 impact conditions. In this section, the performance of the same type of guardrail is compared based on the guardrail heights. Tables 4.7, 4.8, and 4.9 summarize the vehicle redirection characteristics of double-faced W-beam guardrails, double-faced wood-blockout Thrie-beam guardrails, and double-faced steel-blockout Thrie-beam guardrails, respectively. It should be noted that, in Tables 4.7 to 4.9, an impact angle of 25° was used for the small sedan (i.e., Dodge Neon) and pickup truck (i.e., Ford F250) and an impact angle of 15° was used for the single-unit truck and tractor-trailer. An impact speed of 62 mph (100 km/h) was used for the small sedan and pickup truck, 56 mph (90 km/h) was used for the single-unit truck, and 50 mph (80 km/h) was used for the tractor-trailer.

Table 4.7: Vehicle redirection characteristics of double-faced W-beam guardrails

Guardrail Model	Test Vehicle	Guardrail Height	
		29-inch	31-inch
W-beam guardrail	Dodge Neon		
	Ford F250		
	Single-unit truck		
	Tractor-trailer		

With regard to the redirection capability of the double-faced W-beam guardrails at 29- and 31-inch placement heights, the following summarizes the findings from results in Table 4.7 for impacts by the Dodge Neon, Ford F250, single-unit truck, and tractor-trailer.

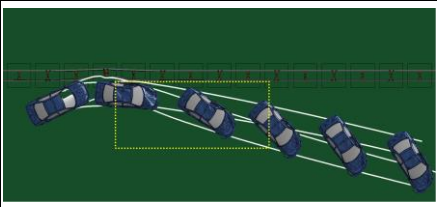
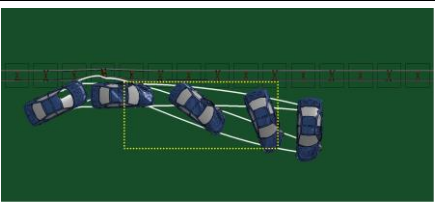
- For both the 29- and 31-inch W-beam guardrails impacted by the Dodge Neon, the simulation results showed that the vehicle partially underrode the guardrail and directly impacted a post. This direct impact on the post caused snagging and pocketing that redirected the vehicle abruptly away from the guardrail with a continuous clockwise rotation and thus failed the MASH exit box criterion. The 31-inch W-beam guardrail redirected the Dodge Neon 0.15 seconds faster than the 29-inch W-beam guardrail and deflected 0.52 ft (0.16 m) further throughout the impact. The Dodge Neon experienced lower rotational motions (i.e., with smaller yaw, pitch, and roll angles) impacting the 31-inch W-beam guardrail than impacting the 29-inch guardrail.
- For impacts by the Ford F250, the simulation results show that both the double-faced 29- and 31-inch W-beam guardrails redirected the vehicle with small exit angles enough to pass the MASH exit box criterion. The exit angle of the Ford F250 impacting the 29-inch W-beam guardrail was slightly smaller than that of the 31-inch W-beam guardrail. Unlike the Dodge Neon impact cases, the 29-inch guardrail redirected the Ford F250 0.12 seconds faster and deflected 0.29 ft (0.07 m) less than the 31-inch W-beam guardrail. The Ford F250 experienced low rotational motions (i.e., with small yaw, pitch, and roll angles) when impacting the 31-inch W-beam guardrail.

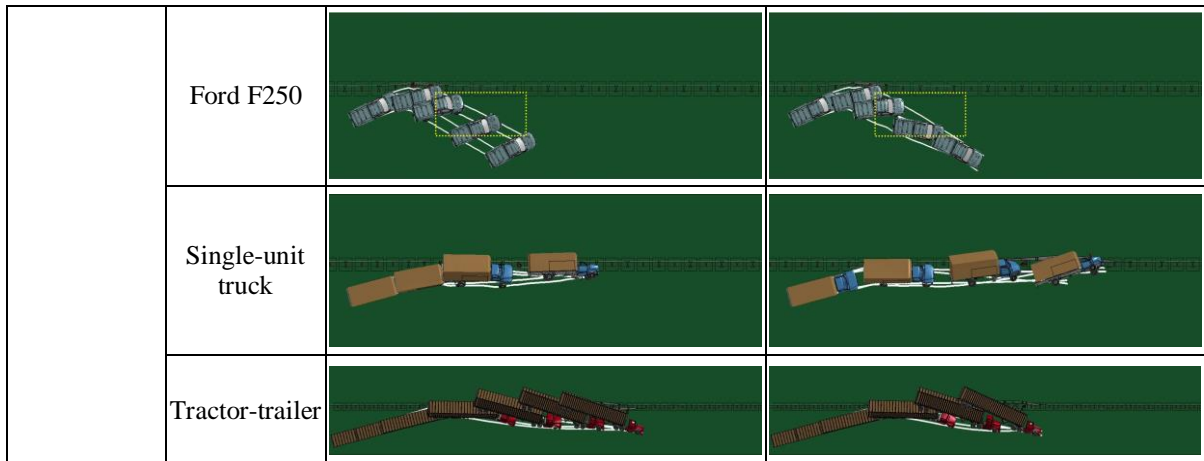
- For impacts by the single-unit truck, the vehicle failed to remain upright and rolled onto the guardrail in both cases; therefore, there was no determinable exit angle and the MASH exit box criterion was not used. These impacts failed the MASH evaluation criterion F , which specified a maximum 75° roll or pitch angle. However, remaining upright was not required by MASH as per the statement “although it is preferable all vehicles remain upright, this requirement is not applicable for tests involving the 10000S (i.e., single-unit truck) and 36000V (i.e., tractor-trailer) vehicles.” This exception of allowing a 90° roll for heavy vehicle impacts relies on the fact that the primary goal of the heavy-vehicle impacts is to demonstrate the guardrail’s ability to contain and redirect the vehicle.
- In both impacts against the double-faced 29- and 31-inch W-beam guardrails, the tractor-trailer was successfully redirected and the two cases passed the MASH exit box criterion. The 31-inch W-beam guardrail redirected the tractor-trailer with a smaller exit angle and 0.16 seconds faster than the 29-inch W-beam guardrail. The 31-inch W-beam guardrail had a maximum dynamic deflection of 8.623 ft (2.63 m), which was 0.52 ft (0.16 m) larger than that of the 29-inch W-beam guardrail. As for the rotational motions (i.e., yaw, pitch, and roll angles), the tractor-trailer experienced low pitch and roll and yaw rotations in both impacts.

The results in Table 4.7 show that both the 29- and 31-inch double-faced W-beam guardrails could retain the four vehicles on the impact side, though the single-unit truck did protrude into the opposite sides of both guardrails. In regard to redirection of the impacting vehicles, both W-beam guardrails were capable of redirecting the four vehicles and passed the MASH exit box criteria for impacts by the Ford F250 and tractor-trailer. It should be noted that for the two impacts by the Dodge Neon, the vehicle experienced severe snagging and pocketing due to direct impact on the posts. Consequently, the Dodge Neon had a large rotation after losing contact with the guardrails and traveling towards the travel lane.

Table 4.8 summarizes vehicle trajectories of the four test vehicles impacting the double-faced 29- and 31-inch wood-blockout Thrie-beam guardrails impacts from the four test vehicles. Note that the impact speeds were 62 mph (100 km/hr) for the Dodge Neon and Ford F250, 56 mph (90 km/hr) for the single-unit truck, and 50 mph (80 km/hr) for the tractor-trailer. The impact angles were 25° for the Dodge Neon and Ford F250, and 15° for the single-unit truck and tractor-trailer.

Table 4.8: Vehicle redirection characteristics of double-faced wood-blockout Thrie-beam guardrails

Guardrail Model	Test Vehicle	Guardrail Height	
		29-inch	31-inch
Wood-blockout Thrie-beam guardrail	Dodge Neon		



With regard to the redirection capability of the double-faced wood-blockout Thrie-beam guardrails at 29- and 31-inch placement heights, the following summarizes the findings from results in Table 4.8 for impacts by the Dodge Neon, Ford F250, single-unit truck, and tractor-trailer.

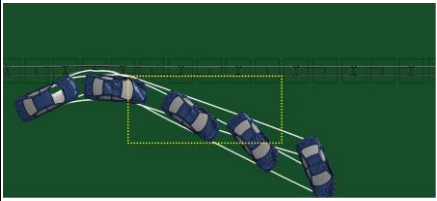
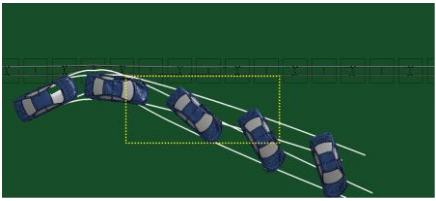
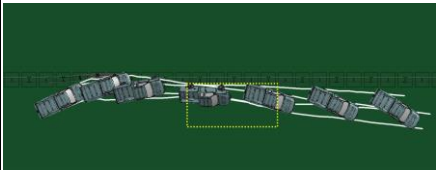
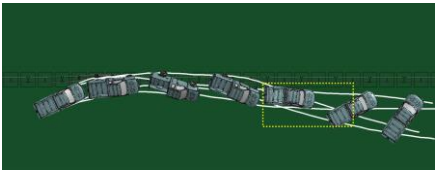



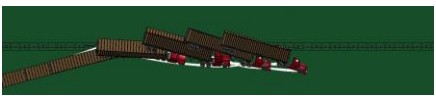
- The double-faced wood-blockout Thrie-beam guardrails at 29- and 31-inch placement heights were able to redirect the Dodge Neon with low exit angles to pass the MASH exit box criterion. In both cases, vehicle snagging and pocketing, as seen on the W-beam guardrails, were not apparent in the cases with these two wood-block Thrie-beam guardrails. The Dodge Neon experienced lower rotational motions in terms of pitch and roll angles; however, the vehicle had continuous yaw rotations after impacting and leaving the guardrails.
- Under impacts by the Ford F250, both the 29- and 31-inch wood-blockout Thrie-beam guardrails were capable of retaining the vehicle on the impacting sides of the guardrails, yet failed to pass the MASH exit box criterion. Upon impacting the 29-inch wood-blockout Thrie-beam guardrail, the Ford F250 was not fully redirected before losing contact with the guardrail towards the travel lane. In the case with the 31-inch wood-blockout Thrie-beam guardrail, the Ford F250 was redirected with a large exit angle and went out of the exit box from the long side. In both impact cases, the Ford F250 experienced a low rotational motions in terms of pitch and roll angles.
- In the two impacts against the double-faced 29- and 31-inch wood-blockout Thrie-beam guardrails, the single-unit truck failed to remain upright and rolled onto the guardrail. Therefore, no determinable exit angle was available and the MASH exit box criterion was not used. These two impact cases failed the MASH evaluation criterion *F*, which specified a maximum 75° roll or pitch angle. As per MASH, “although it is preferable all vehicles remain upright, this requirement is not applicable for tests involving the 10000S (i.e., single-unit truck) and 36000V (i.e., tractor-trailer) vehicles.” This exception of allowing a 90° roll for heavy vehicles relies on the fact that the primary goal of the impact scenarios is to demonstrate the guardrail’s ability to contain and redirect the vehicle.
- Similar to the cases of the single-unit truck, the tractor-trailer failed to remain upright and rolled onto the guardrails during impacts on the double-faced 29- and 31-inch wood-

blockout Thrie-beam guardrails. Therefore, no determinable exit angle was available and the MASH exit box criterion was not used. These impacts failed the MASH evaluation criterion *F*, which specified a maximum 75° roll or pitch angle. As per MASH, “although it is preferable all vehicles remain upright, this requirement is not applicable for tests involving the 10000S (i.e., single-unit truck) and 36000V (i.e., tractor-trailer) vehicles.”

At both 29- and 31-inch placement heights, the double-faced wood-blockout Thrie-beam guardrails were capable of retaining all four test vehicles on the impacting side of the guardrails, though portions of the single-unit truck and tractor-trailer did protrude into the opposite side of the guardrail.

Table 4.9 summarizes vehicle trajectories of the four test vehicles in the impacts against the double-faced 29- and 31-inch steel-blockout Thrie-beam guardrails. The impact speeds were 62 mph (100 km/h) for the Dodge Neon and Ford F250, 56 mph (90 km/h) for the single-unit truck, and 50 mph (80 km/h) for the tractor-trailer. The impact angles were 25° for the Dodge Neon and Ford F250, and 15° for the single-unit truck and tractor-trailer.

Table 4.9: Vehicle redirection characteristics of double-faced steel-blockout Thrie-beam guardrails

Guardrail Model	Test Vehicle	Guardrail Height	
		29-inch	31-inch
Steel-blockout Thrie-beam guardrail	Dodge Neon		
	Ford F250		
	Single-unit truck		
	Tractor-trailer		

With regard to the redirection capability of the double-faced steel-blockout Thrie-beam guardrails at 29- and 31-inch placement heights, the following summarizes the findings from results in Table 4.9 for impacts by the Dodge Neon, Ford F250, single-unit truck, and tractor-trailer.

- Under impacts by the Dodge Neon, the double-faced 29- and 31-inch steel-blockout Thrie-beam guardrails were capable of redirecting the vehicle; however, the exit angles were large in both cases and failed to pass the MASH exit box criterion. The Dodge Neon experienced small roll and pitch rotations and passed the MASH criterion *F*. The vehicle had a large yaw rotations in both cases, with a continuous clockwise rotation after being redirected and leaving the guardrail.
- For both impacts by the Ford F250 on the double-faced 29- and 31-inch steel-blockout Thrie-beam guardrails, the vehicle partially vaulted onto the guardrails but landed on the impacting sides of the guardrails. Due to vaulting on the guardrails, the Ford F250 stayed in contact with the guardrails for an extended period of time compared to the cases of the wood-blockout Thrie-beam guardrail. In both cases, the vehicle had low exit angles that were small enough to pass the MASH exit box criterion. In addition, the Ford F250 experienced low rotational motions in terms of the pitch and roll angles, which passed the MASH criterion *F*. It was observed that, after impacting and leaving the 31-inch steel-blockout Thrie-beam guardrail, the Ford F250 experienced a counterclockwise yaw rotation, which was due to the vaulting but was not seen in the case of the 29-inch guardrail..
- In the four impacts by the single-unit truck and tractor-trailer against the double-faced 29- and 31-inch steel-blockout Thrie-beam guardrails, both vehicles were redirected but failed to remain upright and rolled onto the guardrail; therefore, no determinable exit angle was available and the MASH exit box criterion was not used. These impacts failed the MASH evaluation criterion *F*, which specified a maximum 75° roll or pitch angle. As per MASH, “although it is preferable all vehicles remain upright, this requirement is not applicable for tests involving the 10000S (i.e., single-unit truck) and 36000V (i.e., tractor-trailer) vehicles.” This exception of allowing a 90° roll for heavy vehicles relies on the fact that the primary goal of the impact scenarios is to demonstrate the guardrail’s ability to contain and redirect the vehicle..

At both 29- and 31-inch placement heights, the double-faced steel-blockout Thrie-beam guardrails, were capable of redirecting/retaining the Dodge Neon, Ford F250, single-unit truck, and tractor-trailer. For the impacts by the Dodge Neon, vehicle snagging and pocketing did not occur on the steel-blockout Thrie-beam guardrails; however, the vehicle had large exit angles and failed to pass the MASH exit box criterion. It should be noted that, although portions of the single-unit truck and tractor-trailer protruded into the opposite side of the guardrails during impacts, the two guardrails were capable of preventing the vehicles from penetrating through and retained the majority of the vehicles on the impacting sides.

5. Findings and Conclusions

In this project, finite element simulations were conducted to study the performance of one double-faced W-beam and two Thrie-beam guardrails installed on flat terrain, each with 29- and 31-inch placement heights. The two Thrie-beam guardrails differed in the blockout materials used, one with wood and the other with steel. The impact scenarios were simulated using four MASH test vehicles, a 1996 Dodge Neon passenger sedan, a 2006 Ford F250 pickup truck, a 1996 F800 single-unit truck, and a 1991 GMC day cab tractor-trailer. All crash simulations were conducted at MASH Test Level 4 (TL-4) and Test Level 5 (TL-5) impact conditions. At TL-4 conditions, the guardrails were impacted by the Dodge Neon and Ford F250 at 62 mph (100 km/h) and a 25° impact angle, and by the single-unit truck at 56 mph (90 km/h) and a 15° impact angle. At TL-5 conditions, the guardrails were impacted by the Dodge Neon and Ford F250 at 62 mph (100 km/h) and a 25° impact angle, and by the tractor-trailer at 50 mph (80 km/h) and a 15° impact angle. The simulation results provided insight into the vehicle redirection characteristics of double-faced W-beam and Thrie-beam guardrails for different test vehicle classes as well as guardrail performance in relation to guardrail placement heights and blockout types for the Thrie-beam guardrails. Some of the major research findings are summarized as follows.

- At both 29- and 31-inch placement heights, the W-beam guardrails were capable of retaining the vehicles on the impacting sides of the guardrails in all impacts. In the impacts by the Ford F250 and the tractor-trailer, the W-beam guardrails at both heights safely redirected the vehicles with low exit angles that passed the MASH exit box criterion. In the two impacts by the Dodge Neon, the vehicle experienced tire snagging and pocketing on the post, resulting in undesirable post-impact trajectories and failing to pass the MASH exit box criterion. For impacts by the single-unit truck against the two W-beam guardrails, the vehicle failed to remain upright and rolled onto the guardrails but remained on the impacting sides of the guardrails.
- For the double-faced 29- and 31-inch wood-blockout Thrie-beam guardrails, all the four test vehicles were retained on the impacting sides of the guardrails. In both impacts by the Dodge Neon, the vehicle was redirected with low exit angles and passed the MASH exit box criterion. The Ford F250 was also redirected by the two wood-block guardrails, but with large exit angles, traveling transversely away from the guardrails, and failing the MASH exit box criterion. In all the impact cases by the single-unit truck and tractor-trailer, both vehicles failed to remain upright and rolled onto the guardrails, but remained on the impacting sides of the guardrails. The rollover of the single-unit truck and the tractor-trailer, however, was considered acceptable post-impact behavior according to MASH, under the stipulation that the vehicles were contained and did not fully penetrate the guardrails.
- For the double-faced 29- and 31-inch steel-blockout Thrie-beam guardrails, all the four test vehicles were retained on the impacting sides of the guardrails. In both impacts by the Dodge Neon, the vehicle was redirected with large exit angles and failed to pass the MASH exit box criterion. In both impacts by the Ford F250, the vehicle vaulted up the face of the guardrails, deflected the impacted post, and landed on the impacting sides with low exit angles that passed the MASH exit box criterion. In all the impact cases

by the single-unit truck and tractor-trailer, both vehicles failed to remain upright and rolled onto the guardrails, but remained on the impacting sides of the guardrails. The rollover of the single-unit truck and the tractor-trailer, however, was considered acceptable post-impact behavior according to MASH, under the stipulation that the vehicles were contained and did not fully penetrate the guardrails.

- The maximum dynamic deflections on all guardrails were relatively small and localized in the impacts by the Dodge Neon and Ford F250. Considering the impacts from these two test vehicles, the guardrail deflections were generally larger on the 31-inch guardrails than those on the 29-inch guardrails for the same vehicle. For impacts by the single-unit truck and tractor-trailer, the W-beam guardrails deflected much further than the Thrie-beam guardrails, and the 31-inch guardrails deflected further than the 29-inch guardrails for the same vehicles. The largest maximum dynamic deflection of the guardrail occurred on the double-faced 31-inch W-beam guardrail impacted by the tractor-trailer, with a deflection of 8.62 ft (2.63 m).
- The MASH evaluation criterion F , which specified a maximum roll or pitch angle of 75° , was satisfied in all the impacts by the Dodge Neon and Ford F250. All of the impacts by the single-unit truck and the tractor-trailer, excluding the W-beam guardrails, failed to pass the MASH evaluation criterion F , which were not required for impacts by the single-unit truck and tractor-trailer.
- In all the impact cases of this study, the test vehicles were retained on the impacting side of the guardrails without fully penetrating the guardrails, eliminating the possibility of entering the oncoming traffic lanes and causing a head-on collision. It should be noted that in some impact cases by the single-unit truck and tractor-trailer, the test vehicles rolled onto the barrier and partially overrode the guardrails, but the majority of both vehicles remained on the impacting sides of the guardrails.
- For the double-faced W-beam and Thrie-beam guardrails of this study, vehicle snagging and pocketing were present in all impact cases, resulting in undesirable post-impact vehicle trajectories (i.e., Dodge Neon impacting the 29- and 31-inch W-beam guardrails, Ford F250 impacting the 29- and 31-inch wood-blockout Thrie-beam guardrails, and the Dodge Neon impacting the 29- and 31-inch steel-blockout Thrie-beam guardrails). Except for the above mentioned undesirable post-impact vehicle trajectories, the double-faced W-beam and Thrie-beam guardrails satisfied the MASH TL-4 and TL-5 requirements.
- In all of the impacts by the single-unit truck and tractor-trailer on the Thrie-beam guardrails, the vehicles experienced rollover that is caused by the elevated center-of-gravity (CG) of these heavy vehicles. This common outcome can be attributed to the fact that the guardrails in this study are typically only designed and tested to pass up to MASH TL-3 impact conditions. The impact cases in this study demonstrated the worst-case scenarios of the guardrails impacted by a variety of vehicles commonly seen on the roadway.
- The simulation results of this project can be used to interpret the performance trends of W-beam and Thrie-beam guardrails. They should not be used to draw definitive conclusions about their performance for a specific crash event because some factors

that could affect the performance were not considered in the simulations for this study. These factors included, but were not limited to, impact locations along the longitudinal axis of the barriers, weather and soil conditions, and pre- and post-impact driver response behaviors. Nevertheless, finite element analysis was demonstrated to be a useful tool in crash analysis and could be used in future investigations of other research issues.

6. Recommendations

Based on the simulation results of this study, it was determined that all guardrails were capable of containing all four test vehicles on the impacting side of the guardrails. Although the post-impact trajectories of the Dodge Neon impacting the double-faced 29- and 31-inch W-beam and steel-blockout Thrie-beam guardrails, as well as the Ford F250 impacting the 29- and 31-inch wood-blockout Thrie-beam guardrails were unsatisfactory, the six aforementioned double-faced guardrails performed adequately well under MASH TL-4 and TL-5 impact conditions. The wood-blockout Thrie-beam guardrails were found to provide safer redirection characteristics than the steel-blockout Thrie-beam guardrails based on the evaluation of exit angles, MASH exit box criterion, MASH evaluation criterion F , transverse displacements and velocities, and maximum dynamic guardrail deflections.

7. Implementation and Technology Transfer Plan

The simulation results of this project will be submitted to NCDOT for consideration in future projects to install or retrofit W-beam and Thrie-beam guardrails when allowed by site conditions and deemed necessary by NCDOT personnel. Detailed simulation results will be provided to NCDOT engineers for a comprehensive understanding in evaluating proposed roadside features and/or improving the safety performance of the current system. The modeling and simulation work, along with research findings, will be presented at technical conferences and submitted for publication in technical journals to help researchers and DOT engineers nationwide with similar needs. The research results of this project will be distributed to the public through this report, which will be made available by NCDOT.

References

1. AASHTO. (2011). "Roadside Design Guide, 4th edition." American Association of State Highway and Transportation Officials, Washington, D.C.
2. Alluri, P., Haleem, K., and Gan, A. (2012). "In-Service Performance Evaluation (ISPE) for G4 (1S) Type of Strong-Post W-Beam Guardrail System and Cable Median Barrier: Volume I." *Final Report FDOT BDK80 977-19*, State of Florida Department of Transportation, Tallahassee, FL.
3. Atahan, A. O. (2002). "Finite element simulation of a strong-post W-beam guardrail system." *Simulation*, 78(10), 587-599.
4. Atahan, A. O., and Cansiz, O. F. (2005). "Impact analysis of a vertical flared back bridge rail-to-guardrail transition structure using simulation." *Finite Elements in Analysis and Design*, 41(4), 371-396.
5. Bligh, R. P., Abu-Odeh, A. Y., Hamilton, M. E., and Seckinger, N. R. (2004). "Evaluation of roadside safety devices using finite element analysis." *Report 0-1816-1*, Texas Transportation Institute, College Station, TX.
6. Bligh, R., Miaou, S.-P., Lord, D., and Cooner, S. (2006). "Median barrier guidelines for Texas." *Report 0-4254-1*, Texas Transportation Institute, College Station, TX.
7. Bryden, J. E., Hahn, K. C. (1981) "Crash Tests of Light-Post Thrie-Beam Traffic Barriers." *Transportation Research Record: Journal of the Transportation Research Board*, 796, 41-50.
8. Buth, C.E., Menges, W.L., Butler, B.G. (1998). "NCHRP Report 350 test 3-21 of the vertical flared back transition." Texas Transportation Institute, Test No. 404211-4, Federal Highway Administration, Publication No. FHWA-RD-99-062.
9. Donnell, E. T., Harwood, D. W., Bauer, K. M., Mason, J. M., and Pietrucha, M. T. (2002). "Cross-median collisions on Pennsylvania interstates and expressways." *Transportation Research Record*, 1784, 91-99.
10. Fang, H., Li, N., and Tian, N., (2010). "Median barrier placement on six-lane, 46-foot median divided freeways." No. FHWA/NC/2009-04. *Final Report NCDOT 2009-04*, North Carolina Department of Transportation, Raleigh, NC.
11. Fang, H., Gutowski, M., Li, N., and DiSogra, M., (2013). "Performance Evaluation of NCDOT W-beam Guardrails under MASH TL-2 Conditions." No. FHWA/NC/2012-11. *Final Report NCDOT 2012-11*, North Carolina Department of Transportation, Raleigh, NC.
12. Fang, H., Gutowski, M., Palta, E., Kuvila, D., Baker, R., and Li, N. (2015). "Performance Evaluation of 29-inch and 31-inch W-beam Guardrails on Six-lane, 46-foot Median Divided Freeways." No. FHWA/NC/2014-14. *Final Report NCDOT 2014-14*, North Carolina Department of Transportation, Raleigh, NC.

13. Ferdous, M. R., Abu-Odeh, A., Bligh, R. P., Jones, H. L., and Sheikh, N. M., (2011). "Performance limit analysis for common roadside and median barriers using LS-DYNA." *International Journal of Crashworthiness*, 16(6), 691-706.
14. Findley, D. J., Cunningham, C. M., Schroeder, B. J., Vaughan, C. L., and Fowler, T. J., (2012). "Structural and safety investigation of statewide performance of weathered steel beam guardrail in North Carolina." *Transportation Research Record: Journal of the Transportation Research Board*, 2309, 63-72.
15. Gabauer, D. J., Kusano, K. D., Marzougui, D., Opiela, K., Hargrave, M., and Gabler, H. C. (2010). "Pendulum testing as a means of assessing the crash performance of longitudinal barrier with minor damage." *International Journal of Impact Engineering*, 37(11), 1121-1137.
16. Gabler, H.C., Gabauer, D.J., and Bowen, D. (2005). "Evaluation of Cross Median Crashes, Final Report.", *Final Report FHWA-NJ-2005-004*, Rowan University, Glassboror, NJ.
17. Gabler, H. C. and Gabauer, D. J. (2006). "Safety audit of fatalities and injuries involving guide rail." *Final Report FHWA-NJ-2007-001*, Virginia Tech, Blacksburg, VA.
18. Hallquist, J. O. (2017). "LS-DYNA Theory Manual rev. 8339." Livermore Software Technology Corporation. Livermore, CA.
19. Hampton, C. E., Gabauer, D. J., and Gabler, H. C., (2010). "Limits of acceptable rail-and-post deflection in crash-damaged strong-post W-beam guardrail." *Transportation Research Record: Journal of the Transportation Research Board*, 2195, 95-105.
20. Hampton, C. and Gabler, H. (2013). "Development of a missing post repair guideline for longitudinal barrier crash safety." *Journal of Transportation Engineering*, 139(6), 549-555.
21. Hiser, N. R., and Reid, J. D. (2005). "Modeling slip base mechanisms." *International Journal of Crashworthiness*, 10(5), 463-472.
22. Hu, W., and Donnell, E. T. (2010). "Median barrier crash severity: some new insights." *Accident Analysis & Prevention*, 42(6), 1697-1704.
23. Jehu, V. J., (1968) "Crash Barrier Developments." *Proceedings of the Institution of Mechanical Engineers*, 183, Pt 3A.
24. Kan, C.-D., Marzougui, D., Bahouth, G. T., and Bedewi, N. E. (2001). "Crashworthiness evaluation using integrated vehicle and occupant finite element models." *International Journal of Crashworthiness*, 6, 387-398.
25. Lewis, B. A. (2004). "Manual for LS-DYNA soil material model 147." *FHWA-HRT-04-095*, U.S. Department of Transportation, Federal Highway Administration, McLean, VA.
26. LSTC (2016). "LS-DYNA Keyword User's Manual, Volume I, Version R9.0 (r:7883)." Livermore Software Technology Corporation. Livermore, CA.
27. Lynch, J. M., Crowe, N. C., and Rosendahl, J. F. (1993). "Interstate across median accident study: a comprehensive study of traffic accidents involving errant vehicles which cross the

- median divider strips on North Carolina interstate highways.” *1993 AASHTO Annual Meeting Proceedings*, 125-133.
28. Mackerle, J. (2003). “Finite element crash simulations and impact-induced injuries: an addendum. A bibliography (1998–2002).” *The Shock and Vibration Digest*, 35(4), 273-280.
 29. Mak, K. K., and Menges, W. L. (1998). “Testing of State Roadside Safety Systems Volume VIII: Appendix G – Crash Testing and Evaluation of the Single Slope Bridge Rail.” *Report No. FHWA-RD-98-043*. Texas Transportation Institute, College Station, Texas.
 30. Mak, K. K., and Bligh, R. P. (2002). “Assessment of NCHRP Report 350 test conditions.” *Transportation Research Record 1797*, 38-43.
 31. Mak, K. K., and Sicking, D. L. (2003). “NCHRP Report 492 roadside safety analysis program (RSAP) – engineer’s manual.” *Transportation Research Board*, 7-28.
 32. Marzougui, D., Bahouth, G., Eskandarian, A., Meczkowski, L., and Taylor, H. (2000). “Evaluation of portable concrete barriers using finite element simulation.” *Transportation Research Record*, 1720, 1-6.
 33. Marzougui, D. (2003). “Freightliner into 42 in. F-Shape concrete barrier at 25 degrees.” *Test Setup Report, Test No. 03008*. Federal Outdoor Impact Laboratory, McLean, Virginia.
 34. Marzougui, D., Zink, M., Zaouk, A. K., Kan, C.-D., and Bedewi, N. E. (2004). “Development and validation of a vehicle suspension finite element model for use in crash simulations.” *International Journal of Crashworthiness*, 9(6), 565-576.
 35. Marzougui, D., Mohan, P., Kan, C.-D., and Opiela, K. S. (2007). “Evaluation of rail height effects on the safety performance of W-beam barriers.” *2007 TRB Annual Meeting*, Washington, D.C.
 36. Marzougui, D., Mohan, P., Kan, C.-D., and Opiela, K. S. (2012). “Assessing options for improving barrier crashworthiness using finite element models and crash simulations.” *Final Report NCAC-2012-W-008*, National Crash Analysis Center, George Washington University, Washington, D.C.
 37. MASH (2009). “Manual for assessing safety hardware (MASH).” American Association of State Highway and Transportation Officials (AASHTO), Washington D.C.
 38. Miaou, S.-P., Bligh, R. P., and Lord, D. (2005). “Developing guidelines for median barrier installation: benefit-cost analysis with Texas data.” *Transportation Research Record*, 1904, 3-19.
 39. Mohan, P., Marzougui, D., and Kan, C.-D. (2007). “Validation of a single unit truck model for roadside hardware impact.” *International Journal of Vehicle Systems Modelling and Testing*, 2(1), 1-15.
 40. Mongiardini, M., and Reid, J. D. (2013). “Investigation of a series of relevant phenomena for modeling the full-scale crash test of a small vehicle with a guardrail system.” *International Journal of Computer Aided Engineering and Technology*, 5(1), 58-75.

41. Murray, Y. D., Reid, J. D., Faller, R. K., Bielenberg, B. W., and Paulsen, T. J. (2005). "Evaluation of LS-DYNA wood material model 143." *FHWA-HRT-04-096*, U.S. Department of Transportation, Federal Highway Administration, McLean, VA.
42. Murray, Y. D. (2007). "User manual for LS-DYNA concrete material model 159." *FHWA-HRT-05-062*, U.S. Department of Transportation, Federal Highway Administration, McLean, VA.
43. NCAC (web1). "NCAC Finite Element Model Archive." <
<https://web.archive.org/web/20160407182838/http://www.ncac.gwu.edu/vml/models.html>>.
44. NCAC (web2). "NCAC Papers & Publications." <
<https://web.archive.org/web/20160419032909/http://www.ncac.gwu.edu:80/filmlibrary/publications.html>>.
45. NCAC (2007a). "Technical Summary – NCAC 2007-T-007: Development & Validation of a Finite Element Model for the 1996 Dodge Neon Passenger Sedan." <
<http://www.ncac.gwu.edu/research/pubs/NCAC-2007-T-007.pdf>>
46. NCAC (2007b). "Technical Summary – NCAC 2007-T-004: Development of a Finite Element Model for W-beam Guardrails." <
<http://www.ncac.gwu.edu/research/pubs/NCAC-2007-T-004.pdf>>
47. NCAC (2008). "Technical Summary – NCAC 2008-T-003: Development & Validation of a Finite Element Model for the 2006 Ford F250 Pickup Truck." <
<http://www.ncac.gwu.edu/research/pubs/NCAC-2008-T-003.pdf>>
48. NCDOT. (2012). "NCDOT Roadway Standard Drawings." North Carolina Department of Transportation, Raleigh, NC.
49. NCHRP 22-14 (2001). "Improvement of the Procedures for the Safety-Performance Evaluation of Roadside Features." <
<http://apps.trb.org/cmsfeed/TRBNetProjectDisplay.asp?ProjectID=687>>.
50. NCHRP 22-16 (2003). "Development of an Improved Roadside Barrier System." <
http://onlinepubs.trb.org/onlinepubs/nchrp/nchrp_rrd_273.pdf>.
51. NCHRP 22-21 (2011). "Project 22-21: median cross-section design for rural divided highways." <
<http://apps.trb.org/cmsfeed/TRBNetProjectDisplay.asp?ProjectID=694>>.
52. NCHRP 22-22 (2010). "Project 22-22: placement of traffic barriers on roadside and median slopes." <
<http://apps.trb.org/cmsfeed/TRBNetProjectDisplay.asp?ProjectID=695>>.
53. NCHRP 22-27 (2012). "Project 22-27: roadside safety analysis program (RSAP) update." <
<http://apps.trb.org/cmsfeed/TRBNetProjectDisplay.asp?ProjectID=2517>>.
54. Nicol, D. A. (2010). "Roadside design: steel strong-post W-beam guardrail." *Memorandum 051710*, U.S. Department of Transportation, Federal Highway Administration, McLean, VA.
55. Ochoa, C. M., and Ochoa, T. A. (2011). "Guardrail optimization for rural roads." *Transportation Research Board of the National Academies*, 2203, 71-78.

56. Orengo, F., Ray, M. H., and Plaxico, C. A. (2003). "Modeling tire blow-out in roadside hardware simulations using LS-DYNA." *IMECE2003-55057*, 2003 ASME International Mechanical Engineering Congress & Exposition, Washington, D.C.
57. Patzner, G. S., Plaxico, C. A., and Ray, M. H. (1999). "Effects of post and soil strength on performance of modified eccentric loader breakaway cable terminal." *Transportation Research Record*, 1690, 78-83.
58. Plaxico, C. A., Ray, M. H., and Hiranmayee, K. (2000). "Impact performance of the G4(1W) and G4(2W) guardrail systems: comparison under NCHRP Report 350 test 3-11 conditions." *Transportation Research Record*, 1720, 7-18.
59. Plaxico, C. A., Mozzarelli, F., and Ray, M. H. (2003). "Tests and simulation of a w-beam rail-to-post connection." *International Journal of Crashworthiness*, 8(6), 543-551.
60. Plaxico, C., Kennedy, J., Simunovic, S. and Zisi, N., (2008). "Enhanced Finite Element Analysis Crash Model of Tractor-Trailers (Phase A)." National Transportation Research Center, Inc., Knoxville, TN.
61. Plaxico, C., Kennedy, J., Simunovic, S. and Zisi, N., (2009). "Enhanced Finite Element Analysis Crash Model of Tractor-Trailers (Phase B)." National Transportation Research Center, Inc., Knoxville, TN.
62. Plaxico, C., Kennedy, J., Simunovic, S. and Zisi, N., (2010). "Enhanced Finite Element Analysis Crash Model of Tractor-Trailers (Phase C)." National Transportation Research Center, Inc., Knoxville, TN.
63. Ray, M. H. (1996a). "Repeatability of full-scale crash tests and criteria for validating simulation results." *Transportation Research Record*, 1528, 155-160.
64. Ray, M. H. (1996b). "Use of finite element analysis in roadside hardware design." *Transportation Research Circular*, 453, 61-71.
65. Ray, M. H., and Patzner, G. S. (1997). "Finite element model of modified eccentric loader terminal (MELT)." *Transportation Research Record*, 1599, 11-21.
66. Ray, M. H., and Weir, J. A. (2001). "Unreported collisions with post-and-beam guardrails in Connecticut, Iowa, and North Carolina." *Transportation Research Record*, 1743, 111-119.
67. Ray, M. H., Weir, J., and Hopp, J. (2003). "In-service performance of traffic barriers." *NCHRP Report 490*, Transportation Research Board, National Research Council, Washington, D.C.
68. Ray, M. H., Oldani, E., and Plaxico, C. A. (2004). "Design and analysis of an aluminum F-shape bridge railing." *International Journal of Crashworthiness*, 9(4), 349-363.
69. Reid, J. D. (1996). "Towards the understanding of material property influence on automotive crash structures." *Thin-Walled Structures*, 24, 285-313.
70. Reid, J. D. (1998). "Admissible modeling errors or modeling simplifications?" *Finite Elements in Analysis and Design*, 29, 49-63.

71. Reid, J. D. (2004). "LS-DYNA simulation influence on roadside hardware." *Transportation Research Record*, 1890, 34-41.
72. Reid, J. D., and Marzougui, D. (2002). "Improved truck model for roadside safety simulations: Part I - structural modeling." *Transportation Research Record*, 1797, 53-62.
73. Reid, J. D., Coon, B. A., Lewis, B. A., Sutherland, S. H., and Murray, Y. D. (2004). "Evaluation of LS-DYNA soil material model 147." *FHWA-HRT-04-094*, U.S. Department of Transportation, Federal Highway Administration, McLean, VA.
74. Reid, J. D., and Hiser, N. R. (2004). "Friction modelling between solid elements." *International Journal of Crashworthiness*, 9(1), 65-72.
75. Reid, J. D., and Hiser, N. R. (2005). "Detailed modeling of bolted joints with slippage." *Finite Elements in Analysis and Design*, 41, 547-562.
76. Reid, J. D., Sicking, D. L., Faller, R. K., and Pfeifer, B. G. (2007). "Development of a New Guardrail System." *Transportation Research Record*, 1599, 72-80.
77. Rosenbaugh, S. K., Sicking, D. L., and Faller, R. K. (2007). "Development of a TL-5 Vertical Faced Concrete Median Barrier Incorporating Head Ejection Criteria [Test No. TL5CMB-2]." *Test Report No. TRP- 030194-07*, Midwest Roadside Safety Facility, University of Nebraska-Lincoln.
78. Ross, H. E., Jr., Sicking, D. L., Zimmer, R. A., and Michie, J. D. (1993). "Recommended procedures for the safety performance evaluation of highway features." *NCHRP Report 350*, Transportation Research Board, National Research Council, Washington, D.C.
79. Schrum, K. D., Lechtenberg, K. A., Bielenberg, R. W., Rosenbaugh, S. K., Faller, R. K., Reid, J. D., and Sicking, D. L. (2013). "Safety performance evaluation of the non-blocked midwest guardrail system (MGS)." *Report TRP-03-262-12*. Midwest Roadside Safety Facility, University of Nebraska-Lincoln.
80. Tiso, P., Plaxico, C., and Ray, M. (2002). "Improved truck model for roadside safety simulations: Part II - suspension modeling." *Transportation Research Record*, 1797, 63-71.
81. Whitworth, H. A., Bendidi, R., Marzougui, D., and Reiss, R. (2004). "Finite element modeling of the crash performance of roadside barriers." *International Journal of Crashworthiness*, 9(1), 35-43.
82. Zaouk, A. K., Bedewi, N. E., Kan, C.-D., and Marzougui, D. (1997). "Development and evaluation of a C-1500 pickup truck model for roadside hardware impact simulation." *FHWA-RD-96-212*, Federal Highway Administration, Washington, D.C.
83. Zaouk, A. K., Marzougui, D., and Bedewi, N. E. (2000a). "Development of a detailed vehicle finite element model, Part I: methodology." *International Journal of Crashworthiness*, 5(1), 25-36.
84. Zaouk, A. K., Marzougui, D., and Kan, C.-D. (2000b). "Development of a detailed vehicle finite element model, Part II: material characterization and component testing." *International Journal of Crashworthiness*, 5(1), 37-50.

85. Zweden, J. V., and Bryden, J. E. (1977). "In-service performance of highway barriers." *Report NYSDOT-ERD-77-RR51*, New York State Department of Transportation, Albany, NY.